(1)

AGARD-CP-435

AGARD-CP-435

AGARD

ADVISORY GROUP FOR AEROSPACE RESEARCH & DEVELOPMENT

7 RUE ANCELLE 92200 NEUILLY SUR SEINE FRANCE

AGARD CONFERENCE PROCEEDINGS No.435

Guidance and Control of Precision Guided Weapons

NORTH ATLANTIC TREATY ORGANIZATION

AGARD-CP-435

NORTH ATLANTIC TREATY ORGANIZATION

ADVISORY GROUP FOR AEROSPACE RESEARCH AND DEVELOPMENT

(ORGANISATION DU TRAITE DE L'ATLANTIQUE NORD)

AGARD Conference Proceedings No.435

GUIDANCE AND CONTROL OF PRECISION GUIDED WEAPONS

Papers presented at the Guidance and Control Panel 46th Symposium held in Geilo, Norway from 3 to 6 May 1988.

THE MISSION OF AGARD

According to its Charter, the mission of AGARD is to bring together the leading personalities of the NATO nations in the fields of science and technology relating to aerospace for the following purposes:

- Recommending effective ways for the member nations to use their research and development capabilities for the common benefit of the NATO community;
- Providing scientific and technical advice and assistance to the Military Committee in the field of aerospace research and development (with particular regard to its military application);
- Continuously stimulating advances in the aerospace sciences relevant to strengthening the common defence posture;
- Improving the co-operation among member nations in aerospace research and development;
- Exchange of scientific and technical information;
- Providing assistance to member nations for the purpose of increasing their scientific and technical potential;
- Rendering scientific and technical assistance, as requested, to other NATO bodies and to member nations in connection with research and development problems in the aerospace field.

The highest authority within AGARD is the National Delegates Board consisting of officially appointed senior representatives from each member nation. The mission of AGARD is carried out through the Panels which are composed of experts appointed by the National Delegates, the Consultant and Exchange Programme and the Aerospace Applications Studies Programme. The results of AGARD work are reported to the member nations and the NATO Authorities through the AGARD series of publications of which this is one.

Participation in AGARD activities is by invitation only and is normally limited to citizens of the NATO nations.

Published November 1988

ISBN 92-835-0486-0

Printed by Specialised Printing Services Limited
40 Chigwell Lane, Loughton, Essex IG10 3TZ

PREFACE

The Guidance and Control Panel held a symposium on the topic of Precision Guided Munitions in Norway in 1982. Due to the rapid advance in guidance and control technology for such weapons, and because the body of engineering experience with such weapons is growing, it is appropriate to review these advances.

The content of the 46th GCP Symposium includes the broad range of precision guided weapons against beyond-visual-range surface targets (moving or not) and helicopters with emphasis on guidance and control aspects of such weapons, and, where appropriate, their airborne or ground platforms.

Topics covered include:

- Acquisition and guidance sensors;
- Target signatures:
- Guidance and control algorithms and software;
- Command and control, targetting and launch considerations as they apply to guidance and control;
- Integration issues such as guidance and fuzing;
- Countermeasures versus guidance techniques: trends.

* * *

En 1982, en Norvège, le Panel du Guidage et du Pilotage avait organisé un symposium sur le thème des armes guidées de précision.

Les progrès réalisés dans la technologie du guidage et du pilotage de telles armes depuis cette date, et l'expérience croissante acquise par les ingénieurs, justifient la reactualisation de ces progrès.

Le Programme du 46ème Symposium du GCP couvre l'ensemble des armes guidées de précision deployées contre les cibles au-delà de la portée optique (mobiles ou non) y compris les hélicoptères, et met l'accent sur les aspects guidage et pilotage de telles armes et, quand cela s'avere nécessaire, sur leurs plate-formes au sol ou aéroportées.

Les sujets traités comprennent:

- Capteurs d'acquisition et de guidage;
- Signatures d'objectif;
- Algorithmes et logiciels de guidage et de pilotage;
- Commandes de vol et de pilotage, acquisition d'objectifs; considération concernant le guidage et le pilotage;
- Les questions d'intégration, telles que le guidage et la mise à feu des fusées de proximité;
- Contremesures opposées aux techniques de guidage: tendances.

GUIDANCE AND CONTROL PANEL OFFICERS

Chairman: Mr Kenneth A.Peebles
Director, Electro-Optics Division
Defence Research Establishment
Valcartier
2459 Pie XI Boulevard Nord
Courcelette, P.Q. G0A 1R0
Canada

Deputy Chairman: Ir P.Ph. van den Broek
Delft University of Technology
Department of Aerospace Engineering
PO Box 5058
2600 GA Delft
Netherlands

TECHNICAL PROGRAMME COMMITTEE

Chairman:	ICA H.Radet	Fr
Members:	Mr U.K.Krogmann	Ge
	Dr O.Hallingstad	No
	Mr R.Dunn	UK
	Mr S.Leek	UK
	Dr W.P.Albritton	US

PANEL EXECUTIVE

From Europe:
AGARD-OTAN
Attention: GCP Executive
7 Rue Ancelle
92200 Neuilly-s-Seine, France
Telephone: (1) 47.38.57.80
Telex: 610176 F

From USA and Canada only:
AGARD-NATO
Attention: GCP Executive
APO New York 09777

HOST NATION COORDINATOR

Dr O.Hallingstad
Norwegian Defence Research Establishment
Division for Electronics
PO Box 25
N-2007 Kjeller
Norway

ACKNOWLEDGEMENTS/REMERCIEMENTS

The Panel wishes to express its thanks to the Norwegian National Delegates to AGARD for the invitation to hold this meeting in their country and for the facilities and personnel which made the meeting possible.

Le Panel tient à remercier les Délégués Nationaux de la Norvège près l'AGARD de leur invitation à tenir cette réunion dans leur pays et de la mise à disposition de personnel et des installations nécessaires.

CONTENTS

* Published in CP-435 Supplement.
† Not available at time of printing.

* Published in CP-435 Supplement.

CO_2 LASER RADAR SYSTEMS FOR TARGET ACQUISITION AND GUIDANCE

A.V.Jelalian, G.R.Osche, D.R.Bates, A.J.Legere
Raytheon Company, Equipment Div.
Mail Stop 91
528 Boston Post Road, Sudbury, MA 01776-3375
USA

I. INTRODUCTION

Laser radar systems combine the narrow beam width associated with optical systems with the target measurement capabilities of microwave radar systems. The combined attributes of these distinctly different technologies lead to a single sensor capable of measuring range, velocity, acceleration and angular location while still providing imaging capability. The best optical source for systems having this capability is the CO_2 laser operating in the infrared band at 10.6 microns. This paper will assess atmospheric propagation, coherent and incoherent detection receivers, and field test data collected over the past two decades.

II. PROPAGATION

In reviewing the electromagnetic spectrum as illustrated in Table I, it may be observed that if all-weather system propagation is desired, long-wavelength microwave radar systems are required. However, these longer wavelength systems lack accurate tracking capability at shallow depression angles due to multipath problems, and do not provide the aimpoint selection capability required by many weapon systems. To this end, shorter wavelength operation toward the optical spectrum is dictated.

Table I illustrates the amount of attenuation as a function of wavelength for both laser and microwave wavebands. The chart is compiled from broadband data and does not include the fine-grain atmospheric absorption values into which laser lines may occasionally drift (and which can be prevented by stable transmitter design).

In the visible waveband where the ruby laser operates (0.7 μm), the atmospheric "seeing" conditions have a dramatic effect upon the amount of attentuation per kilometer that the laser beam encounters. Visibility on a clear day is 15 km, with corresponding one-way attenuation of 1 dB/km. Introduction of haze into the atmosphere reduces the visibility to 3 km and increases the attenuation to 5 dB/km. Moving to the 1.06 μm wavelength (the wavelength associated with a YAG laser), it is seen from the table that these conditions produce less attenuation than they did in the visible region. Further movement to 10.6 μm decreases the haze attenuation to 1 dB/km; the predominant attenuation mechanism in that region is absorption by H_2O. The shaded column under the 10.6 μm wavelength addresses the problems of humidity in sub-arctic, mid-latitude, and tropical environments. McClatchey's [1] data for atmospheric attenuation under tropical environments shows a factor of 3 dB/km. A chief concern is system operation in fog and rain [2-4]. The column under λ = 10.6 μm illustrates that a fog having visibility of 0.5 km would have attenuation of 3 dB/km. These figures may be contrasted with those commonly found in microwave radar textbooks [5,6] for attenuation at microwave wavelength from 1 cm to 0.3 cm. These last two columns indicate the ability of longer wavelength electromagnetic systems to penetrate fog with less attenuation.

The data with regard to rain are not necessarily so apparent. The table indicates that a rainfall rate of 4 mm/hr has equivalent attenuation at 10.6 μm and at 0.3 cm. The last column in this chart shows the attenuation of 1 cm (3 dB/km) systems in 12.5 mm/hr of rain.

III. RECEIVER DETECTION TECHNIQUES

In Figure 1, diagrams are shown for incoherent and coherent detection receivers. The incoherent detection receiver at optical wavelengths is similar to a video radiometer receiver (i.e., an envelope detector at microwave wavelengths). However, the signal-to-noise ratio (SNR) equation has additional terms besides the signal power (P_{sig}) called the optical background (P_{bk}) which is caused by undesired signals such as sunlight, cloud reflections, flares, etc. The received signal competes with these external and other internal noise sources at the receiver. The received optical power, after suitable filtering, is applied to the optical detector; square-law detection then occurs, producing a video bandwidth electrical signal.

The coherent detection receiver is similar to the incoherent; however, a portion of the laser signal is coupled to the optical detector via beamsplitters. As a result, the optical detector has the local oscillator power (P_{LO}) at frequency (f_o) in addition to the received signal power (P_{bk}).

Additionally, the receiver has a dark current or thermal receiver noise, 1/f noise, and generation recombination noise.

Having discussed the noise mechanizations, let us now turn to the SNR expressions.

The SNR equation for incoherent detection may be expressed as:

$$SNR = \frac{\eta P_{sig}^2}{hf\left[2B\,(P_{sig} + P_{bk}) + K_1 P_{dk} + K_2 P_{th}\right]}$$

The SNR equation for coherent detection may be expressed as:

$$SNR = \frac{\eta P_{sig} \quad P_{LO}}{hf\left[B\,(P_{LO} + P_{sig} + P_{bk}) + K_3 P_{dk} + K_4 P_{th}\right]}$$

where:

SNR = electrical signal power/electrical noise power
η = quantum efficiency
h = Planck's constant (6.6×10^{-34} joule-second)
f = transmission frequency
B = electronic bandwidth
P_{sig} = received signal power
P_{bk} = background power
P_{dk} = equivalent dark current power = $\frac{AB}{(D^*)^2}$
P_{th} = equivalent receiver thermal noise = $\frac{4KTBN_F}{R}$
P_{LO} = reference local oscillator power
K_1 = $\frac{\rho i}{q}$
K_2 = $\frac{1}{\rho i\, q}$
K = Boltzmann's Constant
T = receiver temperature (290°K)
N_F = receiver noise figure
R = resistance

where:

A = detector area (cm^2)
ρi = the detector current responsivity
q = the electron charge (1.6×10^{-19} coulombs)

D* = specific detectivity ($\frac{cm - Hz^{\frac{1}{2}}}{W}$)

The SNR for the incoherent system has the received signal power squared in its numerator and has a summation of noise terms associated with the return signal, the background signal, the dark current, and the thermal noise of the receiver in the denominator. The returned signal power and the background power are included as noise sources in the detection process because of the random photon arrival rate. In the coherent detection system, the local oscillator power is an additional source of noise (compared to the incoherent system) and the numerator is related to the product of the received signal power and the local oscillator power. The local oscillator power is very important in the detection process; here, it may be increased so that it overwhelms all of the other noise sources. As a result, the local oscillator power in the denominator cancels out the local oscillator power in the numerator; the SNR is directly proportional to the received signal power, rather than to the received signal power squared (as with the incoherent system). Additionally, because the local oscillator power becomes the predominant noise source, the coherent detection system typically is background-immune.

For coherent detection where the local oscillator power is increased to provide shot-noise limited operation of the receiver, the SNR expression for coherent detection can be reduced to:

$$SNR = \frac{i^2_{sig}}{i^2_N} \quad \frac{\eta P_{sig}}{hfB}$$

Comparing the SNR for a coherent system to the SNR for an incoherent system with the following typical parameters at 10.6 microns:

$\eta = 0.5$
$hf = 1.9 \times 10^{-20}$ joules
$D^* = 2 \times 10^{10}$ cm $\sqrt{Hz}/watt$
$\sqrt{A} = 0.03$ cm
$\rho = 4$ amperes/watt
$R = 1000$ ohms

yields the S/N ratio for a coherent receiver which is 30 dB more sensitive than the incoherent detection systems. Recent detector sensitivity improvements would reduce this to approximately 25 dB.

Figure 2 illustrates the reference transmitter power versus SNR relationship for coherent and incoherent detection laser radar systems utilizing a typical 100 ns pulse width. It may be observed that as the SNR requirement increases, the transmitter power of the coherent system increases linearly and that of the incoherent system increases as the square root. In the limit, incoherent detection systems approach the sensitivity of coherent systems for very large SNRs. For a typical SNR requirement of 100 (20 dB), the coherent system is seen to have a 30 dB increased sensitivity over that of an incoherent system.

Coherent detection laser radar receivers are typically Gaussion noise limited and, as a result, RMS measurement errors may be characterized by those utilized in microwave radar systems.

Due to the short wavelength operation of laser radars, Doppler shifts are extremely large compared to microwave systems. This results in IF signals in the receiver allowing short measurement time intervals, thereby permitting simultaneous range, velocity and angle measurement. This inherent capability of laser radar systems to provide five-dimensional target data R,V,I, angle-angle with optical resolution capability has resulted in laser radar systems being evaluated for precision fire control and autonomous missile guidance applications.

The one sigma range (σ_R) and velocity (σ_V) measurement accuracy for pulse,frequency-modulated, and amplitude-modulated waveforms may be shown to be:

Pulse: $$\sigma_R = \frac{K \; C \; \tau}{2 \; \sqrt{S/N}}$$

FM: $$\sigma_R = \frac{C}{2 \frac{dF}{dT}} \; \sigma_F$$

$$\sigma_F = \frac{3}{\pi T \; \sqrt{2 \; S/N}}$$

AM: $$\sigma_R = \frac{C}{4\pi \; F_{AM} \; M \; \sqrt{S/N}}$$

Velocity: $$\sigma_V = \frac{\lambda}{2} \; \sigma_F \qquad \text{where } \tau = \frac{1}{B}$$

Where:
τ = pulse width
C = speed of light
$\frac{dF}{dT}$ = chirp characteristics
σ_F = one sigma estimate of frequency
σ_V = one sigma estimate of velocity
F_{AM} = AM modulating frequency
M = modulation index
T = measurement time

The pulse, frequency-modulated and velocity measurement accuracy capability as a function of receiver processor bandwidth are plotted in Figure 3. Here it may be observed that there is a tradeoff required for pulse systems to simultaneously measure range and velocity, i.e., good range accuracy - poor velocity accuracy.

This trade is not required for FM systems as the slope of the measurement accuracy plots are in the same direction, and chirp characteristics may be chosen to result in good simultaneous range and velocity measurement accuracy.

The curves are plotted for: S/N = 50 for the FM system, 100 for the pulse systems, and assumes the signals are at an intermediate frequency within the receiver such that the processing bandwidth is the inverse of the pulse width, and that the FM chirp characteristic is 10^{12} Hertz per second.

IV. LASER RADAR FIELD TEST RESULTS

Raytheon 10.6-micron laser radar systems employing coherent detection receivers have been utilized in field and flight test experimentation since 1968 [7]. A typical laser radar block diagram utilized for laser radar applications is shown in Figure 4.

In this configuration the laser is modulated to provide information content to the transmitted signal which is coupled through the interferometer, optics, and scanner to illuminate the scan field of interest. The received signal is then coupled, via reciprocity through the interferometer, to the receiver detector where it is mixed with a sample of the laser signal in the form of a local oscillator.

The receiver output is processed by the signal processor to extract target information and then processed by the data processor where all information is compiled to provide target position, range, velocity, and an image. Figure 5 illustrates a 1968 ground signal returned from a 5-watt coherent 10.6 micron airborne system. Figure 5A and Figure 5B illustrate this Doppler-shifted signal along with an aerial camera photograph with the laser boresighted to the center of the frame. Figure 5C illustrates the Doppler-shifted signal of a pedestrian crossing at a crosswalk, as observed in the aerial camera photograph to the left. In the next sequence, the laser footprint passes over the pedestrian and one observes the aircraft ground speed in pictures 5D and 5E. Early success of these experimental systems encouraged further technology development. However, laser devices were too large, weighing as much as 450 pounds. Subsequently, Raytheon developed an air-cooled 5-watt laser weighing 7.5 pounds including power supplies and cooling. The coherent 5-watt laser was configured into the scanning laser radar shown in Figure 6. This system was designed, fabricated and flight-tested under USAF and DARPA sponsorship [8] in 1975. A conceptual diagram of the system is shown in Figure 6. Here the 0.5-milliradian beam was propagated to the terrain via a Palmer scan. The beam advances in a contiguous manner across the terrain (via aircraft flight velocity) to yield a coherent Doppler spectrum in the receiver.

The backscattered Doppler-shifted target signal was then processed in a surface acoustic wave signal processor, recorded on tape, and subsequently played back on the ground through a CRT display. The system was configured for a remotely piloted vehicle (RPV) application with the tape recorder simulating the data link. Thresholding of the Doppler-processed signal intensity resulted in gray scale rendition on a photographed CRT. Figure 7 illustrates a strip made in such a manner. The CO_2 laser radar map, made at a 50-degree depression angle, is shown as the central image in Figure 7. Surrounding this picture are 70-millimeter aerial camera photographs from a vertically oriented camera. One may readily observe that optical quality photograhic images may be made with CO_2 laser radars, and also that speckle effects may be reduced by suitable processing.

Having demonstrated optical resolution capability, let us now evaluate the MTI radar aspects of this system. Figure 8 illustrates a 70-mm aerial camera scene of a forested area at Fort Devens, Massachusetts. There is a tank suitably noted in Figure 8A traveling on a road. A return signal from the forest or road is Doppler-shifted relative to the aircraft velocity and appears at a frequency $f_o + f_D$ while a return signal from the moving tank appears at a frequency $f_o + f_D + f_{target}$ and, as such, appears in a different Doppler filter. The surface acoustic wave delay line processor is programmed to give an MTI cue, in real time, when a Doppler return greater than 5 knots is indicated in adjacent pixels. Figure 8B illustrates this moving target flag which occurs at full intensity, or one gray shade, on the display. Additionally, it may be noted that several target clutter intensity spots cause false alarm indications which are distributed through the scene. Altering the target detection algorithms to require a "N detections out of M trials" detection approach results in Figure 8C and a significant false alarm reduction. One may also note what appears to be a second target in this scene which was not observed in the photograph. A clutter patch of the duration and continuity of motion, required to pass the MTI target detection requirements, tends to rule out a false target detection.

Forward-looking ground-based systems have been configured to demonstrate target acquisition and imaging capabilities. Figure 9 illustrates MTI detection and imaging over a 6° x 5° raster scan field of a moving tank, obtained by a Raytheon-developed system. These measurements were funded by U.S. Army, Navy and Air Force contracts [9]. Figure 9 shows photographs of a visual picture of an M-48 tank and CO_2 laser radar image of the same vehicle. Tank targets tended to have a significant diffuse component as noted by the number of consecutive returns. This may be contrasted to that of a helicopter noted in Figure 10, where specularities contribute to the image. Helicopter blade rotation caused the Doppler return to be outside the bandwidth of the imaging filter so that the blades were not imaged.

Figure 11 illustrates an amplitude-modulated CW laser received signal from a stationary target which has been processed to illustrate range measurement characteristics. Here color is utilized to portray range measurement. In this image the range ambiguity of the 8 MHz Amplitude-Modulated (AM) tone is seen as horizontal bands over the display. The color scale bar under the picture indicates that returns at longer ranges are color shaded red while shorter ranges are white and blue respectively. Red color highlights the tank turret and gun barrel. Figure 12 illustrates how edge extraction techniques implemented in the computer can be utilized

to identify internal features of another vehicle. Here the windshield, bumpers, truck side body, air conditioner and tractor areas are highlighted.

Simultaneous measurement programs with passive IR systems have been conducted. One of these results indicates the diurnal washout of a tanker truck located at a range of 4 km along with that of a CO_2 laser range image of the same vehicle. Figure 13 also illustrates the ability of the system to measure telephone wires at distances of 2800 meters.

In 1984 Raytheon proposed the use of these Laser Radar principles to the USAF Armament Division, Eglin AFB, Florida, for the purpose of autonomous guidance for tactical standoff weapons. The resultant contract was termed the Tactical Ladar Seeker (TLS) Program. The TLS program consisted of two phases. Phase one was a system design study and Phase two was a captive flight demonstration of the selected approach.

Phase one activities included system simulation studies related to AGM-130, powered glide bombs. A typical system scenario consisted of a 25-nmi mission, wherein aircraft position and inertial transfer alignments occurred. The targets selected were:

- Mobile SAM sites
- Bridges
- Buildings
- Runways
- Buried Targets

System range requirements were determined to be approximately 1 km and necessitated simultaneous active and passive operations at 10.6 microns and 8-12 microns respectively. This hardware was designed and supplied to the USAF by Raytheon for a captive flight demonstration. The purpose of the captive flight test was to demonstrate:

- Autonomous, real time, target detection and classification
- Autonomous aimpoint selection

Figure 14 illustrates the seeker hardware mounted in the nose section of a C-45 aircraft along with photographs of the bridges and tactical target scenes. The bridges included both flat and elevated, while the tactical targets included elements of a HAWK Battery located at the outer clay pad location and a Pershing missile (mock-up) located in the central pad.

Figure 15 illustrates simultaneous active/passive airborne bridge imagery collected from a flight test at Eglin AFB while Figure 16 illustrates MTI target detection of cars and trucks on a highway along with passive imaging of the same scene. In Figure 17 active passive imagery of an airport scene may be observed. Here aircraft parked in front of the hangar area have different characteristics in the two scenes. The range image illustrates two parked aircraft while the passive scene suggests three. This is due to a thermal shadow caused by a recently departed aircraft.

A video TV camera was boresighted to the Raytheon sensor and a computer graphics generator was utilized to indicate target detection via a box generated on the detected target. Real-time classification of the target resulted in the suitable detection box being color shaded red. Figure 18 illustrates the bridge detection box located over several pier structures. Subsequent computer processing resulted in the computer selection of a bridge pier aimpoint. Similar detection, classification and aimpoint selection occurred for mobile targets. These 1987 real time results are illustrated in the video tape to be shown.

In summary, confirmation of the Tactical Ladar Seeker concept feasibility has been demonstrated through system studies and in-flight test results, which have demonstrated successful autonomous real-time target detection, classification and aimpoint selection.

REFERENCES

[1] McClatchey, R., Selby, J.: AFCRL-72-0611, Environmental Research Paper No. 419, AFCRL, Bedford, Massachusetts, 12 October, 1972.

[2] Goodwin, F., Nussmeier, T.: IEEE Journal of Quantum Electronics, Vol. QE-4, No. 10, p. 616, October, 1968.

[3] Rensch and Long: Applied Optics, Vol. 9, No. 7, pp. 1563-1573, July, 1970.

[4] Chu, T.S.: Bell System Technical Journal, pp. 723-759, May/June, 1968.

[5] Barton, D.K.: Radar System Analysis, Artech House, Dedham, Mass., 1976.

[6] Skolnik, M.I.: Introduction to Radar Systems, McGraw-Hill, N.Y., 1962.

[7] Doppler Optical Navigator Program, Technical Report AFAL-TR-68-211, Dated October, 1968.

[8] McManus, R.G., Chabot, A., Young, R., Evett, R., CO_2 Laser Heterodyne Sensor, Technical Report AFAL-TR-75-216, Dated November, 1975.

[9] Jelalian A., Keene, W., Kawachi, D., Sonnenschein, C., Freedman, N., Low Probability of Intercept Multifunctional Tactical Sensors, Volume 2, Phase II, March, 1980 AFWAL-TR-80-1006.

[10] Jelalian, A., Keene, W., Kawachi, D., Sonnenschein, C., Freedman, N., Low Probability of Intercept Multifunctional Tactical Sensors, Phase I, Final Report AF-TR-77-77, January, 1978.

TABLE I. ATMOSPHERIC PROPAGATION

dB/km	λ 0.7 μm	λ 1.06 μm	λ = 3.8 μm	λ = 10.6 μm		0.3 cm	λ 1 cm	λ 3 cm
0.2	EXTREMELY CLEAR	EXTREMELY CLEAR	CLEAR (V = 23 km)	SUB ARCTIC WINTER				12.5 mm/h
0.6	STANDARD CLEAR (V = 25 km)	STANDARD CLEAR		CLEAR			2.5 mm/h	FOG (V = 100 FT)
0.8		CLEAR					FOG (V = 100 FT)	50 mm/h
1.0	CLEAR (V = 15 km)			HAZE SUB ARCTIC SUMMER		ADVECTION FOG (V = 400 FT)		
2	LIGHT HAZE (V = 5 km)		HAZE (V = 3 km)	MID LATITUDE SUMMER	RAIN 2.5 mm/h	RAIN 2.5 mm/h		
3	MEDIUM HAZE (V = 5 km)	HAZE (V = 3 km)		TROPICAL	RADIATION FOG (V = 0.5 km) RAIN 4 mm/h	RAIN 4 mm/h	12.5 mm/h	
5	HAZE (V = 3 km)				SNOW 0.2 mm/h		25 mm/h	

V = VISIBILITY

EOA-1156A

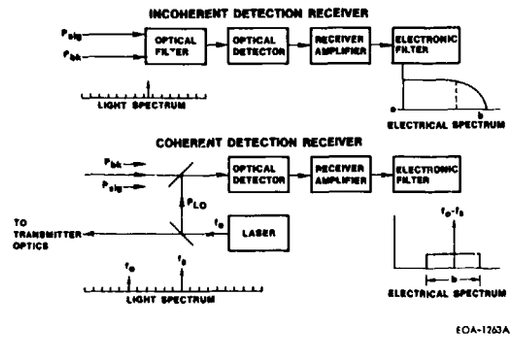

Figure 1. Receiver Systems

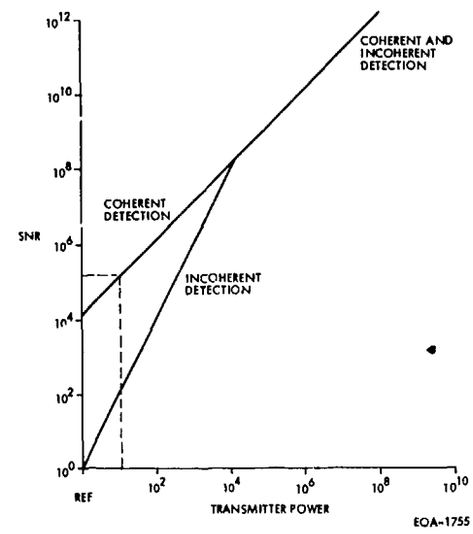

Figure 2. Transmitter Power vs SNR

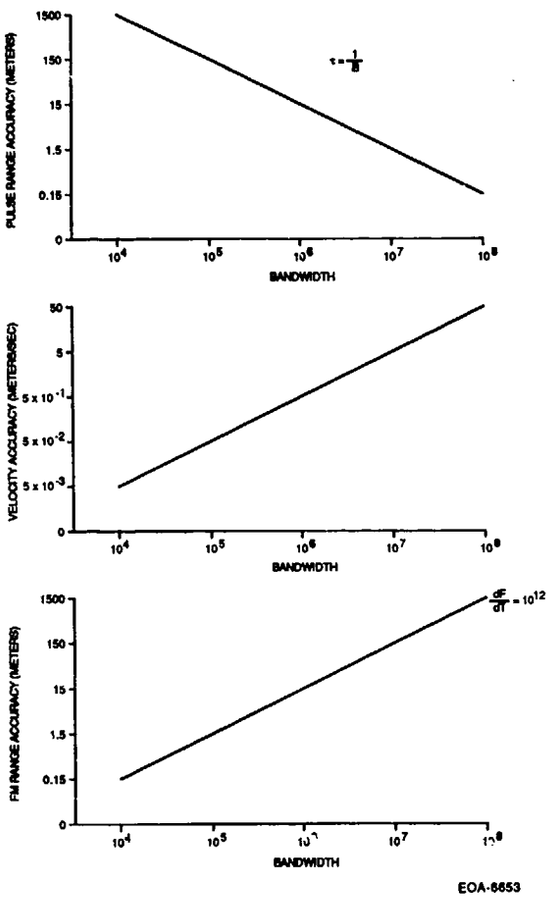

Figure 3. Range/Velocity Accuracy vs Bandwidth

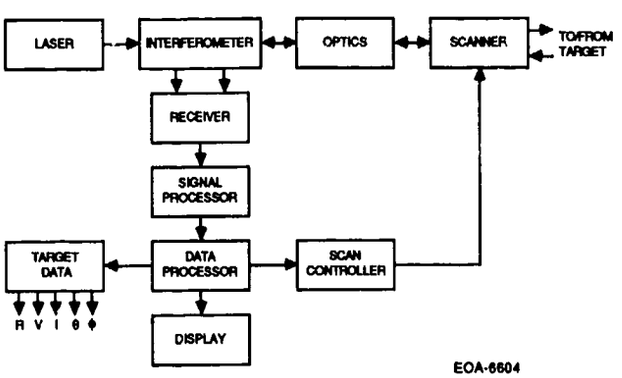

Figure 4. Typical Laser Radar Block Diagram

Figure 5. CO_2 Laser Doppler AMTI of a Person Walking Across an Intersection

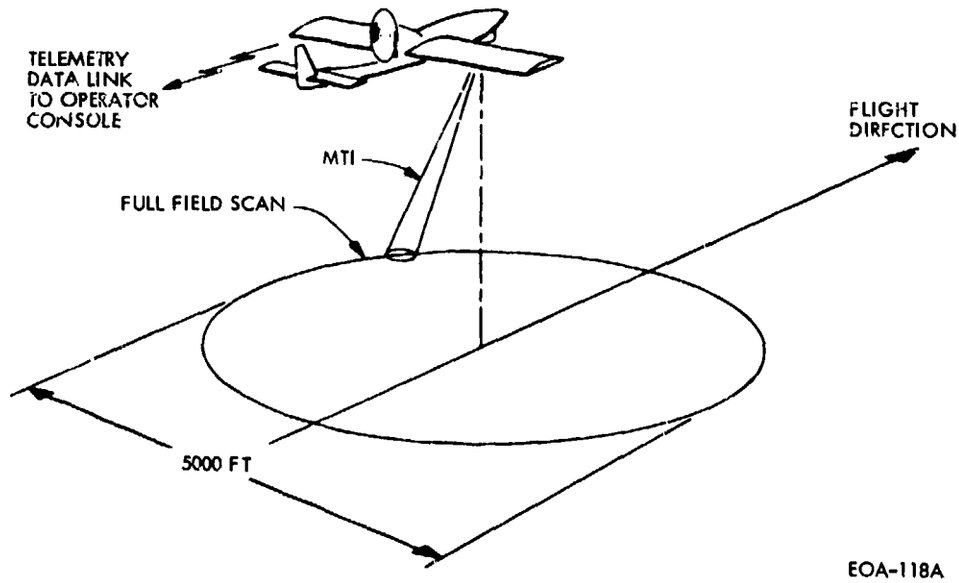

Figure 6. RPV Palmer Scan Geometry

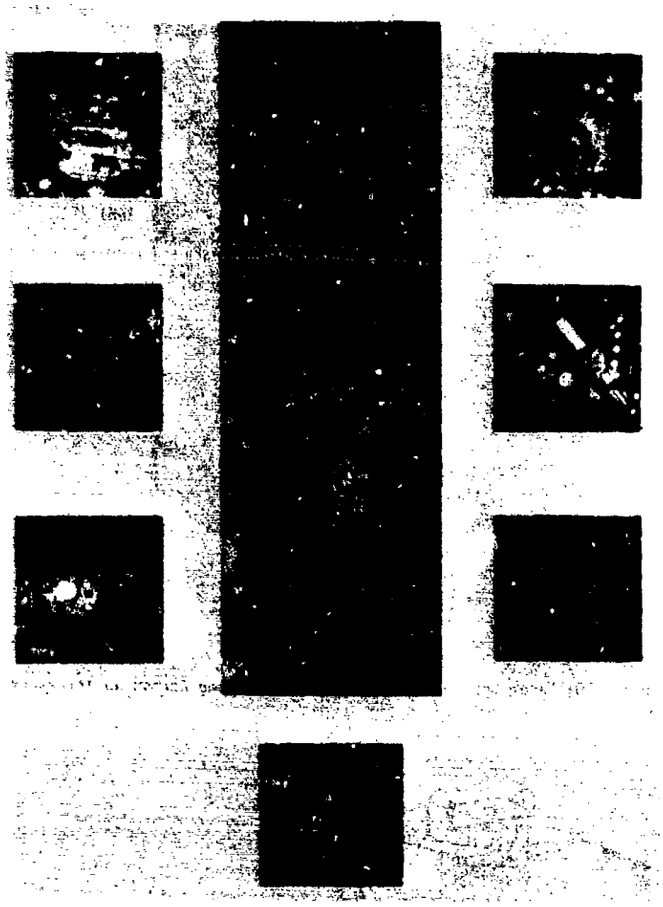

EO-155

Figure 7. Coherent CO_2 Imagery

EO-32

Figure 8. MTI Detection of M-48 Tank at Altitude of 1000 Feet

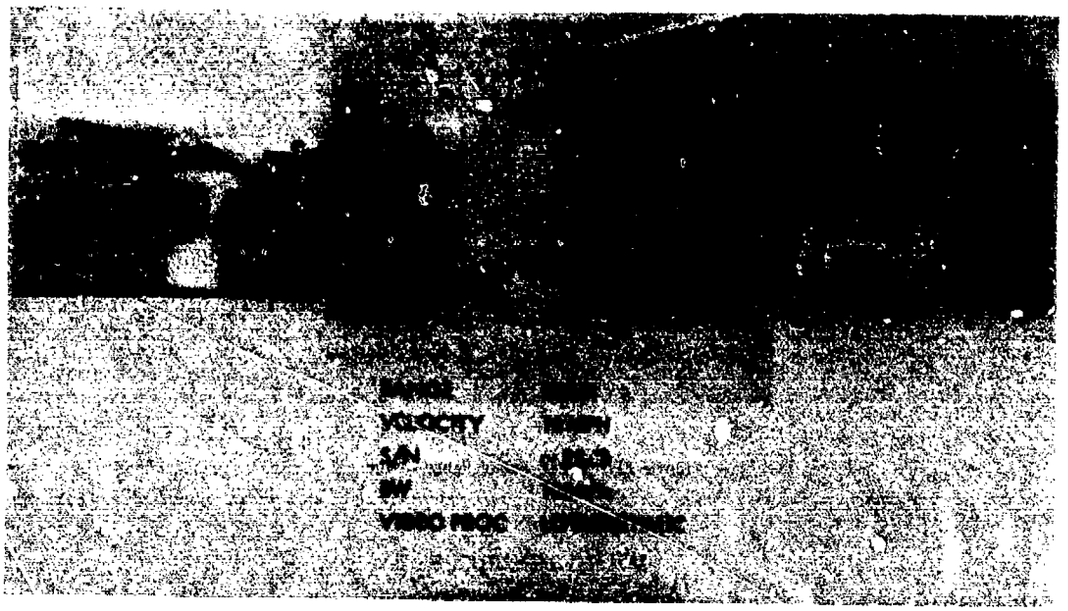

EO-473A

Figure 9. M-48 Tank Approaching

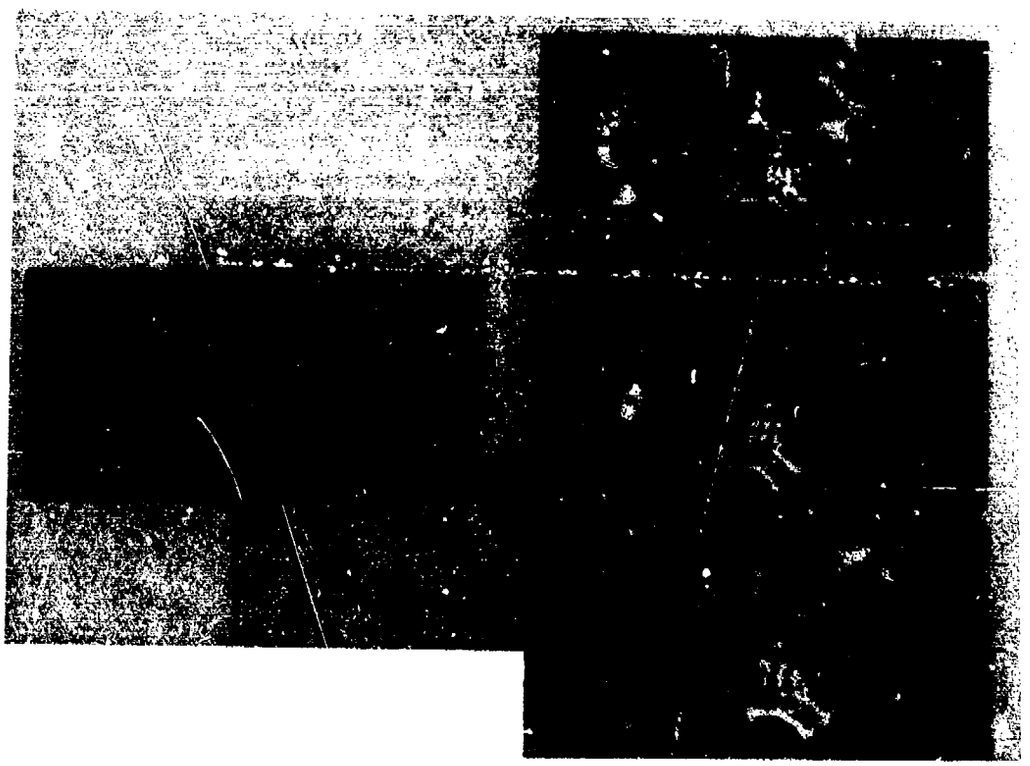

EO-477

Figure 10. UH-1 Helicopter

EO-2622

Figure 11. Laser Radar Range Image

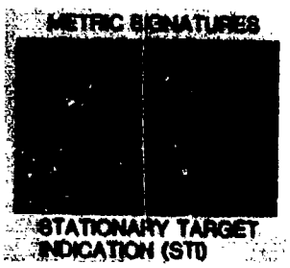

EO-2699

Figure 12. Range Image Edge Extinction

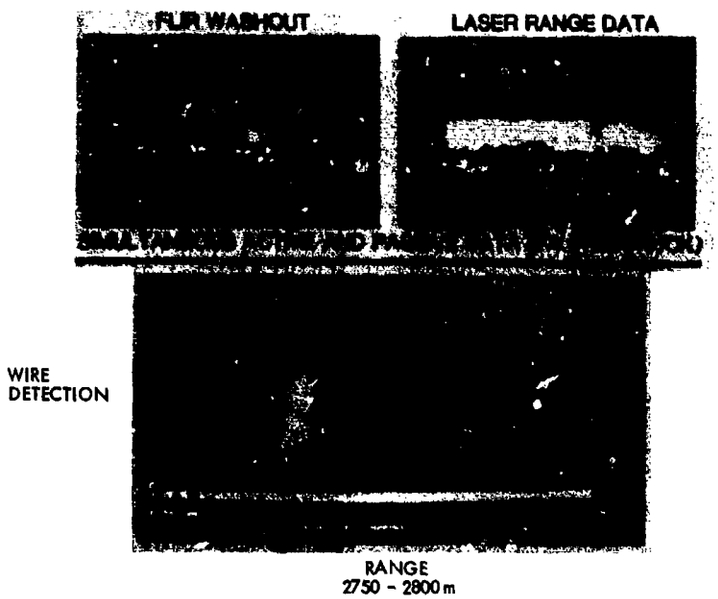

Figure 13. CO_2 Laser Radar Capabilities

EO-2700

EO-2701

Figure 14. Flight Tests

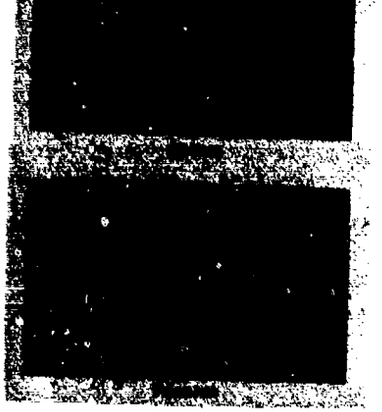

EO-2702

Figure 15. Active/Passive Images Navarre Bridge, Eglin AFB

EO-2703

Figure 16. Active/Passive Images - Eglin Tests MTI Detection

EO-2704

Figure 17. Active/Passive Images - Eglin Flight Tests Hangar Complex

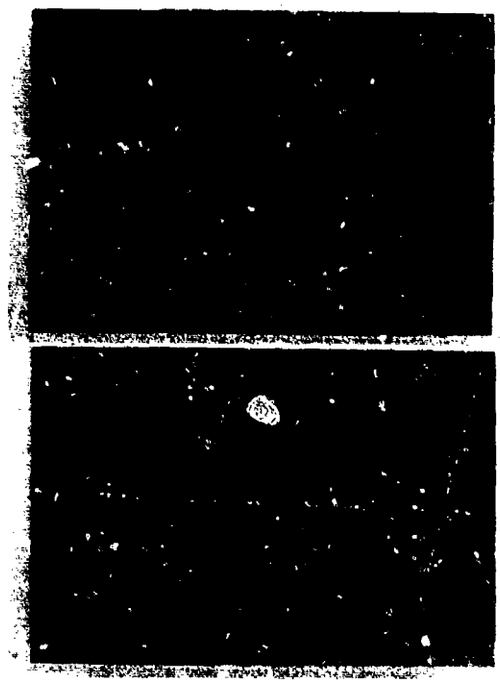

EO-2705

Figure 18. TLS Flight Test Navarre Bridge Detection and Aimpoint Selection

L'AQM - ACCELEROMETRE POUR MUNITIONS DE PRECISION

A. BOURA , Ingénieur . SFENA , BP 128 - 86101 CHATELLERAULT CEDEX
O. AUJAY , Ingénieur . SFENA , BP 128 - 86101 CHATELLERAULT CEDEX
J.L. BOST , Ingénieur . SFENA , BP 128 - 86101 CHATELLERAULT CEDEX

RESUME

La SFENA conduit depuis 1983, en collaboration avec le CEA/D. LETI, un programme d'étude concernant l'utilisation de techniques de micro-usinage collectif pour la fabrication de capteurs inertiels. Des structures accélérométriques pendulaires planes monolithiques d'une surface de quelques millimètres carrés ont été conçues, fabriquées et testées. Les résultats permettent d'envisager leur utilisation dans des systèmes d'armes propulsées à auto-directeur ou dans des obus à correction de dérive.

Les accéléromètres qu'il est possible de construire autour de ces structures sensibles occupent un volume de 1 cm3 à 4 cm3. Selon leur mode de fonctionnement et selon que l'on intègre ou non les circuits électroniques d'asservissement et de mesure.

Certains des prototypes, spécialement calculés, ont résisté à des chocs de 20 000 G (tirs de mortier), alors que d'autres se montrent capables d'un domaine de mesure statique supérieur à 100 G.

On montre comment sont constituées les structures sensibles monolithiques et comment on peut mettre à profit leurs propriétés particulières pour obtenir le meilleur compromis entre le prix, l'encombrement, les performances fonctionnelles et la tenue à l'environnement.

On donne également les résultats expérimentaux récents et les extrapolations qui peuvent en être déduites en ce qui concerne les capteurs utilisables dans des munitions précises.

1. HISTORIQUE DU DEVELOPPEMENT

Le début des travaux de la SFENA (Société Française d'Equipements pour la Navigation Aérienne) dans le domaine des accéléromètres micro-usinés se situe en 1983, année où elle finança une première étude exploratoire au CEA/D. LETI (Division de l'Electronique de la Technologie et de l'Instrumentation). Il s'agissait alors d'essayer d'appliquer les techniques de la micro-électronique à la fabrication d'éléments géométriques susceptibles d'être utilisés dans la définition d'accéléromètres miniatures.

Depuis, la coopération entre la SFENA et le CEA/D. LETI s'est poursuivie sans interruption, matérialisée par des contrats d'étude et développement pluri-annuels dont le financement est partiellement assuré par la DRET (Direction des Recherches, Etudes et Techniques).

Les spécifications techniques objectives adoptées en début de développement (1984) étaient assez ambitieuses. Avec le modèle d'erreur suivant :

$$\frac{\Delta\gamma_E}{\Gamma} = K_0 + \frac{\Delta K_1}{K_1}\frac{\gamma_E}{\Gamma} + K_2\left(\frac{\gamma_E}{\Gamma}\right)^2 + K_1\frac{\gamma_1}{\Gamma} + K_3\frac{\gamma_3}{\Gamma} + \varepsilon_0$$

où

Γ = domaine de mesure,
γ_E = accélération selon l'axe d'entrée,
K_0 = erreur de zéro,

$\frac{\Delta K_1}{K_1}$ = erreur de facteur d'échelle,

K_2 = coefficient de non linéarité quadratique,
K_1, K_3 = coefficients de sensibilité aux accélérations dans le plan transverse,
ε_0 = résidu de modélisation,

les coefficients avaient pour bornes :

Coefficient	Valeur maximale entre -40°C et +80°C
$\lvert K_0\rvert$	10^{-4}
$\lvert\Delta K_1 / K_1\rvert$	10^{-4}
$\lvert K_2\rvert$	10^{-3}
$\lvert K_1\rvert$ et $\lvert K_3\rvert$	10^{-3}
$\lvert\varepsilon_0\rvert$	10^{-5}
Γ	$> 1000\ m/s^2$

La bande passante utile devrait être supérieure ou égale à 100 Hz, et le capteur capable de résister à des ambiances vibratoires assez sévères (15 G crête en vibrations sinus, 30 G efficaces en vibrations aléatoires).

Ces spécifications situaient le capteur à concevoir au niveau des capteurs de prix moyen sur le marché des accéléromètres. Deux autres caractéristiques objectives en constituaient l'originalité :

1) une possibilité de fabrication collective permettant un prix nettement inférieur au prix du marché pour les séries importantes,
2) un volume total inférieur à 2 cm3, permettant à l'utilisateur une intégration extrême.

Ces spécifications ambitieuses ont été utilisées chaque fois que possible pour dimensionner les structures sensibles de l'AQM.

Début 1988, le processus de fabrication mis au point par le CEA/D. LETI est maîtrisé. Des investissements sont réalisés à l'établissement de la SFENA à Châtellerault. Ils vont permettre d'y effectuer le cycle complet de fabrication. Les études d'industrialisation, devant permettre de contrôler au mieux le prix du capteur en phase de production en série, sont menées parallèlement à cette mise en place progressive des moyens matériels.

Ajoutons, avant de décrire plus précisément ces structure et les résultats de mesure obtenus, que leur constitution fait l'objet de plusieurs depôts de brevets avec additions, en France et à l'étranger, tant par le CEA/D. LETI que par la SFENA.

2. CONCEPTION MECANIQUE

Les structures sensibles que nous utilisons sont usinées collectivement dans un substrat plan monocristallin de quartz. On n'utilise pas les propriétés piezo électriques bien connues de celui-ci, mais plutôt que le fait qu'il s'agit d'un matériau isolant usinable par voie humide. De plus, il a fait l'objet d'études théoriques et expérimentales très importantes et sa disponibilité industrielle est assurée. (cf [1] et [2]).

La lame cristalline utilisée mesure 150 à 300 µm d'épaisseur ; l'usinage comprend de multiples étapes : dépôts sous vide, masquages, insolations, dépôts électrolytiques, attaques chimiques cf. [3]. Le nombre de structures de détection par substrat est passé progressivement de 4 en début de développement à 20 sur les derniers jeux de masques réalisés.

La structure - type comprend une masse sensible mobile, suspendue par deux lames parallèles situées de part et d'autre (cf figure 1-a). La masse suspendue est de l'ordre du milligramme ; les lames de suspension mesurent 5 à 7 µm de large et 2 à 3 mm de long.

Sous l'effet d'une accélération parallèle au lames de suspension ou perpendiculaire au plan du substrat, la masse mobile ne se déplace pratiquement pas, compte tenu des raideurs effectives réalisées par le système de suspension. Par contre, une accélération parallèle au plan du substrat et perpendiculaire aux lames de suspension provoque une flexion en S de ces lames et un déplacement de la masse sensible (cf figure 1-b). Il est clair qu'on peut alors mesurer cette accélération soit en mesurant le déplacement relatif de la masse mobile (le rappel des lames étant élastique) soit en mesurant la force nécessaire pour l'annuler.

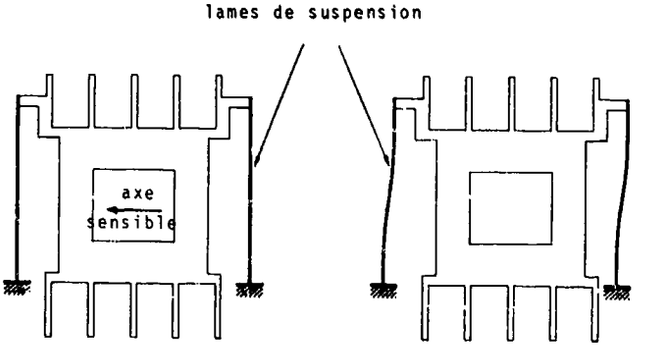

1-a 1-b

Figure 1 Constitution de la masse sensible

1-a au repos

1-b sous accélération, hors asservissement

Un tel dispositif possède des avantages fonctionnels certains :

1) La position relative de la masse sensible dépend d'un équilibre de forces plutôt que d'un équilibre de couples. En effet, les couples agissant perpendiculairement au plan du substrat (direction équivalente à celle de l'axe charnière des accéléromètres pendulaires classiques) sont équilibrés par des efforts de traction/compression dirigés le long des lames de suspension. Ceci implique une sensibilité nominalement nulle aux effets d'anisoinertie et à l'accélération angulaire autour de l'axe charnière.

2) La structure sensible ayant une excellente planéité, on peut positionner les pièces voisines à proximité immédiate (quelques µ-m ou quelques dizaines de µ-m) lorsque c'est nécessaire. Cette possibilité est intéressante, soit pour des pièces de circuit magnétique (bonne concentration du flux magnétique et bonne dissipation thermique) soit pour créer des butées (bonne résistance aux fortes accélérations transverses et aux chocs).

3) Les organes de détection de position associés à la masse mobile (peignes capacitifs) créent un amortissement gazeux du mouvement que l'on peut moduler dans une certaine mesure en agissant sur les paramètres géométriques de l'ensemble (nombre de dents, valeur des jeux, proximité latérale des autres pièces...).

4) Lorsqu'on utilise la structure en mode asservi, la force de rappel doit équilibrer la totalité de la force d'inertie, ce qui élimine les erreurs dues au pivotage rencontrées sur certains accéléromètres de conception classique, particulièrement pour les grands domaines de mesure.

5) La structure elle-même ne fait appel à aucun ingrédient organique (colles, isolants..) ce qui lui donne les meilleures chances de fonctionner correctement à haute température.

6) Malgré un volume extrêmement réduit, une telle structure peut présenter de très bonne références géométriques et un positionnement correct de l'axe sensible par rapport au boîtier.

7) Il est en principe possible de graver deux structures orientées différemment sur le même substrat, ce qui réduit le coût et le volume global tout en améliorant le calage relatif lorsqu'on a besoin d'un capteur "2 axes".

3. UTILISATION DES STRUCTURES EN ACCELEROMETRE

3.1. Accéléromètre électromagnétique asservi

Pour cette utilisation, le moteur est constitué de conducteurs en spirale déposés sur chaque face, éventuellement épaissis par un procédé électrolytique. Le courant arrive par les deux flancs d'une lame de flexion, et repart par les deux flancs de l'autre lame de flexion. Le circuit magnétique est constitué comme l'indique la figure 2 et le système de détection de position est capacitif. La figure 3 donne un exemple de système de détection, et le circuit électrique équivalent.

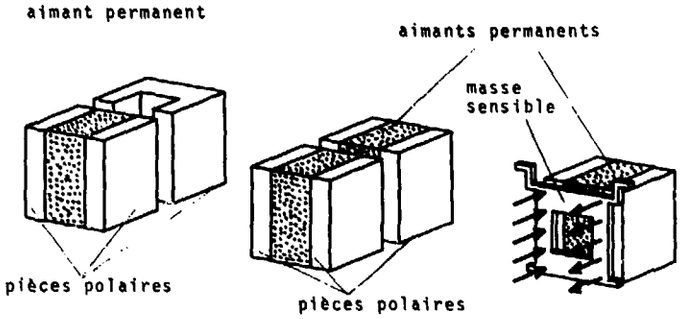

2-a 2-b 2-c

Figure 2 Circuits magnétiques

2-a et 2-b : deux réalisations possibles

2-c : position de la masse sensible par rapport au circuit magnétique et orientation de l'induction utile par rapport au substrat.

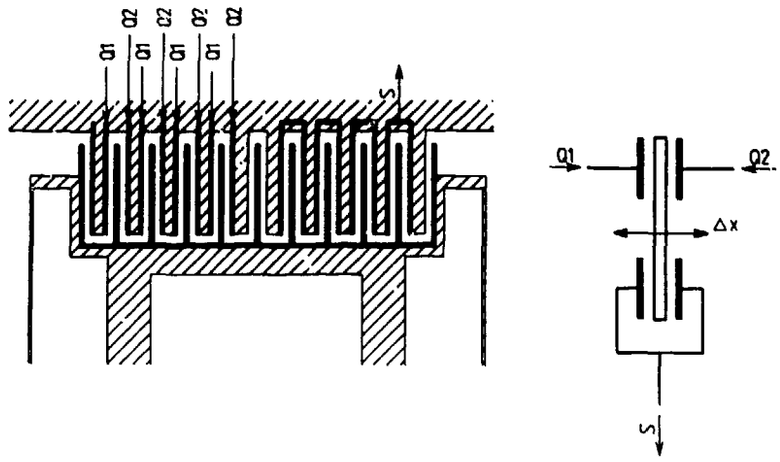

Figure 3 Système de détection de position et schéma électrique équivalent

Les signaux Q1 et Q2 sont deux signaux alternatifs en opposition de phase. La surface métallisée portée par la masse mobile est à un potentiel flottant (fonction du déplacement Δx).

Notons au passage que le moteur de rappel représenté en détail fig.4, fournit en principe une force de rappel proportionnelle au courant le traversant (pas d'erreur quadratique due au déplacement du point de fonctionnement du circuit magnétique ou à une variation de reluctance des bobines avec la position de la masse sensible).

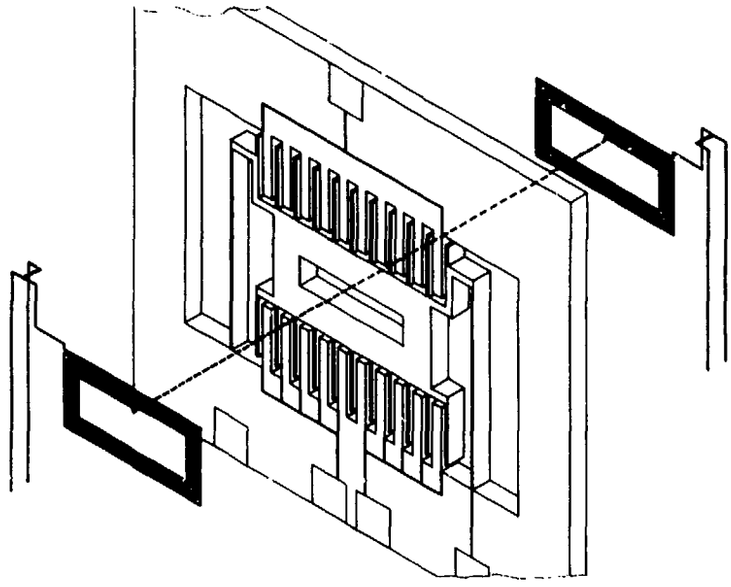

Figure 4 Spires du moteur de rappel

Ces spires sont représentées décollées de la masse sensible pour la compréhension de leur cheminement.

La figure 5 montre la structure de la chaîne d'asservissement en position de la masse sensible et le principe physique de la mesure (mesure du courant de rappel). D'autres architectures (conversion courant --> fréquence, digitalisation dans la boucle, etc...) sont utilisées sur d'autres capteurs fabriqués par la SFENA et seront adaptés à l'AQM lorsque le besoin s'en fera sentir.

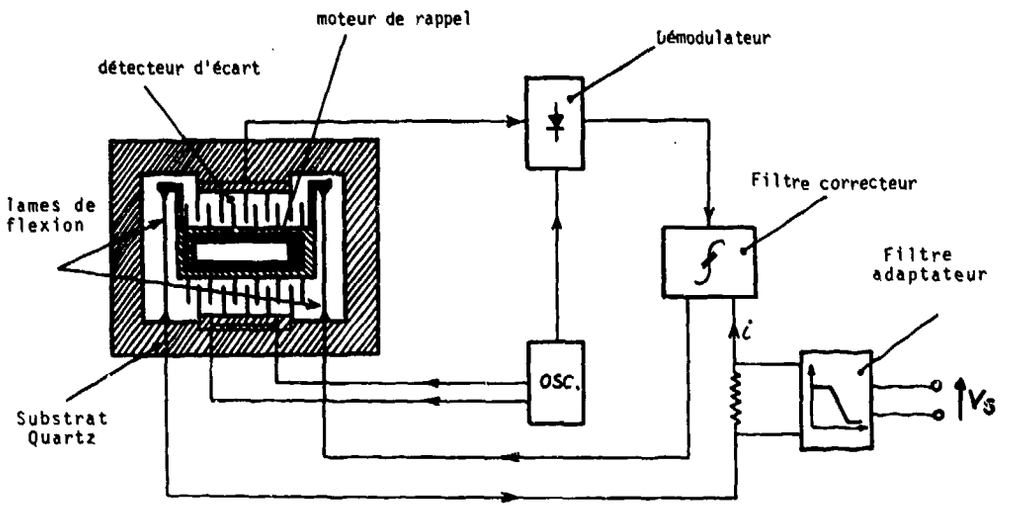

Figure 5

Architecture de la chaîne d'asservissement

du micro-accéléromètre AQM électro magnétique asservi

La figure 6 montre comment la maquette de développement a été intégrée dans un volume global de 2 cm3. Ceci comprend la structure sensible, le circuit magnétique associé et l'électronique d'adaptation d'impédance, le bouclage se faisant actuellement par un circuit hors capteur. On estime que l'intégration complète de l'électronique d'asservissement nécessitera 0,5 à 1 cm3 supplémentaire.

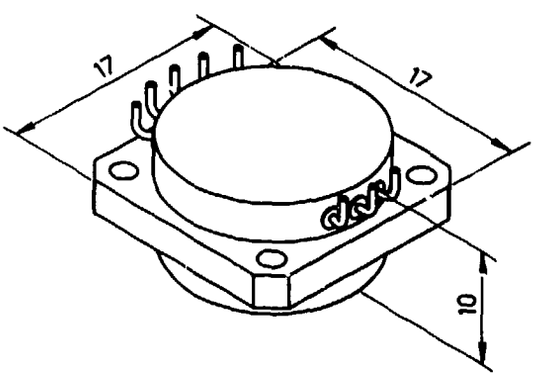

Figure 6

Dimensions extérieures des maquettes fonctionnelles

Le boîtier est hermétique et électriquement isolé du plan de pose. Il contient la structure sensible, le circuit magnétique et l'électronique d'adaptation d'impédance.

Le tableau ci-dessous présente les performances actuelles AQM, après réglage et calibration mais hors tri.

Domaine de mesure	± 100 G
Bande passante utile	⩾ 100 Hz
Biais brut	0,1 G
Facteur d'échelle	⩽ 0,15 mA/G
Dérive de biais en température (-40°C à +80°C)	⩽ 0,01 G
Dérive de facteur d'échelle en température (-40°C à +80°C)	⩽ 0,6 %
Dérive de l'axe sensible (-40°C à +80°C)	⩽ 0,5 mrd
Tenue aux chocs (hors fonctionnement)	100 G/11ms
Tenue aux vibrations sinus (en fonctionnement)	15 G
Tenue aux vibrations aléatoires (en fonctionnement)	30 G RMS (50-2000 Hz)

Ces performances sont assez proches des performances objectives. Elles permettent dès à présent, d'envisager l'utilisation de l'accéléromètre AQM asservi pour les besoins de pilotage/stabilisation des missiles guidés à courte portée.
Des améliorations issues de la maîtrise du processus sont d'ailleurs encore probables en ce qui concerne la dérive de biais et l'hystérisis thermique, étant donné que ces termes d'erreur décroissent de façon ininterrompue depuis l'époque des toutes premières réalisations de structures. Des applications plus ambitieuses ne sont donc pas à éliminer à l'heure actuelle.

3.2. Accéléromètre sans circuit magnétique

Un tel accéléromètre n'a pas besoin de spires métalliques parcourues par un courant. A masse suspendue égale, on peut donc réaliser un bien plus grand nombre de dents sur les peignes de détection et de la sorte obtenir une meilleure sensibilité et un meilleur amortissement du mouvement relatif de la masse sensible. L'absence de circuit magnétique diminue le coût et le volume global par rapport à la version à rappel électromagnétique.

La figure 7 représente une structure de détection comportant un grand nombre de dents constituant des capacités de détection à surface variable.

Des capacités de détection à entrefer variable auraient aussi bien pu être dessinées.

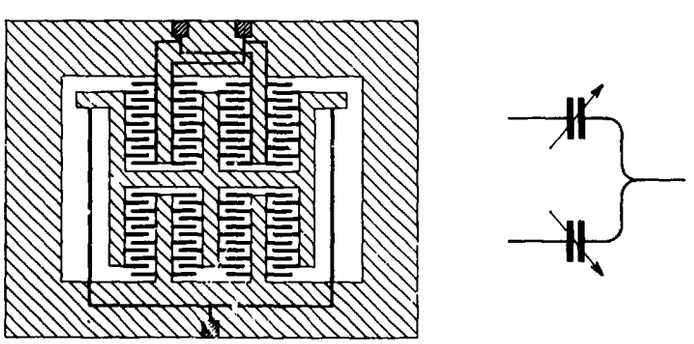

Figure 7

Structure de détection capacitive

à variation de surface et schéma électrique équivalent

De telles structures peuvent fonctionner en mode asservi en appliquant des tensions élevées aux surfaces en regard, pour créer des forces de rappel électrostatiques, ou en mode non asservi en mesurant les variations de capacité au moyen de tensions alternatives de quelques volts d'amplitude, créant des forces de rappel négligeables, voire nulles.

Une application remarquable des propriétés mécaniques de ces structures a été faite dans un montage en sandwich (fig.8) entrant dans un boîtier métallique (fig.9). Le capteur ainsi créé fonctionne en boucle ouverte avec une électronique de servitude située dans un boîtier annexe.

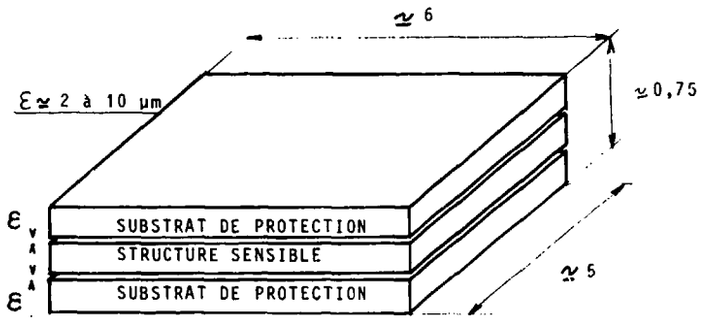

Figure 8

Montage en sandwich d'une structure sensible

(Dimensions en mm)

Des substrats de protection, également en quartz, offrent une protection mécanique et électrique (métallisation externe) à la structure sensible. Ils sont fabriqués par les mêmes procédés que la structure sensible.

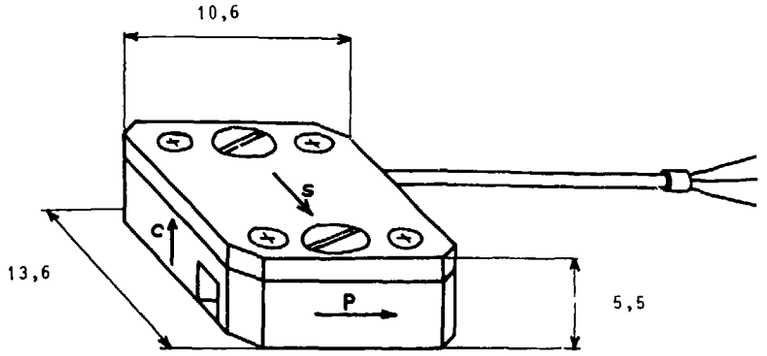

Figure 9

Boîtier d'essai (cotes en mm)

Ce boîtier contient la structure en sandwich de la figure 8 et les connexions électriques nécessaires.

Plusieurs de ces boîtiers ont été fixés dans des obus de mortier qui ont été tirés avec des charges leur donnant des accélérations initiales de 10 000, 15 000, puis 20 000 G. A l'issue de cette série de tirs, 80 % des structures ont montré des valeurs de biais et de facteur d'échelle différant de moins de 1 % des valeurs avant tir. Les 20 % restant ont subi des fractures mineures dues à un défaut de conception localisé (aucune des lames de suspension ne s'est rompue).

Les performances obtenues avec ces structures en mode non asservi nous permettent d'envisager les spécifications suivantes pour le modèle "série" de ce type de capteur.

. Domaine de mesure Γ ..... $\pm$ 20 G

. Bande passante utile ..... $\geq$ 100 Hz

. Biais brut ..... 0,1 G

. Erreur de linéarité sur le domaine de mesure ..... 2 %

. Dérive de biais (-40°C à +80°C) ..... $5.10^{-3} \times \Gamma$

. Stabilité de facteur d'échelle.(-40°C à +80°C) ..... 3 %

. Tenue aux chocs ..... 20 000 G , 5 ms

Ces chiffres, compte tenu d'un volume objectif de l'ordre de 2 cm3 et d'un coût minimal pour des séries importantes font de l'AQM non asservi un candidat prometteur pour les applications du type munition à guidage terminal, où un volume réduit et une excellente tenue aux chocs sont primordiaux.

4. CONCLUSION

Les structures de détection accélérométrique développées par la SFENA en coopération avec le CEA/D.LETI sont susceptibles de satisfaire un grand nombre de besoins, et en particulier ceux des concepteurs de missiles guidés à courte portée et de munitions à trajectoire corrigée. L'étude d'industrialisation en cours permettra de situer plus précisémment les coûts de ces appareils. Une de leurs caractéristiques essentielle est leur capacité à être produit collectivement de façon fiable et répétitive : les spécifications techniques ont donc toutes les chances d'être satisfaites au meilleur prix.

5. REFERENCES

1 B. DULMET
LCP - ENSMM - Besançon - France
Valeurs numériques des constantes physiques du quartz
Novembre 1980

2 V.E. BOTTOM
Introduction to quartz crystal unit design - 1982 .
Van Nostrand Reinhold Electrical/Computer Science and Engineering Design.

3 P. PARRENS
CEA/LETI Grenoble - France
Note technique LETI/MSC n°1419 : Etat de l'art en lithographie
Février 1982

6. REMERCIEMENTS

Nous remercions la DRET pour le support assuré lors de la phase d'étude/développement de cet accéléromètre, ainsi que Madame MICHEL et Messieurs DELAPIERRE et DANEL, du CEA/D.LETI pour la qualité et la créativité de leur travail durant toute la durée de cette coopération SFENA/CEA/D.LETI.

Packaged Fiber Optic Gyros

H.-J. Büschelberger, W. Schröder
LITEF (Litton Technische Werke) GmbH,
D-7800 Freiburg, Lörracher Straße 18, West Germany

Summary

LITEF is developing a family of different Fiber Optic Gyroscopes (FOG) for different applications. The main program is the development of a FOG with a drift stability of 0.1 °/h, which is the class for strapdown attitude and heading reference systems (AHRS). The status of the accuracy meets their requirements. Flight tests with a LTR-81, LITEF's standard AHRS, are scheduled for the end of 1988.

The requirements of guided munitions to the accuracy of the gyro are much less. But the instrument has to be ruggedized to survive the initial shock. The second task is the miniaturization of the gyro and its electronics.

This paper gives an overview of the FOG-AHRS program and outlook to the FOG for Smart Munitions.

Introduction

The international APGM-program and different national programs force the development of inertial sensors for this application. In contrast to the AHRS-class these gyros have to meet a quite different specification. The sensor drift error and the scale factor linearity are not the drivers but the capability of the instrument to withstand the high g-load during launching.

Over its mechanical competitors the FOG has the big advantage of having no moving parts. So to say it seems to be the ideal candidate for this application. The dimensions have to be miniaturized to fit into the compartment in the shell. The packaging of its components has to be done with respect to the expected accelerations. The accuracy of a fiber optic gyro is related to its size. The formulas in the first chapter of this paper show the relations between the rotation rate and the sensor signal. The sensitivity is proportional to the fiber length and the coil radius. Reduction of the dimensions does not only affect the sensitivity but also the noise level. Scaling the appropriate values from the today achieved numbers shows that the requirements can be met with low risk.

The mission profile of a guided weapon requires a gyro drift stability in the order of 100 - 500 °/h. The linearity of the scale factor has to be within 1 %. The outer diameter of the sensor coil in this development program is chosen to 30 mm. As in the AHRS-FOG the sensor module and opto module are in separated housings. Three of the sensor modules can be put together to form a sensor triade, which is equipped with one opto module. This concept saves parts and space.

Basic Relationships of an Interferometer Gyro

The Sagnac effect in the fiber optic gyro causes a phase shift in the sensor coil during rotation with rate Ω relative to inertial space: [1-3]

$$\phi_S = 4 \frac{L \cdot R}{\lambda \cdot c} \cdot \Omega = \Omega / SF$$

L = fiber length
R = radius of fiber coil
λ = source wavelength
SF = scale factor

A Sagnac interferometer converts this phase shift into an output light intensity variation.

The transfer function of a fiber gyro with an unsymmetrically located phase shifter is:

$$I(t) \sim I_o \cdot (1 + \cos(\phi_S + \phi(t) - \phi(t-\tau)))$$

I = intensity on detector
ϕ_S = Sagnac phase shift
$\phi(t)$ = phase modulator phase
τ = fiber coil round trip time

Due to the delay time of τ which the light needs to travel through the sensor coil, the clockwise and counter-clockwise light beams which interfere at the main coupler pass the modulator at different times.

Assuming linear detector response and a linear phase modulator with high bandwidth (which is a good approximation for a $LiNbO_3$ phase modulator), the gyro transfer function is:

$$U_{out}(t) = U_o\,(1 + \cos(SF\cdot\Omega + K(U(t)) - U(t-\tau)))$$

with

$$\phi(t) = K \cdot U(t)$$

K = phase modulator scale factor

In contrast to a mechanical gyro, no integrating term arises. When the gyro is excited with a sinusoidal $U(t) = U \cdot \sin \omega t$, the output amplitudes of first ($U_{1\omega}$) and second ($U_{2\omega}$) harmonics are:

$$U_{1\omega} = 2U_o \cdot \sin(SF\cdot\Omega) \cdot I_1\,(2\cdot \sin\tfrac{\omega\cdot\tau}{2})$$

$$U_{2\omega} = 2U_o \cdot \cos(SF\cdot\Omega) \cdot I_2\,(2\cdot U\cdot K\cdot \sin\tfrac{\omega\cdot\tau}{2})$$

Modulation of the gyro improves sensitivity by use of a demodulator, the output of an unmodulated gyro being very insensitive to rotation at low rates.

The effect of other modulation schemes can be calculated by Fourier series expansions (or visualized by simple drawings). For example, a rectangular modulation is quite useful.

Closed-loop gyro operation can be implemented by letting

$$SF \cdot \Omega + K(U(t) - U(t-\tau)) = n\pi \quad (N \varepsilon Z)$$

from which follows

$$\Omega = \frac{K}{SF}\,(U(t) - U(t-\tau)) - \frac{n\pi}{SF}$$

Any function U(t) which satisfies this equation (for instance ramp or staircase) can be used to restore the gyro.

In contrast to the open-loop approach which gives nonlinear (trigonometric) gyro scale factor behaviour, a closed-loop scheme offers the advantage of a linear scale factor and higher scale factor repeatability.

Fiber Optic Gyro K-2010

The gyro optics are built using the standard interferometer approach [4] and comprising two parts (Fig.1).

The opto module contains: The light source (a pigtailed temperature-stabilized superluminescent diode), a read-out coupler and an avalanche photodiode for optical detection. The opto module is rigidly connected with the sensor module via a fiber link which feeds light into the sensor module and also guides light back to the detector. The sensor module contains a thermally symmetric, wound [5] and potted sensor coil using 500 m of polarization maintaining fiber, an integrated optics phase shifter, a main coupler, and a polarizer. The sensor module housing is made of μ-metal and is gas-tight. A temperature sensor is built into the sensor module. All modules are assembled at LITEF from the basic components (laser diode chip on heatsink, Peltier cooler, avalanche diode, PM-fiber, integrated optic chip, etc.). Fig. 2 shows a photograph of the completed gyro.

The opto module dissipates about 250 mW for light source operation, and in addition 400 mW (2 W) for diode temperature stabilization at 20 ° C (60 ° C respectively) environmental temperature. The gyro excitation phase modulator needs less than 1 mW so that the sensor module does not generate heat. This gyro layout approach has, despite its unfamiliar look, the advantage that, due to the "remote" heat dissipation, no switch-on drifts are expected. The temperature influence of the Peltier cooler on the gyro coil, as well as electromagnetic interference problems, are avoided. Also, good heat removal from the Peltier element is provided if the opto module is mounted on one of the outer walls of the system box.

Test Results

Several similar gyros with this design were built and tested, especially for bias stability over temperature. During test the gyro is mounted in an east-west direction in an environmental chamber where the temperature is set between 10 ° C and 60 ° C. The gyro is excitated with a square wave excitation of 205 kHz and an amplitude of typically 1 V. The amplified avalanche diode signal is demodulated with a commercial lock-in detector. The scale factor is calibrated by observing the change in output signal after rotating the gyro's input axis from the east-west to the north-south direction. Typically several temperature cycles were performed (Fig. 3), from which the bias repeatability was calculated. Random noise measurements were performed by recording the output signal with a 3-secs.-integration time and subsequently forming the RMS value. Data measured are shown in Tab. I.

Generally, the absolute bias is low (< 0.5 °/h), as in general should be the case for a reciprocal design and correctly assembled optics. In our case, a linear temperature model

is sufficient for 0.1 °/h gyro accuracy (Fig. 4).

For scale factor versus temperature evaluation the gyro was rotated on a rate table in an environmental chamber at different temperatures. To overcome the influence of the gyro electronics on scale factor, the change with temperature of the zero crossing of the 2nd harmonic at about 110 °/sec. (sinusoidal excitation) was used to measure the change of the geometric scale factor (Fig. 5) (see "Basic Relationships of an Interferometer Gyro"). The light source temperature was held constant to ensure a constant wave length.

Due to measurement accuracy limitations it may only be stated that the scale factor repeatability is better than 1000 ppm and the scale factor versus temperature sensitivity is less than 100 ppm/° C.

To investigate vibrational sensitivity, one gyro was mounted on a vibration table and was vibrated in operation with a 4 g sinusoidal acceleration between 40 - 3000 Hz. Dominant resonances occurred above 2000 Hz. From 40 Hz to 500 Hz, no change in bias due to vibration with a measurement accuracy of 0.3 °/h was observed. Theoretically, the interferometer has no rectification terms due to vibration; however, non-linearities in the demodulator electronics give rise to signal rectification and an apparent bias shift for high rotational vibration amplitudes occurring due to resonances (10 - 50 °/sec. peaks).

The magnetic sensitivity of the unshielded fiber coil is about 2 °/h/G, the packaged gyro has a sensitivity of 0.015 °/h/G.

The change in input axis alignment versus temperature was measured by rotating the gyro in the two axis orthogonal to the input axis. The change is typically 2 arcsecs/° C; Fig. 6 shows data for the two axes of one gyro. There is no sign of a g-sensitivity of the gyro bias, although the alignment may be slightly sensitive to acceleration.

Tab. II summarizes the measured data. The performance of the current gyro optics performance is sufficient for attitude and heading reference applications.

Electronics

Almost all known gyro-operating schemes can be used for the K-2010, due to the high bandwidth of the phase modulator and the linearity of the detector output. We prefer a closed-loop scheme, the electronics of which are currently under test with a K-2010 fiber gyro. In contrast to a mechanical gyro, the gyro bandwidth is very high (dead time 2.5 µs), which simplifies the loop electronics.

Acknowledgement

The work described in this paper is partly supported by the German Ministry of Research and Technology. The authors alone are responsible for the content.

References

[1]) P. Gröllmann, J. Herth, M. Kemmler, K. Kempf, G. Neumann, S. Oster, W. Schröder
"Passive Fiber Resonator Gyro"
1986, DGON

[2]) W. Schröder
"Entwicklung eines faseroptischen passiven Resonator-Kreisels für die Luftfahrt"
BMFT-FB (LFL 8473 5)

[3]) W. Schröder
"Kurs/Lage-Referenzsystem mit Faserkreiseln"
BMFT FB (LFL 8671 8)

[4]) R. Ulrich
"Fiber Optic Rotation Sensing with low Drift"
Opt. Lett. 5, p. 173 - 175, 1980

[5]) D.M. Shupe
"Thermally induced Nonreciprocity in the Fiber Optic Interferometer"
Appl. Opt. 19, p. 654, 1980

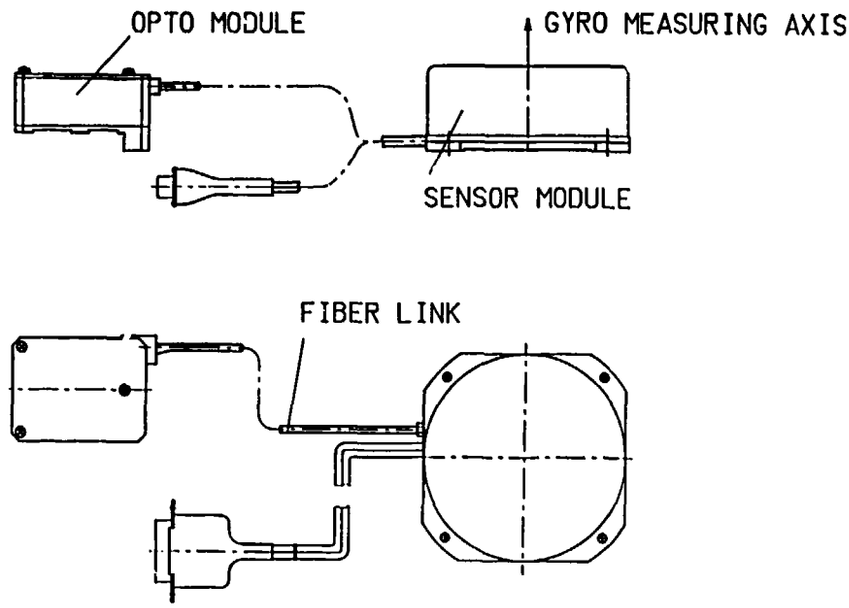

Fig. 1: Outline drawing of fiber optic interferometer gyro K-2010

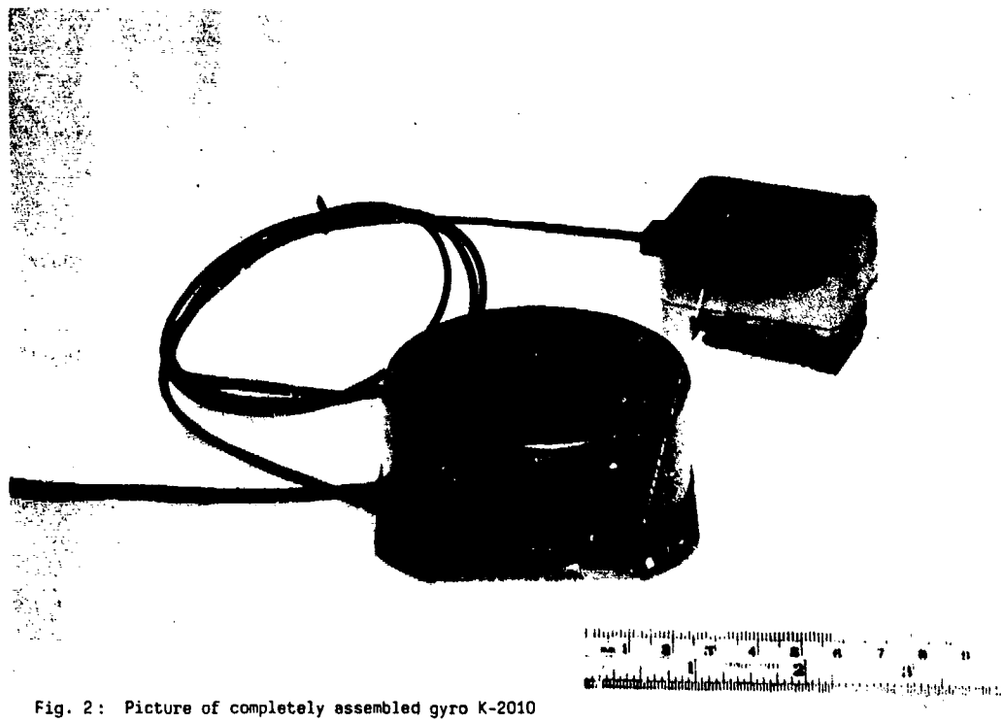

Fig. 2: Picture of completely assembled gyro K-2010

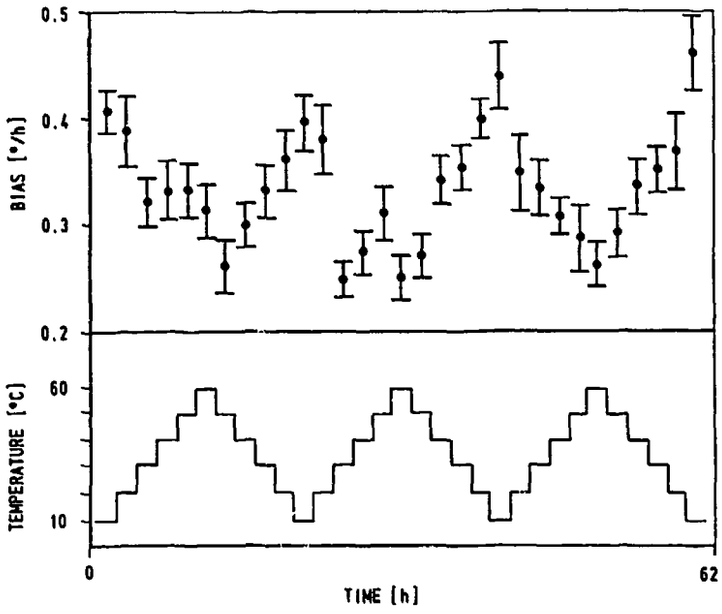

Fig. 3: Temperature changes in environmental chamber over 62 hours and associated bias change of gyro K-2010 #3. The gyro was operated open-loop with square-wave excitation.

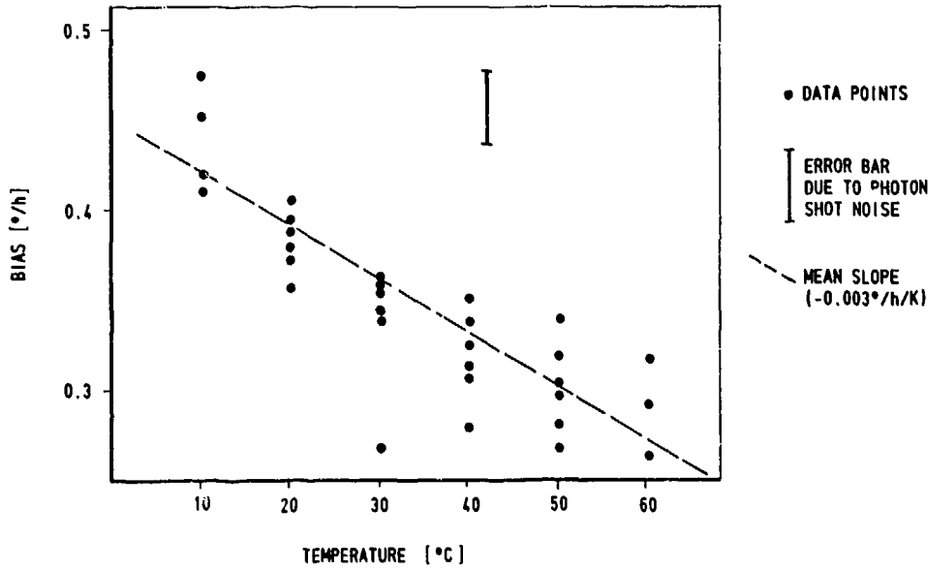

Fig. 4: Bias versus temperature of K-2010 #3

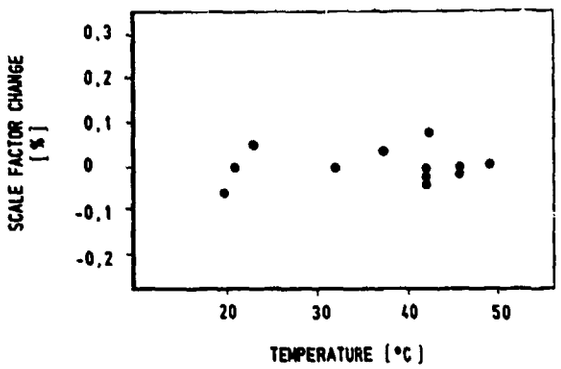

Fig. 5: Scale factor versus temperature

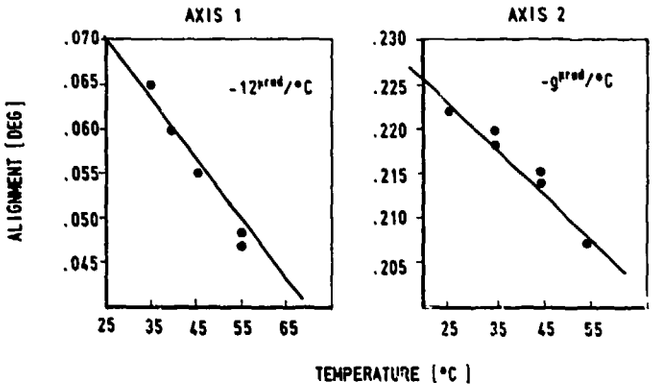

Fig. 6: Alignment versus temperature for the two axes orthogonal to the input axis

K - 2010 Measured Data

	Gyro	# 1	# 2	# 3
Bias Absolute	(°/ h)	0.2	0.4	0.4
Bias Rep. (1σ , 20°C)	(°/ h)	0.06	0.13	0.03
Random Walk	(°/ $\sqrt{h}$)	0.017	0.034	0.03
Δ Bias / Temperature	(°/ h / k)	$5 \cdot 10^{-3}$	$8 \cdot 10^{-3}$	$3 \cdot 10^{-3}$

TABLE I

K - 2010 Performance Data

Bias Absolute	< 0.5 °/ h
Bias Rep. (1σ , 20°C)	< 0.2 °/ h
Random Walk	< 0.04 °/ $\sqrt{h}$
Δ Bias / Temperature	< $8 \cdot 10^{-3}$ °/ h / K
Magnetic Sensitivity	< 0.02 °/ h / G
Alignment / Temperature	< 15 μrad / K
Scale Factor Rep (1σ ,20°C)	< 0.1 %
Scale Factor / Temperature	< 0.01 % / K
Bias Change (Operating)	
During Vibration (4g, 40Hz - 500Hz)	< 0.3 °/ h

TABLE II

DEMONSTRATION OF FOG-M CAPABILITIES BY MEANS OF SIMULATION AND EFFECTS OF PROPRIOCEPTIVE FEEDBACK ON THE CONTROL

B. J. Damen
Prins Maurits laboratory TNO (PML)
P.O. Box 45
2280AA Rijswijk
the Netherlands

R.N.H.W. van Gent & H. Schuffel
Institute for Perception TNO (IZF)
P.O. Box 23
3767ZG Soesterberg
the Netherlands

SUMMARY

This paper consists of two parts. The first part, for which the Prins Maurits laboratory is responsible, describes a simulated scenario with the Fibre Optic Guided Missile (FOG-M) with the aid of a 6 degree of freedom simulation model for investigating manoeuvrability and footprint areas against both stationary and moving ground targets. Also the performance against moving helicopters was investigated. Some conclusions are made as far as manouevrability and seeker field of view concerns.

The second part, for which the Institute for Perception is responsible, describes a simulator built for research on the FOG-M system including man-in-the-loop control. Demonstration studies indicated some possible problem areas, such as the manual control characteristics. A study was started concerning which type of joystick-system would enhance performance of persons with minimal experience. A first experiment examined the proprioceptive feedback effect on the control of FOG-M. It showed that providing the operator with proprioceptive feedback on the manoeuvrability would enhance control performance.

PART 1

1. OVERVIEW

One of the new anti-tank guided weapons in the 10 km range is the FOG-M, which stands for Fibre Optic Guided Missile.

The principle of fibre optic guidance is that the missile is equipped with a camera in the nose which relays the video data by means of an optic fibre to the operator. See Figure 1 for a generic concept.

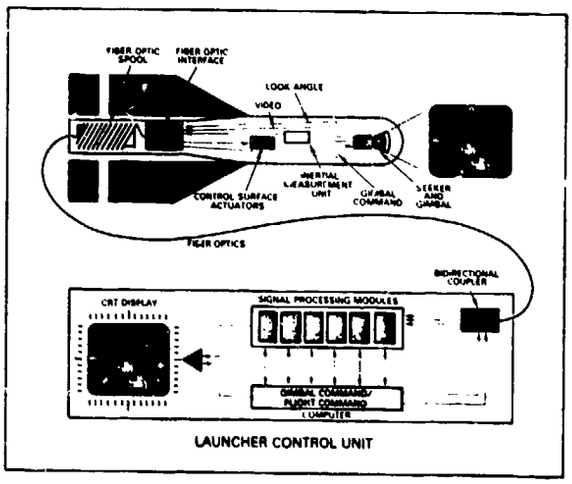

Figure 1. Generic concept of FOG-M.

The operator, who receives the data on a television screen, then steers the missile by means of a joystick. These steering commands are transferred back to the missile through the optic fibre. An example of how this concept would work when operational is shown in Figure 2.

Figure 2. An operational concept of FOG-M.

The operator sits in a vehicle equipped with one or two work stations on which the video pictures are displayed. Also there is a batch of missiles in a trailer or in another vehicle. Both the operator and the missiles can be hidden at some distance from the battle area in order to reduce vulnerability to enemy fire. At some moment an array of targets is spotted by a forward observer or by other means and the operator launches one or more missiles in the direction as indicated. The flight towards the target area can be by autopilots with altitude hold, or via waypoints or other means to relieve operator tasks. Cross-winds and unfamiliarity with the terrain can be high load factors to the operator. Because of target speed and observation delay time, the missile should fly as fast as possible towards the designated area. On arrival of the missile in this area the operator starts searching for targets.

Search altitude, missile speed, camera depression angle, zoom capability and a daylight or an IR camera are all variables which influence the search process. Once the operator finds a target, he locks the camera on the target, making it possible for the missile to execute a top-attack on the target by means of autotrack.

2. FOG-M CONFIGURATION

For the purpose of simulation and investigation of a Fibre Optic Guided Missile, the FOG-M configuration of U.S. Army MIssile COMmand was chosen, shown in Figure 3.

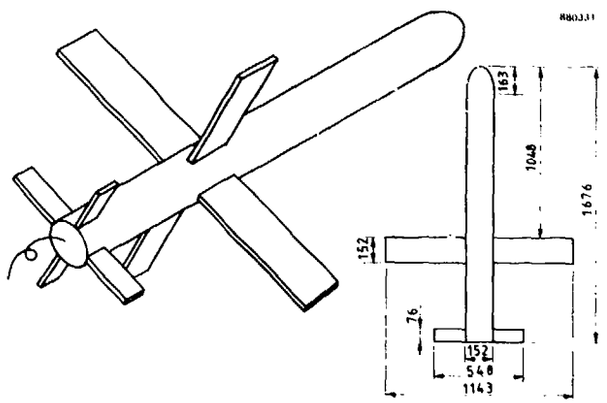

Figure 3. FOG-M configuration.

The four wings and the four tail fins are deployed after launch. An optic fibre payout is mounted on the rear with a fibre length of about 10 km. The nose houses the IR or daylight camera. Performance parameters such as thrust levels, speeds and operating heights were investigated as part of this study.

3. THE SIMULATION MODEL

On the basis of this configuration a trajectory simulation model for the FOG-M was developed. It is a 6 Degrees Of Freedom model (6 DOF) , a picture of which is presented in Figure 4.

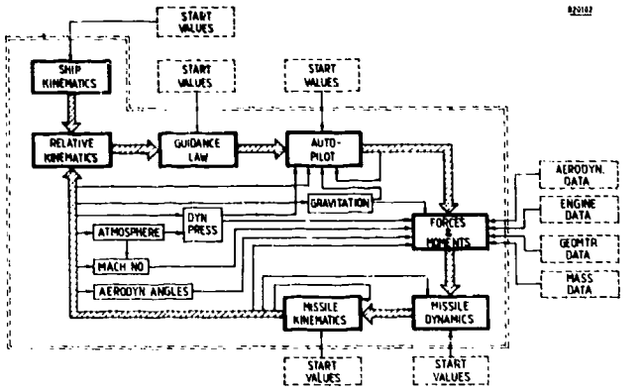

Figure 4. 6 DOF simulation model.

The main inputs to be determined for this model are the aerodynamic and the guidance module. The aerodynamics were determined from the geometric configuration of the FOG-M graph and are given in table 1. With this data an autopilot was designed.

FOG-M AERODYNAMIC COEFFICIENTS			
C_{Z_α}	= -62.0	$C_{M_{\delta_p}}$	= 127.2
C_{M_α}	= -129.0	$C_{Y_{\delta_r}}$	= -24.0
C_{Y_β}	= -62.0	$C_{N_{\delta_r}}$	= 127.2
C_{N_β}	= 129.0	$C_{L_{\delta_a}}$	= 21.8
$C_{Z_{\delta_p}}$	= 24.0	C_X	= -0.3

Table 1. The aerodynamic data of the FOG-M.

It is a Skid To Turn autopilot with proportional navigation guidance. The search phase uses an altitude autopilot and the autotrack phase an feedback of acceleration. The FOG-M flies with a roll attitude of 45 degrees. The autopilots are shown in Figure 5.

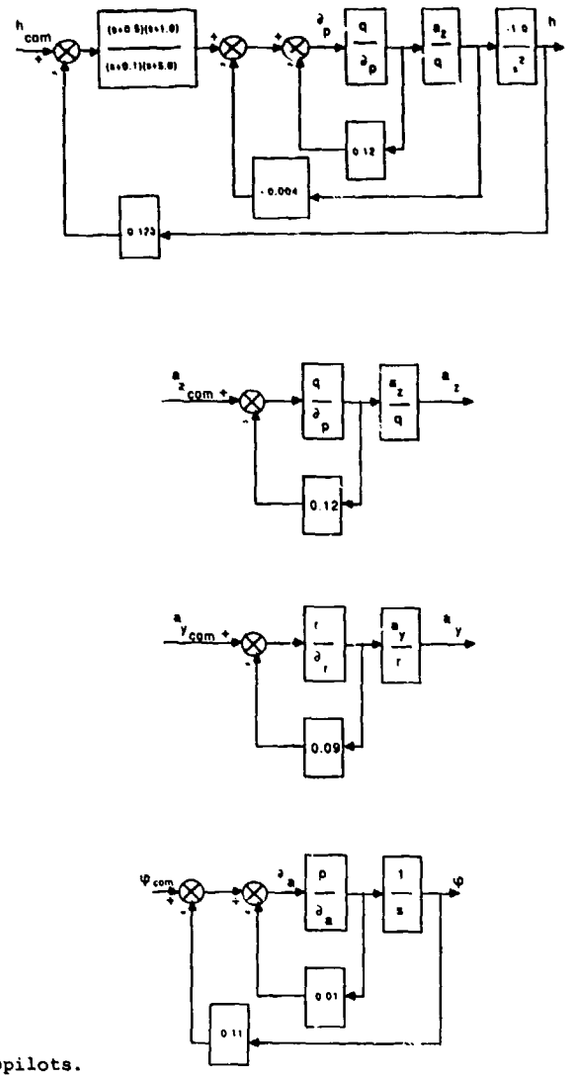

Figure 5. The autopilots.

With the estimated aerodynamics and the autopilot the 6 DOF model is completed.

The principle of the model is as follows. From the motion of the missile and the target the relative motion is calculated. A second-order differential equation seeker model with a 50 Hz frequency update rate then converts this movement into two line of sight (LOS) rates. These are the LOS rates in pitch and yaw in body axes coordinates. The autopilot then computes the pitch, yaw and roll rudder deflections from these LOS rates. These rudder deflections, together with gravity, aerodynamics and missile dynamics result in the new missile kinematics and the loop is closed.

Some limits were imposed on the model, such as angle of attack less than 15 degrees and a g-limiter of 3 g with a rudder limit of 15 degrees.
The video camera in the nose is not limited in its movement or depression angle for the purpose of this simulation. A tentative model uses 15 degrees depression angle and a zoom capability of 4 to 16 degrees.

4. MANOEUVRABILITY OF FOG-M

For the search phase some flight characteristics of the FOG-M were investigated, such as turn capability and minimum speed for two different speeds and thrust levels. Turn capability is investigated in order to see if FOG-M is able to return over the target area if a first search does not show any targets. The scenario in which this would take place will be discussed later. Some results are shown in table 2.

COMMANDED ACCELERATION	1.0 g	1.5 g	2.0 g
CHANGE IN COURSE UNTIL VELOCITY DROPS BELOW V_{MIN}	270°	210°	180°
TIME NECESSARY FOR TURN	45 sec	24 sec	16 sec
TURN RADIUS NECESSARY	750 m	500 m	400 m
FIBRE LENGTH USED	3600 m	1900 m	1200 m

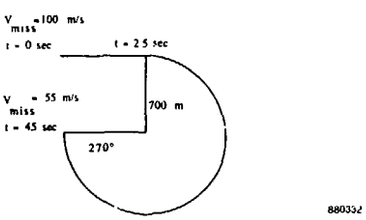

Table 2. Flight characteristics of FOG-M.

The turn capability and turn radius are rather poor at low speed. The time to complete a 270 degree turn, for example, is 33 s and the fibre length used is 3300 m. This turn radius is so wide because during manoeuvres the missile will lose speed and the minimum turn speed will be exceeded, in this case 90 m/s. This is due to the high drag and gravity component at high angles of attack, which forces are not compensated by the thrust. So the missile will lose speed at a high rate when the commanded acceleration is too large. At high speed the situation is a bit better, but shows large side-slip angles, so a new search over the target area or a turn over a missed target does not seem very attractive at this moment. Loss in altitude is reasonable at these thrust levels.

During search for targets, the operator would like the missile to fly as slow as possible, in contrast with the navigation phase. So the low speed of 100 m/s, which is well above the stall speed of about 45 m/s, is chosen as the operating speed for the simulation. This 45 m/s is not a stable situation, for the lack of thrust will cause the missile to decelerate quickly at this angle of attack and the missile will fall down quite fast after this moment.

5. SIMULATION RESULTS AGAINST GROUND TARGETS

When a target has been identified and a lock on is acquired, the missile must be able to hit it. A few footprints were made to identify the minimum distance necessary, also called slant range, to manoeuvre the missile to the target for several operating heights. The first is Figure 6, which shows two footprints when the missile is flying at an altitude of 150 m and 200 m respectively. All targets are stationary. The minimum distance necessary to manoeuvre the missile to the target is a circle around the missile, formed by its maximum dive capability. This is influenced by its elevator limit of 6 degrees. The left and the right turn capabilities are restricted by the same rudder limit.

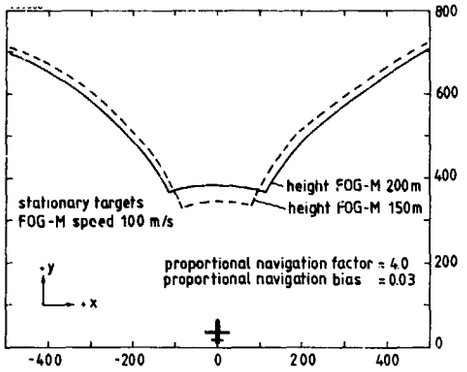

Figure 6. Footprint against ground targets.

The rudder limits are 6 degrees instead of 15 degrees in the navigation and search phase, for the height autopilot makes FOG-M move much smoother than this simulated autotrack autopilot which would drive the angle of attack over 20 degrees. There is just a small difference in footprints for the different heights, so from the footprint aspect there is no preferable flying height. All the hits are top-attacks with an impact angle of at least 40 degrees. This is done with a proportional navigation factor of 4.0 and a bias on the line of sight rate of 0.03.

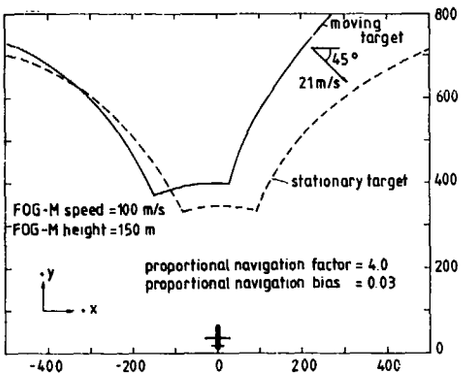

Figure 7. Footprint against moving ground targets.

Figure 7 shows how the footprint is influenced by a moving target with the missile at an altitude of 150 m. The target has a speed of 15 m/s as shown in the figure and so the footprint is shifted accordingly , but well within the lower field of view of the camera as shown in Figure 8. Here a footprint is given for all reachable targets with a speed of 15 m/s in any x and/or y direction which can result in a maximum speed of 21 m/s. The flying height is 150 m. Also the lower camera window is shown with a depression angle of 15 degrees and a field of view of 16 degrees. For this camera angle the operator is able to reach every target he detects, regardless of the way the target is moving. Then the missile hits the target with an impact angle of at least 40 degrees.

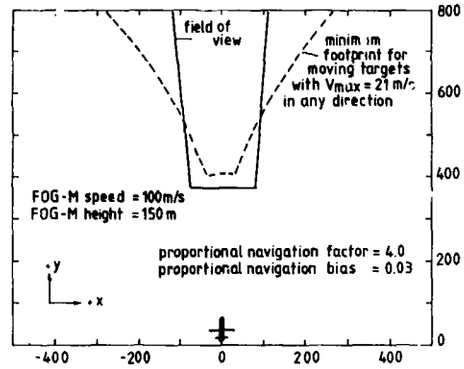

Figure 8. Footprint against moving ground targets.

6. SIMULATION RESULTS AGAINST HELICOPTERS

Also the performance against helicopters was investigated. A few helicopter speeds were simulated for several altitude differences with FOG-M. The proportional navigation factor was kept at 4.0 but the bias was removed.

First shown in Figure 9 is a helicopter some 150 m below the FOG-M missile which moves toward the missile. Three footprints are shown here, all for a missile speed of 100 m/s. The upper one is for a helicopter speed of 60 m/s towards FOG-M. It shows that the helicopter must be recognized and locked at a distance of at least 600 m in order to obtain a hit. For the slower helicopter speed of 30 m/s this distance is 450 meter. And for the stationary helicopter this is 350 m. For these speeds there is no problem.

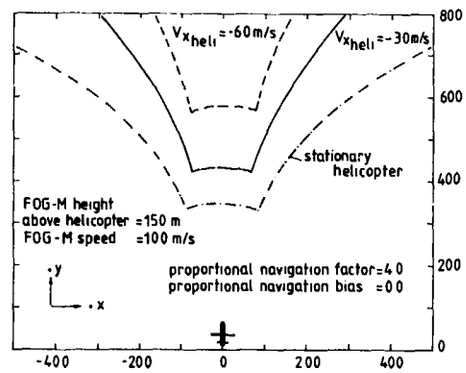

Figure 9. Footprint against helicopters.

The next footprint in Figure 10 is for a crossing helicopter 150 meter below FOG-M. When the helicopter has a cross speed of 30 m/s from left to right, the footprint is shifted to the left. For a speed of 60 m/s this is even worse and the footprint is not in the center of the camera anymore. The FOG-M operator has to anticipate this and must see the helicopter coming from the left at a relatively large offset angle.

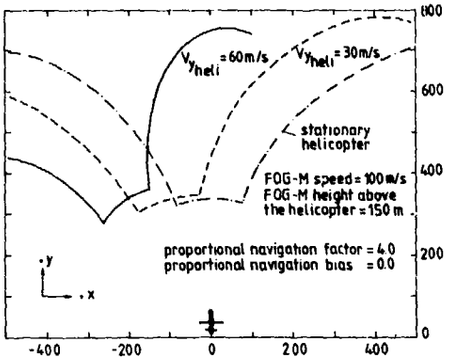

Figure 10. Footprint against crossing helicopter.

This means that FOG-M must have a steerable gimballed camera in order to direct the camera towards the target for searching and attacking a helicopter at short range. For the leftmost figure the camera angle must be some 30 degrees to the left to see the target at short range. This will have influence on operator tasks. However, for a helicopter at a range of more than 800 m it is possible to chase the crossing helicopter and keep it in the field of view of a fixed camera.

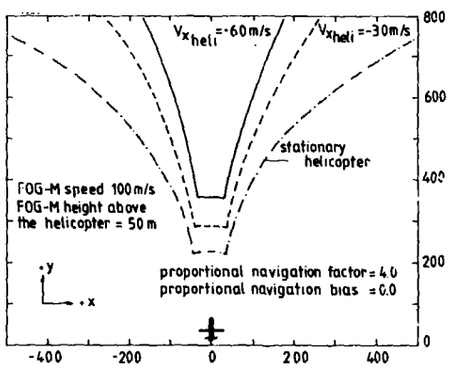

Figure 11. Footprint against helicopter 50m below.

In addition, a helicopter was investigated at some 50 m below FOG-M, to see if the operating height affects the footprint. Figure 11 shows the three footprints: one for a stationary helicopter and the others for a helicopter moving towards FOG-M at a speed of 30 m/s, respectively 60 m/s. It shows that lock on distances for a moving helicopter are much smaller than for the cases in Figure 9.

For the helicopter crossing 50 m below FOG-M, one can see in Figure 12 that lock on ranges are some 100 m shorter than in Figure 10. But to attack a moving helicopter at short ranges, the operator still needs a moving camera.

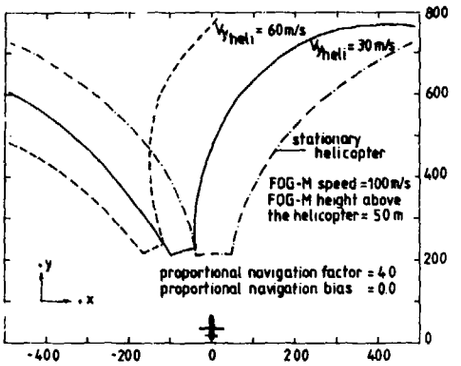

Figure 12. Footprint against crossing helicopter 50m below.

Hence the operating height of FOG-M has no real influence on the size of the footprint, but lock on ranges are better and from an operator point of view this can be very important.

7. SOME TENTATIVE CONCLUSIONS

Some tentative conclusions and remarks are:
- Against moving and stationary ground targets, FOG-M has a good footprint with impact angles above 40 degrees.
- With the estimated aerodynamics, the FOG-M has relatively poor turning capability. From a tactical point of view this is a disadvantage.
- Variable thrust would give the advantage of high speed towards the target area, low speed during the search for targets and a greater capability against moving helicopters.
- For engaging moving helicopters at short range the operator must be able to move the camera in order to see the target in time.

So much for the technical side of FOG-M. The role of the operator will be discussed next.

PART 2

1. INTRODUCTION

The Fibre-Optic-Guided Missile (FOG-M) using a man-in-the-loop promises to be a very interesting weaponconcept for the following reasons:

-it uses passive systems for search and tracking and a fibre-optic wire for the transmission of signals which make detection and jamming of the system virtually impossible;
-the broadband fibre-optic transmission capability makes it possible to reduce the number of expensive equipment needed on the missile itself;
-using a man-in-the-loop, system effectiveness would be enhanced by the adaptive capabilities of the human operator.

In order to demonstrate capabilities of the system including the man-in-the-loop control, a simulator study is being conducted.
The simulator consists of a modelboard to simulate the environment in which the missile is operating. A videocamera assembly, controlled by computers and moving according to the dynamic characteristics of the missile is used to simulate the outside world. The generated pictures are sent to an operator-console where the operator controls the missilesystem with joysticks.
The simulated location roughly resembles terrain in western Germany. Enemy targets can be simulated as well. A diagram of the simulator is shown in figure 1.

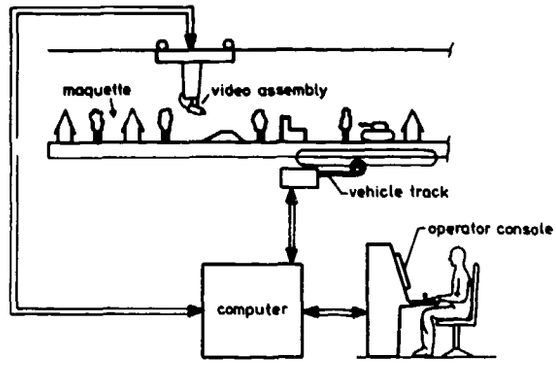

Figure 1. A schematic diagram of the simulator.

The following photos will show the type of image the operator could expect while flying the missile in an european type of environment (figure 2 & 3).

Figure 2. Typical TV-image of the area with village and the canal. The field of vision (FOV) is approximately 25 degrees.

Figure 3. TV-image of area with targets (tanks). FOV is 15 degrees and the distance to the target is 600 meters.

The altitude is set at 155 meters and the velocity at 110 m/s.
Results of the demonstration study suggest that the detection of a target is a critical issue of this weapon system. However if a target is detected and locking can not be immediately accomplished, it is possible due to the length of the fiber optic wire to pass the target on the first run and turn around and come back for a lockon.
Using a simple videocamera in bad weatherconditions renders the system inoperative. Therefore an IR sensor (especially in western european weather) will be needed in a very large number of situations. The last photo (figure 4) shows an operation using an view resembling IR.

Figure 4. Typical IR image. FOV is 25 degrees.

During these pilot experiments some possible problems have been noticed:

-searching for a single target at a relative high speed without prior knowledge of its whereabouts could be ineffective in an european type of landscape where camouflage is relatively easy.
-the detection problem is accentuated if the target is stationary.
-a fast target (like a helicopter) can sometimes be detected without it being possible to attain the target.
-the transferfunctions of the joysticks controlling the videocamera and the missile itself are of large importance due to the sometimes high relative speeds of the target.

As stated, the demonstration study indicated that the characteristics of the joysticks greatly affected the controllability of the system. Therefore a research program has been started to investigate which type of joystick-system would enhance performance of persons with little or no experience in flying (as would be the case of a normal FOG-M operator).
In particular the effect of proprioception on the controllability was a topic of interest.

Joystick-systems used in most aircraft consist of a free-moving stick connected mechanically (through cables, push-rods, or hydraulics) to the control surfaces. In the very modern aircraft the direct connection does not exist any more, but instead the output of the joystick is fed into a computer and after being processed is fed to the control surface actuator. This is also the case in FOG-M where there cannot be a mechanical link between the joystick and the control surfaces for obvious reasons. Therefore the feel of the aircraft responses to control adjustments has to be artificial. The thought behind the following experiments is that if one desires a person to learn a motor control task the fastest way possible, then one should provide the person with the best possible proprioceptive cues, or feel in the control lever, for supporting decisions on control movements. In short, the definitions of proprioception and exterioception as they are used in the experiments are as follows:
-Proprioception can be considered a category of responses from those receptors in the body which are stimulated by the actions of the body itself as opposed to the information provided by visual or auditory receptors, which is called exterioception.
For example a pilot's perception of attitude change through his vestibular system is proprioception, whereas his interpretation of the artificial horizon is exterioception.
The control of a FOG-M can be conceived of as a perceptual motor task. A generally accepted theory about learning such a task is shown by Fitts and Posner (1967). They divide the learning of a task into three phases: the cognitive, the associative and the autonomous (figure 5).

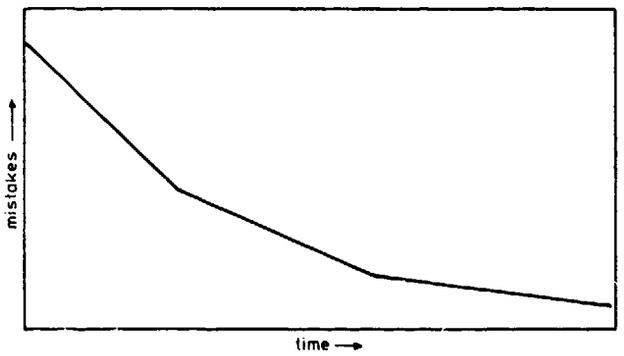

Figure 5. The cognitive(a), associative(b) and autonomous(c) phase of learning according to Fitts and Posner(1967).

The cognitive phase of learning, when instructions and demonstrations are the most effective, can be considered as a first step in the development of an executive program for the activity. This stage allows for the selection of an initial repertoire of subroutines. During this stage the largest improvements are accomplished.
During the associative phase of learning, the new patterns begin to stabilize. Errors, which are often frequent and very large in the cognitive phase, begin to decrease and to lessen in amplitude.
During the autonomous phase, the task becomes increasingly autonomous, less directly subject to cognitive control, and less subject to interference from other ongoing activities. Errors are seldom made and are very small.

Both Adams(1971) and Schmidt(1975) have developed theories concerning the learning of motor control tasks in the cognitive and autonomous phase. They state that:

-When performing motor perceptual tasks we may expect with proprioception superior results in all parts of the learning curve.

For testing this hypothesis the following joysticks have been used:
-an isometric joystick;
-a variable spring force centered joystick;

These controllers differ in the way they provide the operator with proprioceptive feedback.
The isometric joystick produces feedback of the control variable through the pressure on the arm, whereas the last type offers not only proprioceptive feedback of the control variable through the position of the arm but also of the effort needed and thus over the controllability of the vehicle (figure 6). The last type requires feedback from the vehicle, whereas the second type does not.

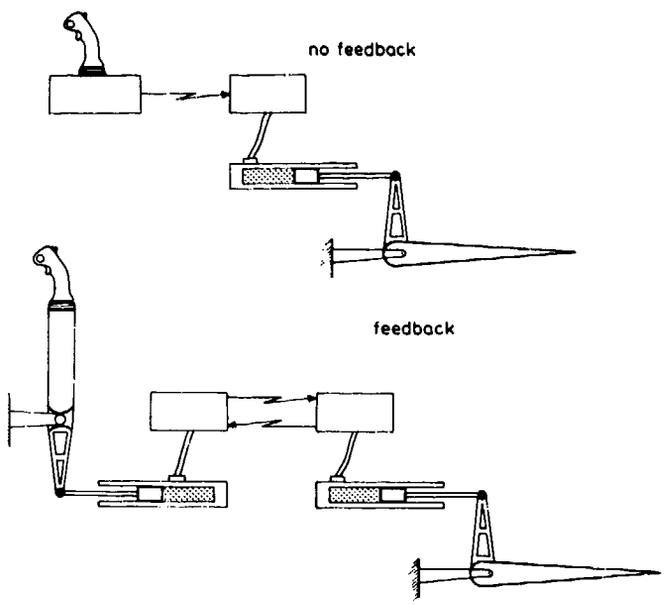

Figure 6. The force-stick (a) without feedback from the vehicle and the variable spring force centered joy-stick (b) with feedback from the vehicle.

In practice the joystick will feel firm but agreeable when the controllability is at a high level. It will feel sluggish if the FOG-M is flying extremely slow and close to the stall speed and at the other extreme, if the airspeed is so high that the manoeuvrability is low, the joystick will feel to heavy. Hence, it was expected that the more effective proprioceptive feedback controller would enhance:

-learning speed;
-accuracy of performance;
-avoiding limits of manoeuvrability.

2. METHOD

The manoeuvre of interest was a dive onto a ground target, because of the critical nature of this type of task.
The task consisted out of flying the vehicle from a situation with a previously determined altitude and velocity on to the target in such a way that:
a, the target was hit dead center;
b, the target was hit as vertical as possible;
c, the aircraft was not stalled.
The aircraft was aligned with the target hence only pitch control was needed. This was simulated on a computer, which was connected to one of the two different joysticks. A mathematical model of an air-vehicle, approximately resembling the FOG-M characteristics without an autopilot and therefore rather difficult to fly manually , was used in order to accentuate possible differences in controllability offered by the joysticks. The computer was also used to provide a perspective image of a target on a monitor. This was done by simple computer generated imaging.

Twelve subjects were asked to fly the simulator with the two joysticks mentioned before. The subjects were all male students between the age of 18 to 25. They had no flying experience, were righthanded and had normal or corrected visual acuity. Only the type of joystick was varied between the subjects. A first group of six subjects flew with the isometric joystick, a second group flew with the variable spring force centered joystick. The subjects were seated in an isolated room, containing the joystick assembly and the computer with the monitor. Each subject was tested on 250 successive trials. Knowledge of results at the end of a trial was provided by showing the subject the distance to the center of the target and the tangent of the angle with which it was hit. The two criteria were stored in a data file for analysis. At the same time a plot of the flight path was shown.

3. RESULTS

a) The target distance to dead center:

The average and the standard deviation of the distance was subjected to an analysis of variance. The average values are shown in the figures 7 and 8.
Both the average distance and the standard deviation showed no significant effects of joysticks, replications and their interaction.

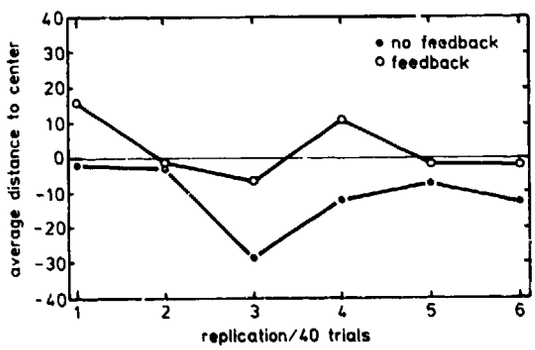

Figure 7. The distance to the target per 40 trials as a function of joystick and replication, averaged over subjects.

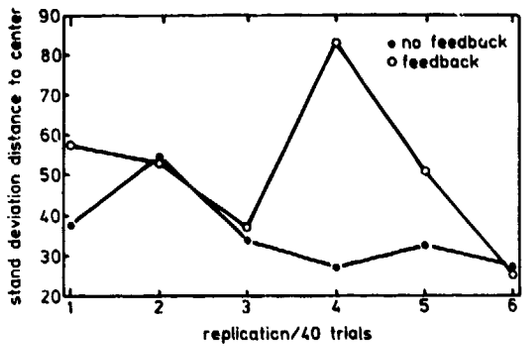

Figure 8. The standard deviation of the distance to the center of the target per 40 trials as a function of replication and joystick, averaged over subjects.

b) The angle to the vertical:

The average and the standard deviation of the angle was subjected to an analysis of variance. The average values are shown in the figures 9 and 10.

The average angle to the vertical showed no significant effects of joysticks. The effect replication was significant (p 0.05). There was no significant interaction. The standard deviation showed no significant effects of joysticks, replication and their interaction.

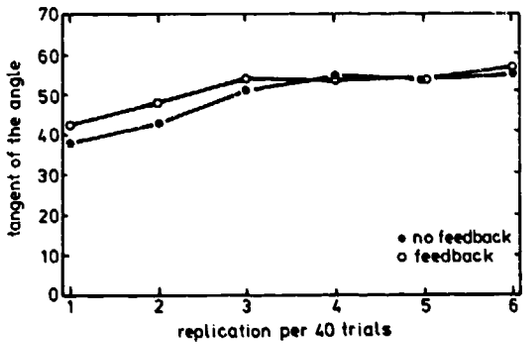

Figure 9. The tangent of the angle to the vertical per 40 trials as a function of joystick and replication, averaged over subjects.

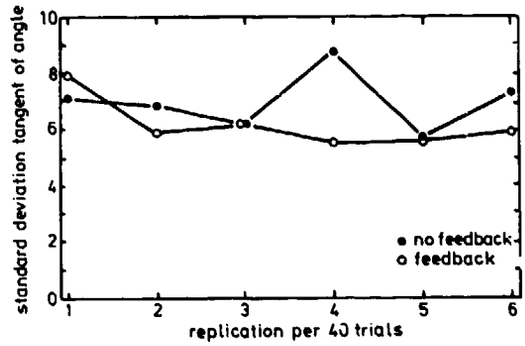

Figure 10. The standard deviation of the of the tangent of the angle to the vertical per 40 trials as a function of replication and joystick, averaged over subjects.

c) The number of stalls:

The number of stalls per 50 trials were analyzed by a T-test. Results showed a significant difference of performance between the two joysticks in favor of the one with feedback from the aircraft (see Fig 11).

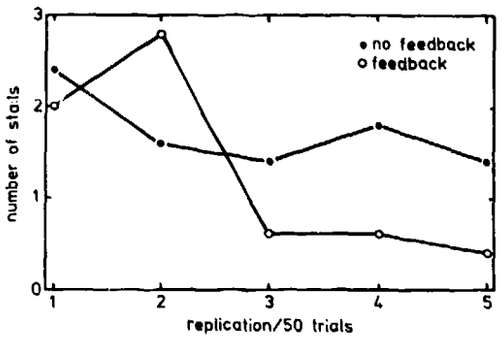

Figure 11. The average number of stalls per 50 trials as a function of joystick and replication, averaged over subjects.

4. DISCUSSION

a) Learning speed:

It was expected that the learning speed would improve as a function of proprioceptive feedback. The results only showed a general effect of learning in the average angle to the vertical and the number of stalls. As regards the number of stalls, a significant interaction between joysticks and replication was found aswell . No improvement was detected in the average distance. This would indicate that the additional proprioceptive feedback is more effective for avoiding the limits of manoeuvrability and not for improving the accuracy of performance.

b) Accuracy of performance:

No significant difference was found between the two joysticks as regards the accuracy of performance. Concerning the distance to the target no significant learning effect could be noticed. A positive learning effect was detected with the angle to the target. Apparently subjects tried in the cognitive phase of learning to keep the distance to the target constant, while improving the angle. This is a well known phenomenon (e.g. Crossman and Cooke 1962) and this suggests extending the number of practice trials for further research.

c) Avoiding limits of manoeuvrability:

Significant improvement was found with the joystick having feedback from the vehicle as extra proprioception. One can therefore assume that subjects used the feedback of the additional variable (namely the manoeuvrability) only for that purpose and did not improve the accuracy of performance. This would indicate that the performance of this particular task could not be enhanced by the knowledge of the manoeuvrability of the aircraft. A task where the accuracy of performance could be enhanced by such knowledge would therefore be an interesting topic for the future.

5. REFERENCES

Adams, J.A. Human tracking behaviour. In: W.C. Howel & I.L. Goldstein (Eds.), Engineering Psychology, Current Perspectives in Research. New York: Meredick Corporation 1971.

Crossman, E.R.F.W. & Cooke, J.E. Manual control of slow response systems. International Congress on Human Factors in Electronics, Long Beach, California, 1962 (Reprinted in Edward and Lees, 1974, op. cit) London.

Fitts, P.M. & Posner, M.I. Human performance. Belmont, CA: Brooks/Cole, 1967.

Schmidt, R.A. A schema theory of discrete motor skill learning. Psychological Review, 1975, 82, no. 4, 225-261.

APPLICATIONS OF IMAGE ANALYSIS IN PRECISION GUIDED WEAPONS

by
S. Grinaker
Norwegian Defence Research Establishment
P Box 25, N-2007 Kjeller
Norway

SUMMARY

An autonomous fire and forget weapon will have to automatically navigate from the launch site to the target area, detect and recognize the target, home onto in, and in the terminal phase, select an aim-point. All these tasks can be performed by utilizing an imaging seeker-head. Image based target acquisition and tracking are well established ideas and implemented in weapons in operation or under development. A brief survey of the involved image processing techniques are provided, including a few examples of state-of-the-art algorithms. If an imaging sensor-head and processor are already employed, these instruments can also be utilized for other purposes. The basic ideas of image based navigation and aim-point selection are introduced and accompanied by examples, and the possibility of replacing the gyro stabilization by image processing is discussed. Finally, the problems concerning the implementation of image analysis for real-time processing are adressed, and some principles for system designes are provided.

1 INTRODUCTION

The professional conference participant has just arrived to a big city he has never visited before. He went by taxi to the hotel and he now wants to find a restaurant where to get a good meal. The lady at the reception desk recommends a restaurant 15 minutes walk away. He gets a map so he can find his way through the busy city with its labyrinth of streets. Well outside the hotel he turns left as the map tells him. He walks along the pavement, crosses streets, turns around corners, all the time comparing names, directions and sequences of streets with those on the map. Finally he arrives at the block where the restaurant is supposed to be. There he looks for the restaurant and soon recognizes the name he is searching for. The restaurant has two doors, but he easily finds the one to enter. And well inside he eventually gets his much desired meal. This man was able to reach his goal simply by the use of a map, his eyes and his long experience in solving similar problems. In a city where he had never been before he succeeded in finding his way from the hotel to the area where the resturant is located, he detected his target - a restaurant he had never seen before, and finally he found the door where to enter.

The tasks performed by this professional conference participant are in principle the same as those to be performed by a completely autonomous homing missile. Also the missile will have to navigate from the launch site to the target area, detect and recognize the target, home onto it, and in the terminal phase, decide on a point of impact. Therefore, the aids necessary for the missile to perform its mission are a map, an imaging device and a computer properly programmed and with the necessary "experience" stored in its memory.

By the end of this century the NATO forces will have in service autonomous weapons based on imaging IR sensors and advanced signal processing. Such weapons are passive (non-radiating), thus difficult to detect, they can obtain a high probability of hit and be very resistant against counter-measures. The IR sensor provides full night capability, and the inherent "intelligence" and autonomy make this kind of weapons extremely simple to operate, even under stress of combat. Furthermore, the time the infantryman is exposed to fire from the enemy is reduced, thus increasing survivability. Autonomous IR imaging seekers are effective against almost all kinds of targets; mobile and stationary, sea, land and air targets. Several studies within NATO and in the individual member nations have concluded that such weapons will be highly cost-effective, and that they significantly improve the defence against Warzaw Pact forces.

This paper addresses the image processing part of such missile seekers. The content is more or less general and true for all imaging seeker heads, but the imaging IR sensor is the most realistic and timely one and is the one we bear in mind. The sensor head and image processor are employed primarily for automatic target acquisition and tracking. As indicated above, however, if these instruments already exist they can also be utilized for other purposes. In Section 2 image analysis based navigation will be discussed, and Section 3 deals with the possibility of replacing the gyro-stabilized platform by image processing. Section 4 and 5 cover the well-established automatic target acquisiton and tracking applications respectively, and aim-point selection is covered in Section 6. Finally, in Section 7 the implementation of the image processing techniques for real-time processing is addressed.

2 NAVIGATION

The essential result of navigation is the current position relative to the destination. This means that the task to be performed by a missile navigation system is to update the missile position when the missile moves along a preprogrammed trajectory to the target area. A prerequisit is that the positions of the launch site and the target area are known initially. The navigation should, ideally, be accurate enough to assure that the target is covered by the missile search area. For weapons attacking mobile targets this will not always be possible because of the uncertainty in target position, but the more accurate the position estimate is the higher the probability of acquiring the target is. If the uncertainty in navigation becomes much less than that for the target position estimate, however, there is of course nothing more to gain. As long as the system does not get lost map based navigation can keep the position error close to the uncertainty of the map data, and this uncertainty is time invariant and therefore does not increase for long missions. However, the probability of getting lost increases with the distance to go. Essential in map based navigation is therefore always knowing the position on the map. This process is by humans performed by comparing map features and landmarks in the real scene. When a match between the features of the scene and the map is obtained, a quite accurate estimate of position and orientation in map coordinates can be determined. The accuracy is, however, not determined from the map accuracy alone, but is also dependent on how well the landmark positions are

defined. If there are very distinct features like rivers, roads, ponds, and coastlines to be used for matching, the overall accuracy can get close to that of the map. The edge of a meadow or a marsh is, however, not so well defined, and the highest point of a mountain may be difficult to locate exactly. If only such "vague" features are available less reliable estimates of the position can be determined. Therefore people make an accurate update when distinct features are available, and when confident matching is not possible, they track major landmarks (mountains, etc) to fix the orientation.

Automating this process by image analysis techniques requires the navigation system to

1) automatically recognize map features in the scene

2) determine the sensor position in terrain (and map) coordinates

If the navigator is completely vision based, the system should also

3) automatically track landmarks by use of image data

It is well known that the accuracy of inertial navigation systems decreases with operation time, and high quality systems are extremely expensive. Automatic image analysis can be used to improve the inertial navigator by updating the position at recognized landmarks.

This kind of navigation is used in cruise missiles, but based on radar data rather than electro-optical (EO) data. In principle, this makes little difference, but radar data are courser and provide less reliable and accurate landmark recognition than IR and visual data do. Radar data provide, on the other hand, all-weather capability. To the knowledge of the author EO image data have never been used for navigation purposes in tactical weapons. However, weapons already employing an imaging device for homing purposes can utilize this also for navigation. An EO navigation system has the potentiality of being less expensive and more accurate than the traditional system based on plain inertial navigation. Even though research and development work along these lines has not been reported for weapon applications, similar work for autonomous land vehicle navigation has been published in the open literature (1, 2, 3).

2.1 Image processing in automatic navigation

In land vehicle navigation the problem is to keep track of the position when the vehicle follows a predetermined path from point A to point B. Provided the initial position is on a road, a major subproblem is to track the road edges to determine the exact position. As long as there are no intersections, rest areas, bus stops and so on, it is assumed that the road is smoothly curved. Therefore, having detected an edge element, the continuation of this is assumed to be along the same general direction, and consequently the search area can be restricted to a small portion of the image (Figure 1). When failing in detecting an edge inside the search window alternative hypotheses are investigated (Figure 2)

a) An intersecting road
b) A curved road
c) A continuation of the road further away

Standard image processing techniques are used to perform edge detection inside the search windows.

If the system detects some unexpected obstacle, e g the road is closed due to construction work or enemy activity, or the continuation of the road simply cannot be found locally, a detour is to be determined. Artificial intelligence techniques have been used in this process. Such situations may also force the vehicle to leave the road and explore new land to circumvent the obstacle. This exposes the image processing system to several challenging problems which cannot be addressed in this paper.

The general approach in image based navigation is firstly to detect features in the image and secondly to recognize these in the map data. However, detailed map data can provide information which significantly simplifies the interpretation of the image. If the current position already is known fairly accurately, the search problem can be reduced considerably by attacking the problem the other way around: Pick a few near-by distinct features from the map data, transform the features' map coordinates to image coordinates and search for the features in the image data. A present project at The Norwegian Defence Research Establishment (NDRE) indicates that this approach makes the interpretation of edge data extracted from the image much easier, and the smaller the search area is the easier the interpretation is. (The process of restricting the search area to a minimum also includes corrections for sensor imposed geometric distortions). The basic steps in the processing are illustrated in Figure 3.

Usually the above mentioned techniques applicable in land vehicle navigation are easily adapted to missile navigation.

3 ELECTRONICALLY STABILIZED SENSOR HEAD

Precision guided weapons performing long range target acquisiton and tracking (and sensor based navigation) need stabilized sensor heads. This requirement stems from the need

- to steer the sensor to view a specified ground area independent of the exact missile orientation

- to achieve maximum sensor head resolution as limited by the detector and optics

Today sensor head stabilization is realized by use of gyros. Regrettably, a gyro stabilized platform adds considerable weight, volume and cost to the seeker head. The idea in this section is to extract the necessary information for sensor head stabilization from the sensor data themselves. In imaging seeker head systems this will in many cases be possible. The basic procedure is to measure the sensor head panning and rotation from image data and, through a closed control loop, compensate for unwanted motion. The measurements are determined from the image data basically by computing the shift and rotation of the image due to sensor

motion. The idea of using image data for sensor head stabilization is not new, but only recently work directly related to this problem has been reported (4).

A possible approach to the stabilization problem is

1) Register consecutive images
2) Compute the translation and rotation parameters
3) Restore motion blurred image, e g by Wiener filtering
4) Geometric restoration (panning and rotation) - for visual inspection only
5) Determine steering commands

Image registration is, for two images covering partly the same ground area, to determine all pixel pairs which combine two pixels, one from each image, covering the same area on the ground (see Figure 4). This problem has been extensively studied by many researchers, and various approaches to solve the problem have been proposed (5, 6).

In homogeneous image areas the pixel registration problem cannot be solved locally because the pixels cannot be unambiguously distinguished. Therefore, pixel registration is firstly performed in inhomogeneous image areas. For instance, if distinct features like lines, corners, edges, crossing lines etc, can be recognized in both images, several pixel pairs can be determined. Information about change in position of these distinct pixels can then help to determine the correspondences of less distinct pixels. In this way the pixel registration can propagate into the homogeneous regions. For the technical details about how to perform image registration the interested reader should consult the specialized literature.

How can sensor motion be computed from image information? Let us consider the situation in Figure 5, where F is the sensor focal length, Δx, Δy, Δz are the components of the sensor displacement between consecutive images, and (X, Y, Z) and (X', Y', Z') are sensor based cartesian coordinate systems at the two instants. A fixed 3-D point with coordinates (x, y, z) and (x', y', z') in the two coordinate systems, will be projected onto the image plane at coordinates (X, Y) and (X', Y') respectivley. If the sensor motion is pure translational then, from Figure 5:

$$\frac{X}{X} = \frac{F}{Z} \rightarrow X = F\frac{X}{Z} \qquad X' = F\frac{X'}{Z'}$$

$$Y = F\frac{y}{z} \qquad Y' = F\frac{y'}{z'} \qquad (1)$$

$$x' = x-\Delta x$$
$$y' = y-\Delta y \qquad (2)$$
$$z' = z-\Delta z$$

$$\Delta x = X\frac{z}{F} - X'\frac{z-\Delta z}{F}$$

$$\Delta y = Y\frac{z}{F} - Y'\frac{z-\Delta z}{F} \qquad (3)$$

If the sensor is also rotated (Figure 6) the mathematics becomes slightly more complicated, but it can easily be shown that the motion parameters are related by the following set of equations:

$$X = F\frac{X}{Z} \qquad X' = F\frac{X'}{Z'}$$

$$Y = F\frac{y}{z} \qquad Y' = F\frac{y'}{z'}$$

$$\begin{bmatrix} x' \\ y' \\ z' \end{bmatrix} = R \begin{bmatrix} x - \Delta x \\ y - \Delta y \\ z - \Delta z \end{bmatrix} \qquad (4)$$

$$R = \begin{bmatrix} \cos\beta\cos\gamma & \cos\beta\sin\gamma & -\sin\beta \\ -\sin\alpha\sin\beta\sin\gamma - \cos\alpha\sin\gamma & -\sin\alpha\sin\beta\sin\gamma + \cos\alpha\cos\gamma & -\sin\alpha\cos\beta \\ \cos\alpha\sin\beta\cos\gamma - \sin\alpha\sin\gamma & \cos\alpha\sin\beta\sin\gamma + \sin\alpha\cos\gamma & \cos\alpha\cos\beta \end{bmatrix}$$

where α, β and γ are the angles of rotation around the X, Y, and Z axes respectively.

Eq (4) is true for every 3-D point projected onto both images. For every pair of registered pixels the quadruple (X, Y, X', Y') is known, and for each pair a new set of equations (4) is valid.

If two pixel pairs are registered, eq (3) can be solved. In presence of noise we will, however, need more than two pairs, and Δx, Δy and Δz are determined as the least-square solution. Similarly, eq (4) can be

solved from 6 pairs of pixel registrations, but usually some tens of pairs are necessary to make the solution reasonably noise insensitive.

If the image motion is large compared to the pixel resolution the motion will cause blurring and reduce the over-all seeker resolution. Let the pixel exposure time (the period in which energy is collected for one pixel) be T_E , and let the image frequency be $1/T_I$. The displacement of the image representation of a fixed point in 3-D, measured in pixels, is (X-X', Y-Y'). Some of this displacement, (ΔX_{T_E}, ΔY_{T_E}), occurs during the exposure time,

$$\Delta X_{T_E} = (X - X') \frac{T_E}{T_I}$$

$$\Delta Y_{T_E} = (Y - Y') \frac{T_E}{T_I}$$

If the displacement, (ΔX_{T_E} , ΔY_{T_E}), is much smaller than the pixel size (detector resolution), the motion imposed blurring is neglectable. For large T_E/T_I (e g staring arrays) and for low performance stabilization systems, however, the detector resolution will usually not be retained.

The pixel intensity value is a time integral of the radiation from the instantanious field of view (IFOV) onto the detector element. If the IFOV is constant during the exposure time, the received energy is simply an image of the IFOV. If there is motion, however, the received energy is an integral of energy contributions from a continuously varying IFOV. Provided the 3-D energy radiation distribution is known, the imaging process can be computed when the IFOV position and velocity, i e the motion parameters, are known. Let I be the radiation onto the detector element. If the function

$$\int_{t=T_0}^{T_0 + T_E} I(IFOV(t))\, dt,$$

mapping energy from IFOV into a pixel intensity, has an inverse function, image deblurring can be accomplished by determining the IFOV radiations from the pixel intensities. A lot of attention has been paid to this problem by image processing scientists, and several techniques for restoring motion blurred images can be found in the text books. Figure 7 shows an example of motion restoration.

4 TARGET ACQUISITION

Automatic target acquisition accomplished by image analysis is by now a well accepted idea adopted in several PGW development programmes. In 1980 AGARD held a symposium (7) allocated to this topic, and several presentations in various fora have covered such techniques and concepts in much more detail than can be done in this paper.

Automatic image analysis systems are usually designed as succesive steps of data reduction. In this context image based target acquisition can be subdivided into segmentation, feature extraction and classification, as shown in Figure 8.

In general, segmentation is to subdivide the image into psychophysical, connected areas, named segments. In target acquisition the term "segmentation" usually means the separation of target candidates from the background. The same basic requirements apply to electronic vision as to human vision. There must be some contrast between object and background to permit separation. Furthermore, to constitute a segment, an area should be homogeneous in some feature, usually grey level or texture. Thus, the homogeneity criterion for IR images usually is that all segment pixels should correspond to areas of approximately the same temperature or, alternatively, areas with a temperature above some threshold. The image of the target can correspond to one or more segments, but each segment (target subpart) should be internally homogeneous and have contrast to the background or neighbouring segments in some selected feature.

The image processing literature covers plenty of segmentation techniques and the more or less well-founded corresponding theories. Not all these methods are applicable for real-time processing in weapon implementations, however, and the weapon concept will often significantly restrict the choice of possible techniques.

4.1 Low resolution target detection

In some applications early target detection is essential, meaning that the detection should be performed on the basis of a very coarse image of the target. Under the NATO Defense Research Group/Panel III, the RSG9 on Image Processing in 1977-80 accomplished a cooperative research project entitled "Discrimination and classification of operating military targets in natural scenes from multispectral data" (8, 9). In this project "The Alabama Data Base" containing thermal low resolution targets like tanks, APCs, jeeps, etc, was processed. A low resolution target is here defined as a target covered by a few pixels only, so that its shape cannot be resolved. In this data base, as in most natural thermal images, the military targets possess a larger thermal signature than the local background. Therefore all participating countries included grey level thresholding in their segmentation procedures. There are three broad categories of such segmentors:

1) the globally adaptive segmentors which assume that the background is uniform and accordingly adapt the parameters once for each whole image

2) the locally adaptive segmentors which assume that the background is composed of large areas which are individually uniform, and adapt the parameters for each local region within each image

3) the object adaptive segmentors which allow target signature variations within each local image subarea by adapting the parameters to the local object/background conditions, i e no single threshold is used to separate the segment from the background, but the threshold will vary around the contour dependent on the local intensity values and the contrast across the edge.

It is obvious from this cooperative work accomplished by Canada, Denmark, France, Germany, Norway and USA that the locally adaptive techniques are superior to the globally adaptive techniques. Any expectations of further improvements by using object adaptive techniques are, however, not supported by this work. This may be due to deficiencies in the algorithms or the data base, but most likely the general class of low resolution segmentation problems is such that there is little to gain by these refinements. Finally, it was clearly indicated that the detailed construction of the segmentor is of minor importance as long as the algorithm is tuned to the data base.

A generalized version of the Norwegian segmentor is shown in Figure 9. Low temperature resolution imaging sensors will produce low contrast images. Scattering in the atmosphere and optics, and frequency limitations in the detector preamplifier and sensor electronics may produce low spatial resolution images even though there are 50-100 pixels covering the target. Therefore, the term "low resolution target images" may span a range from a couple of pixels to nearly 100. To cover this complete range of low-resolution IR images the segmentor in Figure 9 is a combination of two parallel independent segmentors, and the segmented image is determined as the union of the two. One segmentor, which is similar to the one used for The Alabama Data Base, is tuned to detect small high-contrast objects. The other tends to detect somewhat larger, low-contrast objects. The basic scheme is identical for the two segmentors, but the details differ a lot and are also strongly dependent on the actual application (data base).

First a "contrast picture" is produced by applying some kind of gradient operator to every pixel in the input image. For the hot-spot detector this may be the Laplacian, but this is strongly dependent on the sensor and kind of scenario. For the low contrast segmentor a less noise sensitive operator should be applied, for example a band-pass filter or, equivalently, a combination of a noise filtering (low-pass filter) and a gradient operator (high-pass filter). The gradient thresholding can be globally, locally or object adaptive dependent on the amount of a priori information available. The thresholded gradient picture should primarily include object edge pixels. Of course, also some noise generated pixels will be present, but probably these will be randomly distributed throughout the image, whereas the object edge pixels are grouped together around the object contours. Therefore some kind of density filtering and/or pixel grouping (clustering) will identify the potential object locations. Finally, inside the identified windows, the original grey level image is processed by a locally or object adaptive thresholding to determine the objects.

The segmentation process locates the objects in the field of view and defines their silhouettes. However, these objects need not be targets only, also several other target-like objects may be present. Object classification is therefore necessary. Low-resolution images are usually classified by statistical pattern recognition techniques. Firstly some predefined, discriminating features are measured for each segment. These features can be spectral, shape or size descriptive. Only very course shape features are meaningful for low-resolution images, and size features will only discriminate against background or foreground structures much larger than the targets searched for. During design the classifier was taught what the various kinds of targets look like in this feature space. The second step, therefore, is principly to compare the measured features and the previously learned features. If the measured feature vector is reasonably similar to one of the stored patterns, the object is assigned to the corresponding class.

4.2 Subpixel target detection

If very long detection ranges are required, the target should be acquired when its projection onto the image plane still is only a fraction of a pixel. Subpixel target recognition can only be performed by use of contextual information.

The previously mentioned NATO Defense Research Group AC 243/Panel III/RSG9 is currently investigating the possibilities of automatically detecting and recognizing subpixel targets from their formations. This project was initiated in 1986 to develop algorithms which will allow airborne detection of formations of military vehicles at long ranges. Algorithms of this type can increase the useful range of existing IR sensors by allowing the detection of vehicular targets based on their formation as a whole, even though the individual targets appear only as non-resolvable points.

One possible approach follows this basic outline:

1) The individual formation members (being single pixel targets) are detected as contrast points in singular images or as moving points in image sequences (this latter criterion requires careful image registration, change detection and object tracking).

2) The individual target candidates are clustered into formations according to predefined rules. The formations may be incomplete due to missing elements.

3) Missing elements are searched for in locations specified by the formation description. Relaxed detection criteria may be used in this area restricted search.

4) The 3-D to 2-D mapping performed by the imaging process will, in general, distort the appearance of a real target formation, and individual targets may be occluded due to land screening or obscuration from vegetation. Therefore considerable variations from the ideal formation must be permitted, and natural, similar looking structures on the ground may very well cause false alarms. All formation candidates are therefore tracked to reveal whether they behave like true target formations and to discriminate between stationary and moving structures.

It is extremely difficult to reliably acquire subpixel targets, and this research is still in its infancy. Most likely it will take years to reach practical results, and this section has been included solely for the sake of completeness.

4.3 High-resolution target segmentation and classification

If little information about the target location is available a priori, the seeker head may need to search for the target over a large area. In this area there may also be decoys and other non-target objects with signatures similar to that of the target. Reliable target acquisition, consequently, requires detailed information about the objects so that they can be distinguished. In such applications the target should be resolved into at least some hundred pixels. For this kind of imagery much more sophisticated processing techniques are available than for the low-resolution case, but still the current state of electronics and computers seriously restricts the choice of methods for weapon applications.

A survey of image processing techniques applicable to high-resolution images is far beyond the scope of this paper. Nevertheless, we will give one example from NDRE research demonstrating the extended possibilities provided by advanced image analysis.

Reality is that the sensor head produces a sequence of images during the missile's mission. If the images are independently segmented as singular images, i e without making use of information extracted from preceding images, the segmented images will show considerable differences in the details. Due to digital noise the fine structured contours will necessarily vary. Furthermore, high frequency atmospheric fluctuations, wind, clouds etc, may produce local pixel intensity variations changing over time in a probabilistic manner. These variations result in minor statistically distributed disturbances in the segmented images, causing the detailed segmentation to change from image to image. Finally, in the presence of motion, the local contrast between objects and background will change, obvicusly influencing the segmentation results. In natural images very often only fractions of objects can be extracted due to very low contrast between some parts of the objects and the local background (e g camouflaged military targets). In the next moment other parts of the objects can be extracted, however, since the local background has now changed due to relative motion between targets, background and sensor. Based on these observations we can conclude that singular image segmentation generally will be noisy. However, by combining the segments from several images, better and more stable results may be obtained.

A stable and fairly complete and noiseless segment is obtained by the basic scheme shown in Figure 10. The valid segment is determined by taking the union of instantaneous segments for that object extracted from consecutive singular images. To leave out non-object pixels appearing in only a few instantaneous segments the pixels are, however, weighted according to their number of occurrences, and only relatively stable pixels are retained in the final segment. Included in this algorithm is also a careful registration of object pixels.

5 TARGET TRACKING

Image based target tracking has already for a long time been employed in operating weapons, e g the US air-to-surface missile Maverick, and improved performance trackers have been presented in several NATO fora and elsewhere (10, 11, 12, 13).

A prerequisit for target tracking is that the target is acquired. Then image based tracking is to keep record of the target projection (position) in every frame of an image sequence. This makes tracking basically a recognition process in which imaged targets are to be recognized in successive frames. Hence, tracking is nothing but reacquisition and may naturally be performed in a similar way as the initial acquisition. Tracking is easier, however, since more information is available about the target's signature and position. Furthermore, knowledge about its history also indicates how the target will behave in the future. This knowledge may therefore be used to model the target, to predict how it will be projected onto the image plane in later images and to forecast the behaviour of its characteristic features. Successful prediction will increase the probability of recognizing the target later and is therefore essential for stable tracking.

Target tracking can be subdivided into three basic tasks:

1) Image registration
2) Target recognition
3) Target state prediction (primarily position, but also other variables which may be induced in the target model)

The early trackers combined the registration and position prediction by expecting the displacement of the target in the image, $(\Delta X, \Delta Y)$, to be constant in two time spans. This means, basically, that the sensor motion is constant and the target velocity vector is constant. For these assumptions to be acceptable, the predictions must be frequently updated compared to the scene dynamics, and the sensor platform should be stabilized.

It is unlikely that the target will be found exactly at the predicted position, in particular when the prediction is performed in the simple way described above. To permit some noise and to compensate for the inaccuracies stemming from an incomplete dynamic model, a search area around the predicted target position is defined, wherein the target is searched for. The earliest trackers were the contrast tracker, which just recognized a contrast point, and the edge tracker, which recognized two vertical (left and right) and two horizontal (upper and lower) edges to define the outline of the target. Of course, these trackers were very sensitive to contrast points and edges close to the target position, and they were easily fooled.

More recently the correlation tracker appeared. In this tracker a model of the target, an image usually produced from previous images, and a search window in the current image are cross-correlated, and maximum correlation determines the new target position. The target model must be updated during tracking to compensate for changes in aspect angle, increasing size, etc. The update may, for example, be a copy of the target image at distinct moments, or it may be a weighted average of the former model and the current image. Correlation trackers are fairly robust to background disturbances, but they usually have problems in handling obscurations, i e when the target is more or less occluded by terrain, vegetation or other foreground objects. In the most advanced correlation trackers special logic is added, however, to handle some of these problems.

Feature based trackers have the potentiality to further improve robustness and reduce processing requirements. Furthermore, if image based acquisition is already employed, little extra hardware is needed to implement the tracker. In feature based tracking the targets are represented symbolically by their feature vectors rather than by their grey level image, and the image-to-image recognition may be performed by similar pattern recognition techniques as in the acquisition phase.

Image analysis can also be used to perform the measurements in a target estimator, as in the NDRE Intelligent Multi-Target Tracker. This system, which is an integrated target acquisition unit and multi-target tracker, is briefly described in the sequel. For details, see (13, 14).

There will always be some uncertainty in the classification results of the target acquisition unit. For example, an object may be classified as with probability 0.8 being a tank, with probability 0.2 being an APC. Rather than simply acquiring this object as a tank target, the classification uncertainty should also be reflected in the tracker initialization.

The NDRE multi-target tracker consists of a set of tracker banks, a segmentation and classification unit, a target segment calculator and a data base module (see Figure 11). One tracker bank is allocated to one target and may include several individual trackers. Each such tracker is implemented as an estimator, e g a Kalman filter, and a measuring unit. The various estimators in a bank model the alternative hypotheses about the target, i e one Kalman filter models the tank, another models the APC, etc. (Also uncertainties in aspect angle may be taken care of by multi-hypothesis trackers). Initial hypothesis probabilities are provided by the acquisition unit. The individual trackers are independent, parallel trackers monitored by a common controller. Ill-modelled trackers, i e estimators based on false hypothesis, will after some time diverge significantly from the measurements. A modified χ^2-test and a probability test are executed by the controller, and after a while ill-modelled trackers will fail the test. In principle, therefore, only the "correct" estimator survives. The measurements necessary for the estimator are performed through image segmentation, feature extraction and object classification. Also the aspect angle is measured by the same process. This image analysis, performed for target tracking, follows basically the same procedure as that for the acquisition process. The processing for the two purposes is, however, performed on complementary parts of the image. (Segmentation and classification for acquisition are performed outside the tracker search windows only).

The Target Projection Calculator and the Data Base Module in Figure 11 are used to determine the image search area, i e the search window where to perform the above described analysis for state vector updating.

The NDRE Intelligent Multi-Target Tracker has proven the ability to track several targets simultaneously, automaticly acquire targets also during tracking, and to track through obscurations. Sophisticated trackers, like this one, have a much higher potentiality to resist counter-measures and to handle difficult natural situations than the simpler in-service trackers. Therefore, in the near future, this kind of trackers will be introduced in the more sophisticated weapons.

Provided image processors are already employed for target acquisition, the implementation of such trackers will not be much more expensive and will not require much more additional hardware than the old trackers.

To further demonstrate the excellent partnership between image based acquisition and tracking it should be mentioned that object tracking also can be used in the acquisition process. To improve the reliability of the acquisition a target candidate may be tracked for some time so more information can be extracted for the classification. In this approach there is no clear distinction between target acquisition and tracking. The NDRE multi-hypothesis tracker, where improved classification is obtained by leaving out all trackers but the properly modelled one, also indicates that the two modules should be closely integrated in applications covering scenarios of multiple targets, decoys and background clutter.

6 AIM-POINT SELECTION

The missile guidance system always needs a stable point in 3-D to steer against. In non-imaging homing this has not been a topic of much consideration, since the seeker simply has seen a point-target. In such systems, consequently, smoothing of the aim-point position by some kind of filtering (low-pass filtering, Kalman filtering) has been the only processing possible and necessary. In an imaging homing system, however, the target is represented as an areal target. At long distances the target does not seem to be much more than a point and defines an aim-point good enough. At shorter ranges, however, this is no longer true, and a well defined point on the target must be selected so that stable guidance can be accomplished. It is, of course, possible to select some arbitrary aim-point, but one should rather select a "desired point of impact" (DPI), defined by some preselected criteria. This point may, for example, be a distinct contrast point on the target, the centre of interia of the target projection, or a point defined relative to some reference points. In the terminal phase, when the missile gets close to the target, a high resolution image is obtained and detailed information about the target is collected. Hence, there is a great deal of freedom in selecting the DPI, and one should take advantage of this opportunity to optimize some criterium like "maximum probability of hit" or "maximum probability of kill".

The centre of inertia of the target segment is defined as (X_{mean}, Y_{mean}),

$$X_{mean} = 1/N \sum_{i=1}^{N} X_i \,, \qquad Y_{mean} = 1/N \sum_{i=1}^{N} Y_i$$

N is the number of pixels in the segment (target size).

DPI = (X_{mean}, Y_{mean}) would maximize the a priori probability of hit for many targets and provide a high hit probability for most targets. This is generally not true, however, for targets with concave silhouette (as for a catamaran head on).

Choosing the DPI as the point maximizing the probability of hit will usually not maximize the probability of destruction, which is often a more attractive goal. Maximizing this criterium is, however, a non-trivial task and involves target vulnerability studies and weapon performance considerations. The result will certainly also depend on the weapon's angle of impact.

The problems concerned with the selection of an optimal point of impact is, however, not a topic of this paper. Let us therefore just assume that for every target there exists a set of preselected DPIs defined such that for a given angle of attack there is one and only one DPI. Selection of the valid DPI, then, is based on information from the acquisition and tracking modules. Dependent on the control strategy of the missile guidance system the seeker's aim-point may be another than the DPI. If this is the case, however, a well defined relationship exists between the two, and the topic to be solved by image analysis in this terminal phase is to recognize and track the preselected aim-point. An aim-point is properly defined if it is unambiguously referenced to some close, distinct, contrast points. Automatic image analysis can then be used to recognize the aim-point. In practice, to reliably recognize a contrast point requires the image of the target to be segmented into areas corresponding to target subparts, and these subparts (or equivalently target substructures) must then be recognized.

An example will illustrate this idea:

To an anti-tank weapon the preselected aim-point is defined as "the centre-point of the borderline between the hull and the turret" (see Figure 12). In this concept the tank subparts "turret" and "hull" must be found and represented by their image segments. Thereafter it is trivial to determine the optimal aim-point. The image segmentation techniques involved in this task are very much the same as those for high-resolution segmentation in the acquisition module (see section 4.3). As for the tracking, however, the target class and position is already known, and the segmentation process may be supervised by knowledge about the target shape and intensity function. Having segmented the target into its subparts the next problem is to classify the segments. At least the turret and the hull must be identified. Of course this can be done as described in section 4.1 by firstly computing discriminating features and secondly determining the classes by statistical pattern recognition, but the classification should now be supported by the structural information available (the turret is above the hull, the turret is connected to a gun, the hull is above the tracks, etc). Then, when the turret and the hull are located and their shapes are specified by their image segments, the borderline between them is easily determined. The mid-point on the borderline defines the aim-point.

7 IMPLEMENTATION

Image analysis is extremely processing consuming, and special computer architectures with a high degree of parallelism are required to permit the use of advanced image processing in real-time applications. Imaging systems produce very high data rates, and practical algorithms typically demand a processing power of 1-2 Giga-operations (10^9) per second (GOPS) to run in real-time.

A variety of parallel image processing machines are described in the literature (15, 16, 17). These are, however, mainly developed for research applications or to process singular images. In most proposals the machines are bus organized having large image memory systems and special high-speed processors connected. Other typical image processing machines include the array processors, and more recently, multi micro-processors interconnected in various topologies, e g hypercubes. These machines are much faster and more cost-effective for image processing than traditional sequential computers. Nevertheless, for real-time processing they are still too slow, and for weapon applications they are much too large. Therefore special designs are necessary.

No pure sequential machine can provide the computing power requested above. Processing speed-up can, however, be obtained by parallel designs. There are three basic types of parallel architectures:

SIMD — Single Instruction stream Multiple Data stream (array processors)

MIMD — Multiple Instruction stream Multiple Data stream (several microprocessors or signal processors working on separate data)

Pipeline — In this architecture the data flow through a chain of processors, each executing a separate task of data processing on-the-fly (similar to the industrial conveyor belt)

Image analysis systems are very often composed of subsystems as those previously presented in this paper. These subsystems correspond to consecutive steps of data reduction. Segmentation and feature extraction are front end functions on the pixel level involving huge amounts of data. These modules often consist of fairly simple operations processing only local data, e g filter output is computed from the pixel values in a small neighbourhood. Very specialized processors can be employed to efficiently execute this kind of low-order operations, and very often on-the-fly processing is possible. The proceeding cognitive tasks, e g classification and target tracking, need flexibility, however, and may be implemented in expert software modules. These modules, therefore, need to be implemented in programmable hardware. Consequently, to combine necessary processing speed and requested flexibility, real-time image processing systems need a modular architecture. Firstly, there should be a specialized, high capacity hardware processor which can perform real-time processing on-the-fly, and secondly, there should be a powerful, programmable multi-processor system which can run complex programs written in high-level language. Finally, the use of a common data base should be avoided. The use of distributed memory will solve the problem of the Von Neuman bottleneck (a too high data rate on a common bus or data channel), whereas minimizing data storage by on-the-fly processing also reduces vasted memory access time.

Most sensor systems scan the field of view in a raster scan fashion, thus converting the two-dimensional image data to a time series. The pipeline architecture is well fitted for on-the-fly processing of such data and is a natural choice for the front end machine. However, independent program branches are often identified when parallelizing the low-order image processing algorithms to be run by this machine. Therefore parallel pipelines will speed up the processing and provide a more flexible solution. A parallel pipeline implementation of a segmentation algorithm is shown in Figure 13. For a more detailed discussion, see (18).

The on-the-fly processor will be special to a particular application, so that the low-order processing of a specific algorithm can be executed in real-time. For a weapon implementation special hardware processors may be developed, and very compact hard-wired designs can be determined. At NDRE a rather complex algorithm for real-time processing of TV images has been implemented using standard integrated circuits. This processor, providing a processing power well above 1 GOPS, consists of approximately 30 double Eurocards. Preliminary investigations reveal, however, that the size of the computer can be reduced to approximately 10% of this by developing five special VLSI circuits.

In some low-order processing all pixels are to be processed identically. In such cases the SIMD machine can be very efficient. However, as explained above, the data usually are presented sequentially to the low-order processes, and the advantage of the inherent parallelism is partly lost. For weapon applications SIMD architectures, therefore, are most effective if the processors and the sensor are tightly coupled. Provided a multi-element sensor is employed, the various processing elements can process data streams from separate sensor elements at a very low level before the data are converted to the raster scan structure.

The high-order processing, i e target classification, target tracking and aim-point selection, requires a high degree of flexibility. These tasks involve several more or less independent algorithms working on separate data, and how much time is spent in the various modules and how much data are transferred between them cannot be fully foreseen and will vary with the image content. These algorithms should obviously be implemented in a flexible, programmable machine. On the other hand, the range of algorithms to be run on this machine is that of image analysis algorithms, thus being much more restricted than that of general purpose computers. Also these high-order processes are fairly modular, and for a particular weapon implementation rough estimates of the processing power necessary in each module and requirements to the capacity of the interconnecting data channels can be determined. Generally, a multi-microprocessor MIMD machine is best suited for the high-order processing, but often the processors can be loosely connected. In such loosely connected networks processing clusters (one or more processors) are dedicated to special tasks.

In many applications the MIMD machine will be designed along the guidelines of general multiprocessor networks, and there will be examples of several of the most common topologies. However, the way data are organized in image processing, namely as 2-D matrices, is of special concern. There are also some algorithms organizing data in a pyramidal structure, in which the full resolution image is on the bottom and reduced data representations are on the higher levels. In many image processing machines these data structures are mapped over to the processor topologies, thus resulting in two-dimensional processor arrays or pyramides of processors. These architectures also reflect the fact that data dependencies usually are local and most data transferrals will be between connected processors. There are, however, also some image processing algorithms requiring global data information, which is very clumsy to implement in this kind of architecture and results in ineffectiye solutions.

Due to the modularity of image processing algorithms, loosely coupled architectures may be advantageous in specific implementations. In such constructions one processor cluster may perform, for example, the classification, another cluster may accomplish the tracking, and the first cluster will in the terminal phase be ready to perform the aim-point selection. The tasks can, of course, be further subdivided by distributing subtasks to separate processors within a cluster, e g each tracker may be implemented in a separate processor. In a typical implementation 5-15 of today's fastest microprocessors will be necessary to run the high-order processing to be executed by the MIMD machine.

8 CONCLUDING REMARKS

Advanced precision guided weapons involve a number of non-trivial signal processing tasks. Basically these are the same as those performed by hunting animals. The claim of this paper is that, except for accelerometers to sense the upright position, an imaging device is the only sensor necessary to successfully reach the ultimate goal of killing the target. The eagle and the hawk constitute a living proof of this claim. The best solution is not necessarily to copy biology, but the fact that vision based homing systems have worked for thousands of years and that the eagle still is around indicate that the biological solution is a good one.

As for the terminal phase, i e for target acquisition, tracking and aim-point selection, there is little doubt about the superiority of imaging seeker heads compared to any non-imaging homing systems. (Additional information from non-imaging sensors may be valuable, though.) We have in this paper discussed the use of image analysis applied to these problems, and the state-of-the-art of this technology has been demonstrated by a few examples. It is clear, though, that many of the most advanced image analysis techniques cannot be applied to missile seekers today due to limitations in electronics and computer technology. However, by the construction of special hardware computers, powerful algorithms tuned to the particular application can already now be employed for PGWs.

The high quality imaging sensor and the high capacity image processor employed for the primary tasks mentioned above should be utilized also for other processes. We have in this paper paid some attention to the possible use of these aids for navigation and sensor head stabilization, and some basic, preliminary results have been presented.

Even though we are still far from copying advanced biological systems, it is not unlikely that within the end of this century there will exist vision based missile seeker heads accomplishing all the tasks covered by this paper.

9 ACKNOWLEDGEMENT

Most of the examples presented in this paper have been produced by the Image Processing Group at NDRE. In particular I will thank my colleagues I Dyrdal, E Heyerdahl, H C Palm and E Østevold for their contributions and valuable comments. The example algorithm covering Land Vehicle Navigation was developed by Ø Christoffersen, UNIK, University of Oslo as part of his thesis.

10 REFERENCES

(1) A.M. Waxman, J.J. LeMoigne, L.S. Davis, B. Srinivasan, T.R. Kushner, E. Liang, T. Siddalingaiah: A Visual Navigation System for Autonomous Land Vehicles, IEEE Journal of Robotics and Automation, Vol RA-3, No 2, April 1987

(2) H.P. Moravec: The Stanford Cart and the CMU Rover, Proceedings of the IEEE, 71, pp 872-84, July 1983

(3) D.M. Keirsey et al: Intelligent Tactical Autonomous Control (ITAC) System, DAAK70-83-C-0057, Final Report, Hughes Research Labs, Malibu, CA, USA, Feb 1987

(4) R. Engelhard: Electronic Image Stabilization in Real-Time, AGARD Symposium on Electro-Optical Systems and Image Analysis for Airborne Applications, 54th Panel meeting of the Avionics Panel of AGARD, Athens, Greece, Oct 1987

(5) T.S. Huang (ed): Image Sequence Processing and Dynamic Scene Analysis, NATO ASI Series, Series F, No 2, Springer-Verlag, NY, 1983

(6) T.S. Huang (ed): Image Sequence Analysis, Springer-Verlag, NY, 1981

(7) Image and Sensor Data Processing for Target Acquisition and Recognition, 40th Technical Meeting of the Avionics Panel of AGARD (AGARD Conference Preprint No 290), Aalborg, Denmark, Sep 1980

(8) L. Sevigny, G.H. Jensen, N. Bohner, A.M. Navarro, E. Østevold, S. Grinaker, J. Dehne: Discrimination and Classification of Operating Military Targets in Natural Scenes from Thermal Imagery, Final Report, AC/243 (Panel III) D/191, Brussels, Belgium, Oct 1981

(9) L. Sevigny, G.H. Jensen, N. Bohner, E. Østevold, S. Grinaker, J. Dehne: Discrimination and Classification of Vehicles in Natural Scenes from Thermal Imagery, Comp Vision, Graph and Image Proc, Vol 24, pp 229-43, 1983

(10) AGARD Symposium on Electro-Optical Systems and Image Analysis for Airborne Applications, 54th Panel Meeting of the Avionics Panel of AGARD, Athens, Greece, Oct 1987

(11) L. Sevigny, G.H. Jensen, J.-P. Gambotte, N. Bohner, S. Grinaker, R. Cowdaroy: Image Analysis for Target Tracking, AC/243 (Panel III) D/244, Brussels, Belgium, Nov 1985

(12) K.H. Bers, N. Bohner, P. Fritsche: Image Sequence Analysis for Target Tracking, Image Sequence Processing and Dynamic Scene Analysis, NATO ASI Series, Series F, No 2, Springer-Verlag, NY 1983

(13) I. Dyrdal, S. Grinaker, E. Heyerdahl: An Intelligent Multi-Target Tracking System, Proc. 4th Scandinavian Conf on Image Analysis, Trondheim, Norway, June 1985

(14) E. Heyerdahl: A Multi Hypothesis Tracking System, Proc. 4th Scandinavian Conf on Image Analysis, Trondheim, Norway, June 1985

(15) K.S. Fu, T. Ichikawa (Ed): Special Computer Architectures for Pattern Processing, CRC Press, Boca Raton, FL, USA, 1982

(16) M.J.B. Duff, S. Levialdi (Ed): Languages and Architectures for Image Processing, Academic press, London 1981

(17) H. Freeman, G.G. Pieroni (Ed): Computer Architectures for Spatially Distributed Data, NATO ASI Series, Series F, No 18, Springer-Verlag, Berlin 1985

(18) S. Grinaker: Real-Time processing of Rasterscan Images, Image Sequence Processing and Dynamic Scene Analysis, NATO ASI Series, Series F, No 2, Springer-Verlag, NY, 1983

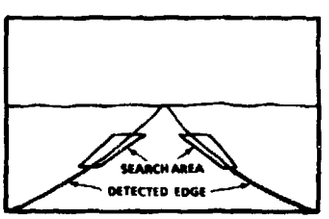

Figure 1 Search area for road tracking

The bold lines are the detected road edges. Expecting the road being smoothly curved, the edge continuations (faint lines) are searched for inside windows lining up with the general diraction of the detected edges

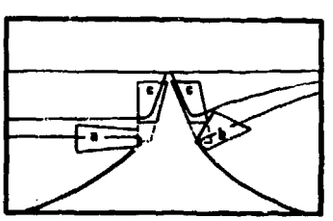

Figure 2 Search area for road tracking

a) Search window for edge of crossing road

b) Search window for edge of curved road

c) Alternative search window for the case that the straight road edge cannot be found locally

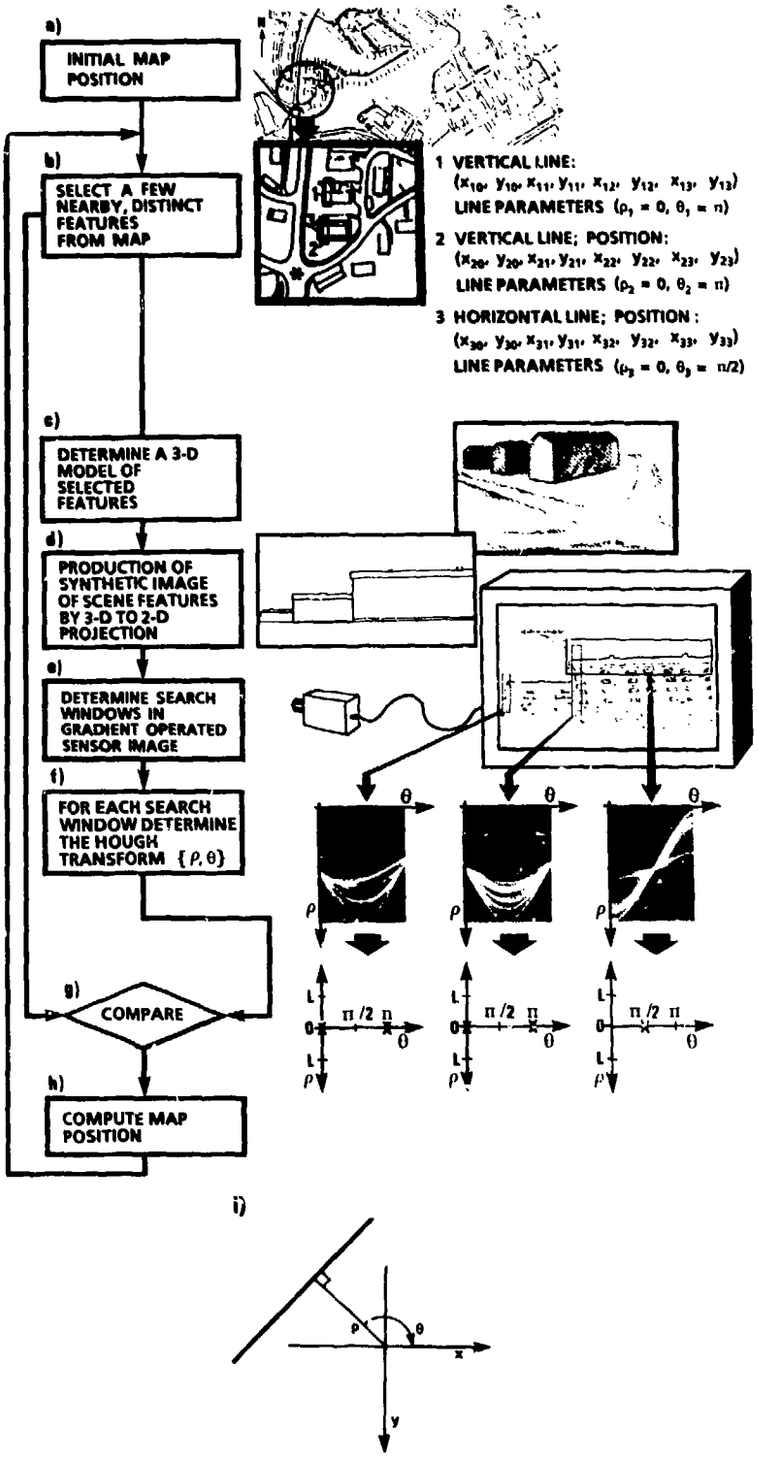

Figure 3 Map supported image navigation (Figure caption to be continued on next page)

Figure 3 Map supported image navigation (Cont)

a) The current position on the map, marked by an asterisk, is known

b) A few distinct features from the neighbourhood are selected, (here two vertical lines and one horizontal line). The line positions are specified by search windows which are defined by their corner coordinates

c) From the map data a 3-D model, depicting the selected features, is produced

d) A synthetic image, resembling the sensor image, is produced by mapping the model onto a plane located in the sensor focal plane

e) Gradient picture with the search windows superimposed. A gradient operator locates edge pixels. The search windows are transferred from the synthetic image to the sensor image

f) For each search window all edge pixels (gradient pixels above some threshold) are Hough transformed. (The parameters ρ and θ are defined in Figure 3 i)

g) Clusters in the Hough transform correspond to colinear edge pixels and determine the corresponding edge parameters. Two windows contain a vertical line along the y-axis ($\rho = 0$, $\theta = 0, \pi$) and one window contains a hurizontal line along the x-axis ($\rho = 0$, $\theta = \pi/2$)

h) The a posteriori sensor position in map coordinates is computed from the feature positions and orientations in the image (the line parameters are used to update the a priori position)

i) The line parameters ρ and θ

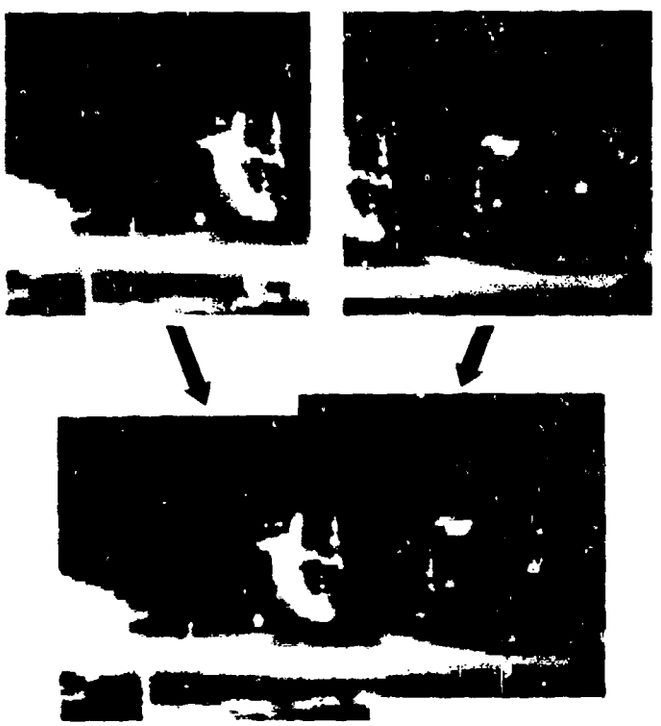

Figure 4 Image Registration

Two images, covering partly the same field of view, are merged to one image covering the union of the singular field of views. Pixel registration is the determination of pixel correspondences

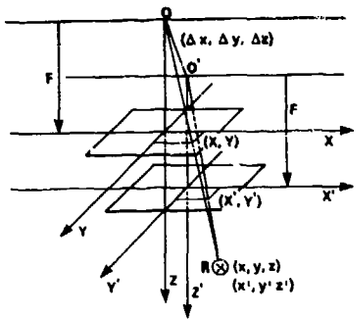

Figure 5 Determination of translational sensor motion by measuring the image displacement of a fixed point

(X, Y, Z): Sensor based cartesian coordinate system at instant T_0

(X', Y', Z'): Sensor based cartesian coordinate system at instant $T_0 + T_I$

(Δx, Δy, Δz): Sensor displacement

(x, y, z): Coordinates of a fixed point, R, in coordinate system (X, Y, Z)

(x', y', z'): Coordinates of R in coordinate system (X', Y', Z')

(X, Y): Coordinates of the image of R at instant T_0

(X', Y'): Coordinates of the image of R at instant $T_0 + T_I$

F: Sensor focal length

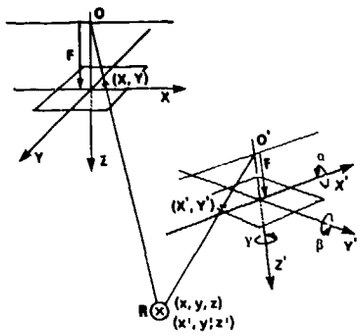

Figure 6 Determination of general sensor motion by measuring the image displacement of a fixed point

Notation is the same as in Figure 5. Additional parameters:

α: Rotation around the X-axis
β: Rotation around the Y-axis
γ: Rotation around the Z-axis

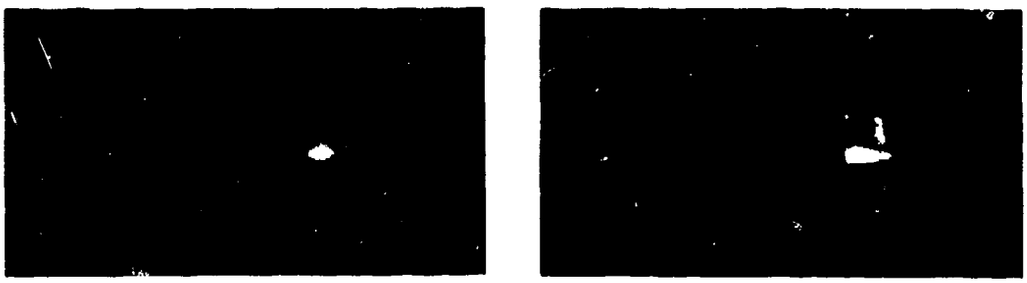

a) b)

Figure 7 Motion restoration

a) Image blurred due to diagonal camera motion

b) Restored image (motion parameters were known)

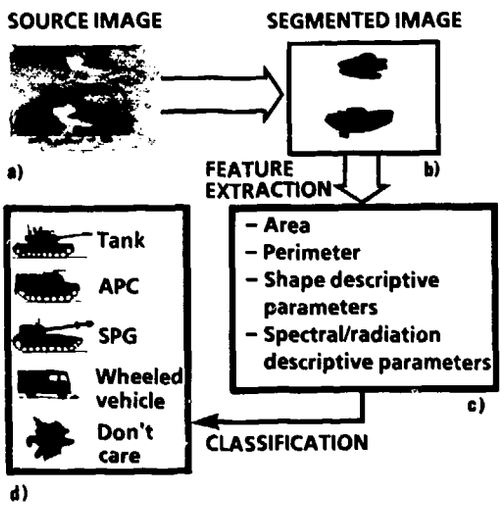

Figure 8 Image analysis for target acquisition

a) Thermal source image of two tanks

b) Segmentation: Separating objects from background

c) Feature extraction: Measuring prespecified, discriminating features, e g segment area, mean segment temperature, etc

d) Classification: Comparison of learned target patterns and measured object features to determine object class

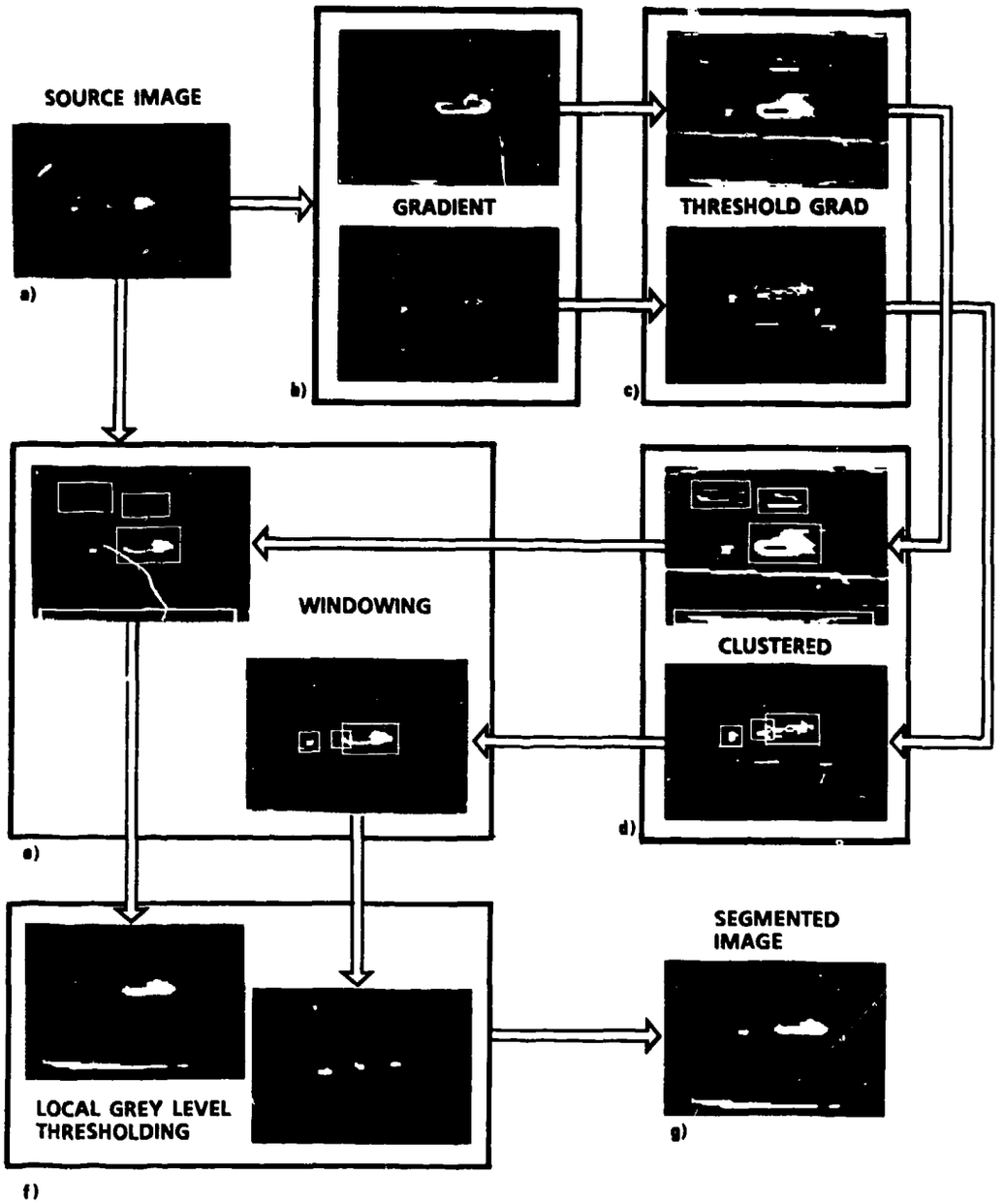

Figure 9 Segmentation of low-resolution IR images

a) Thermal source image

b) Contrast image obtained by convolving the original IR image and a gradient operator

c) Thresholded gradient image

d) Edge localization by clustering contrast points

e) Windowing: Determination of potential object areas
(not all windows are displayed)

f) Local grey level thresholding for separating objects from the background

g) Segmented image taken as the union of all local segments

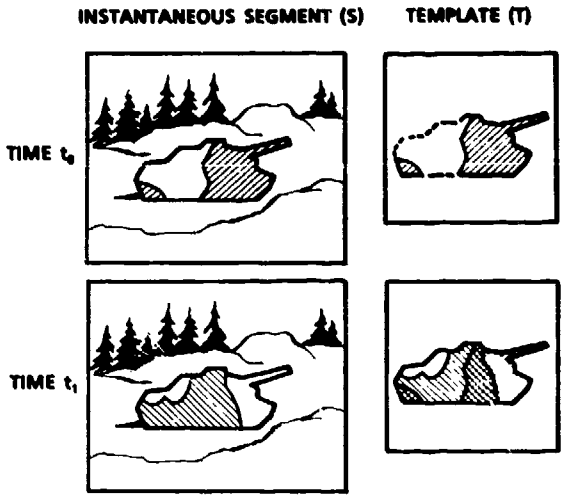

Figure 10 Image segmentation by template matching - Principle scheme

The template always constitutes the valid object segment

a) Segment in image I_0 : $S_0 = R_0$

b) Template at time t_0^+ : $T_0 = R_0$

c) Segment in image I_1 : $S_1 = R_1$

d) Template at time t_1^+ : $T_1 = R_0 \cup R_1$

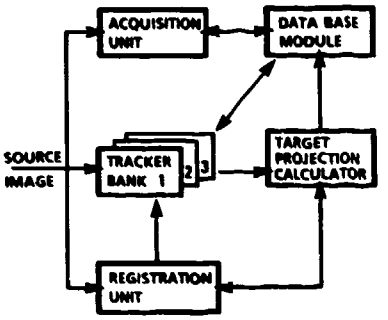

Figure 11 The NDRE Intelligent Multi-Target Tracker

An acquisition unit and multiple target trackers are integrated in one system permitting multi-target tracking, automatic target acquisition also during tracking, and tracking through obscurations. The Target Projection Calculator and the Data Base Module are used to determine the search window in the image. The registration unit extracts the information necessary for determining the sensor motion

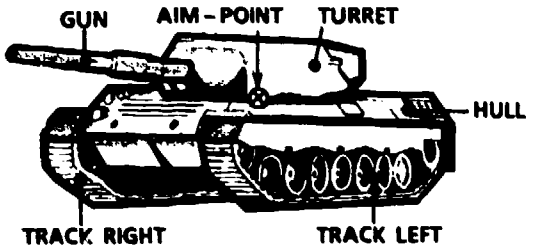

Figure 12 Preselected aim-point on a tank target

Desired aim-point: Centre-point of the borderline between hull and turret. Determination of this aim-point requires the recognition of the target substructures "hull" and "turret".

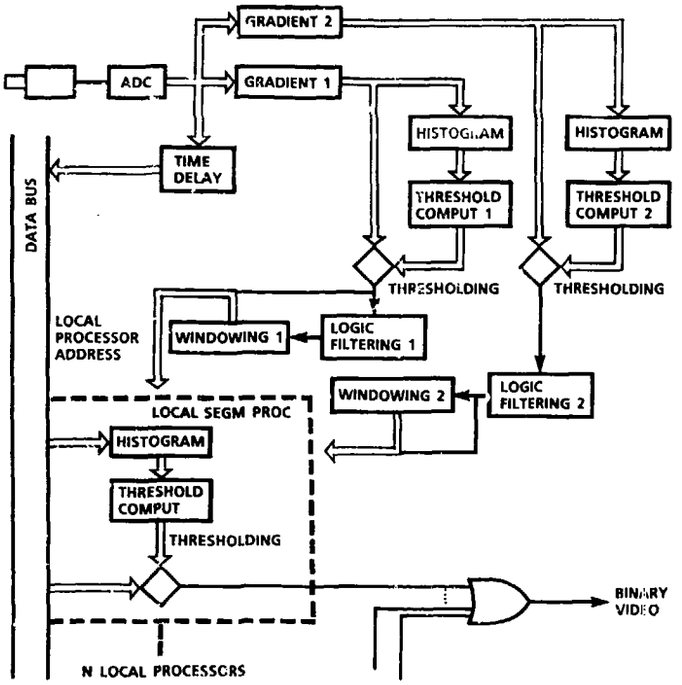

Figure 13 Parallel-pipeline implementation of a segmentation algorithm for low-resolution IR-images (ref Figure 9)

Processing of the two different gradient pictures are performed in parallel, and the local windows can be segmented independently in parallel pipelines.

STATISTICAL TECHNIQUES APPLIED TO ANALYSIS OF AIMPOINT DISTRIBUTIONS

V. Darryl Thornton, Director of the Operations Research Department
Joseph M. Conrad, Senior Engineer
Sverdrup Technology/TEAS Group
P.O. Box 1935 Eglin AFB, FL 32542

SUMMARY

A key element in the assessment of state-of-the-art weapons that are designed to autonomously detect, hit, and kill targets is the evaluation of the test data collected during the early phases of system testing. Typically, early versions of the proposed seekers are captive-flight tested aboard either fixed or rotary wing aircraft and the pertinent test parameters are recorded. During captive flight testing of seekers, detection and aimpoint data are collected over many parameters without knowing a priori which ones are significant. The most significant of these parameters are those that influence the probability of target detection and define the distribution of the aimpoints on the target. Relative to the aimpoint problem, the systems analyst is placed in the position of first identifying which parameters had the greatest effect on the resulting aimpoint distribution, characterizing and testing a proposed distribution against the test results, and finally predicting the aimpoint distribution in situations where there appeared to be a significant dependency on specific parameters and yet test data in these areas were either sparse or completely lacking. .

While no statistical method can completely make up for a paucity of test data, the intent of this paper is to illustrate the application of several statistical techniques that seek to maximize the amount of information gained. A stepwise multiple regression technique is presented that assists in the identification of significant parameters. Having identified these parameters, a Chi-square goodness-of-fit technique is used to test the hypothesis that the form of the proposed aimpoint distribution is, as an example, bivariate normal. Finally, a second regression technique is presented that generates coefficients corresponding to those parameters that were found to be the most significant. Using these coefficients, sensor performance parameters may then be predicted in those areas where data are sparse.

INTRODUCTION

A necessary factor in the assessment of any weapon system is an estimate of its effectiveness. Basically, three events must transpire for a target to be killed: (1) the target must be encountered and detected, (2) it must then be hit, and (3) it must be killed as a result of being hit. Relative to unguided general purpose weapons, which are delivered on the target from above, JMEM (Joint Munitions Effectiveness Manual) methodology is quite sufficient for determining effectiveness. However, for weapons designed to autonomously detect, hit, and kill the target, the traditional JMEM methodology is not appropriate. This is especially true of dispenser weapons that involve sensor-cued or precision-guided submunitions.

Statistical techniques for analyzing test data are presented that allow the use of a methodology that accounts for the stochastic nature of the detection, hit, and kill events. This eliminates the requirement to assume that the corresponding probabilities of these three events are independent and/or constant, which has normally been done heretofore. The statistical techniques presented are meant for application to data from tests of sensor/seeker and warhead performance. These test data provide information on: probability of target detection, distribution of aimpoints, variation of hitpoints, ballistic dispersion, and warhead lethality. Even though the first of these is discussed briefly, this paper deals, for the most part, with techniques for addressing the second: distribution of aimpoints and how said distribution is determined.

The organization of the paper is to first motivate the determination of aimpoint distributions by providing a short description of a methodology that can be used to accurately assess state-of-the-art guided weapons, but which requires information on the aimpoint distribution of the sensor or seeker. After this motivation, some useful statistical techniques for deducing detection probabilities and aimpoint distributions are presented. Finally, an example that demonstrates the usage of the techniques is presented.

METHODOLOGY

Some definitions will prove useful in the discussion to follow: We define:

P_d	=	Probability of detection (given encounter),
$P(H/D)$	=	Probability of hit given detection,
$P(K/H)$	=	Probability of kill given a hit, and
P_K	=	Probability of kill (given encounter).

Most weapon effectiveness methodologies to date have used some combination of the following: (1) $P_K = P_d \cdot P(H/D) \cdot P(K/H)$ or (2) a Monte Carlo simulation of the detection, hit, and kill events based on the values of P_d, $P(H/D)$, and $P(K/H)$, respectively. In actuality, these three conditional probabilities are not constants but vary as a function of such parameters as: the target orientation (aspect angle), the elevation angle between target and submunition, the range of the target from the submunition, target status (e.g., engine running or cold), etc., which are termed "significant variables". Additionally, the hit and kill events are closely tied together, since the probability of kill depends on precisely where the target is hit and not merely whether the target is hit. It can be shown that, for a given set of parameter values:

$$P_K = \iint P_d \cdot f_{HP}(x,y) \cdot P_{KH}(x,y)\,dx\,dy,$$

where x,y is a target-centered cartesian coordinate system; $f_{HP}(x,y)$ is a probability density function corresponding to the distribution of hitpoints given detection has occurred; and, $P_{KH}(x,y)$ is a function that yields the probability of target kill given a hit at the point x,y (frequently called a PK map).

The distribution of hitpoints usually results from a combination of three sources: (1) the distribution of aimpoints, (2) an aimpoint-to-mean-hitpoint translation, and, (3) the variation of the hitpoints about the mean hitpoint as a result of such things as ballistic dispersion.

The second of these sources is dependent on the exact workings of the submunition in question; it is, however, usually deterministic in nature. The third is usually bivariate normally distributed with zero means; consequently, if the aimpoint distribution is bivariate normal, the hitpoint distribution will be bivariate normal with means equal to the aimpoint mean plus translation constants, and standard deviations and correlation coefficient equal to the aimpoint standard deviations and correlation coefficient combined with the standard deviation corresponding to the aforementioned "ballistic" distribution.

Since the aimpoint distribution is independent of the other two contributors to hitpoint (which are independent of each other), there is no real requirement for the aimpoint distribution to be bivariate normal in order to perform the above integration for P_K. As seen above, however, when it is normal, a real simplification is possible. This simplification (a bivariate normal hitpoint distribution) allows for a standard numerical integration routine. Given this fact and the additional fact that the aimpoint distribution is indeed often bivariate normal, this paper is slanted toward that case. The aimpoint distribution for a given set of values for the significant variables (aspect, altitude, or whatever) can be checked for normality using a Chi-square test for each of two orthogonal direction variables (for example, x out the front of the target and y out the right); that is, failure to reject marginal normality will be used as cause to accept it. As it is felt from basic physical considerations that the aimpoint distribution is usually joint normal, substantiation of marginal normality will be taken to allow an assumption of joint normality. Then, the aimpoint distribution can be totally specified by two means and two standard deviations (for each of the two orthogonal variables) along with the corresponding correlation coefficient. These five quantities are termed the "five distribution-defining parameters" here.

The overall process would normally consist of first determining what variables influence the probabilities of detection and the aimpoint distribution; the data would then be grouped together by all combinations of these variables. Review of these data might show "gaps" and discontinuities. A determination as to how to fill these gaps and how to quantify the influence of the significant variables would be made. Some suggested methods are described below.

USEFUL STATISTICAL TECHNIQUES

Detection probabilities and aimpoint distributions generally are multivariate functions. A cursory examination of the data base would hopefully show which of the variables over which data were collected appear to have the greatest chance of explaining the variations. While it is not difficult to assess the marginal effects of the variables, attempting to assess their effects jointly can be quite difficult. To estimate the extent to which each of these variables influences the P_d, the data can be analyzed using a standard statistical analysis package (see Reference 1 for a discussion of several), which performs an analysis of variance for multiple independent variables and will thus indicate those variables that appear to offer the greatest chance of explaining the variance in the data.

Since the data quite often are unbalanced (that is, they contain unequal numbers of observations for each of the variables), a general linear model procedure is suggested. (This procedure fits the data into a linear model using a least-squares method.) The program subsequently tests the F-value produced, by dividing the mean square error of each of the parameters by the total mean square error, to determine if that particular parameter is significant. A small significance probability, PR>F (from F tables), indicates that the probability some linear function of the parameter existing is significantly different from zero. For example, if PR>F is less than 0.01, that variable tests significant at the 99-percent confidence level. To minimize unnecessary effort, it is suggested that only variables significant above the 95 percent level be selected for detailed analysis. Please note that although this statistical technique can be very helpful in identifying and quantifying important variables, it will not be a panacea; nor will it be a stand-alone method for the analysis. Rather, it is simply a first step. Once the statistical package has identified significant parameters, as many combinations of these parameters as possible should be analyzed for trends. The data should be grouped in matrix form across all significant parameters and manually examined. Excursions by grouping data in many different ways can either establish a trend or fail to indicate one. The established trends provide a method for filling "gaps" and for modifying small sample size data that fail to fit the trends.

As is the case for the P_d analysis, a statistical computer program can be used to indicate which variables were significant in affecting the aimpoint distribution (that is, affecting the means, standard deviations, and correlation coefficient). Again as with P_d, a more detailed investigation should be made to establish such things as consistency and reasonableness of trends as a function of such variables. These investigations, relative to significant variables, should be performed for the test targets (for example) with the greatest number of data points (optimally one hundred or more). Because of the usual paucity of aimpoint data (since only target detection events and not all acquisition opportunity events result in an aimpoint), it is not desirable to have the aimpoint distribution (for a given sensor-target combination) expressed as a function of too many variables (probably no more than two).

After a determination of significant independent variables has been made (that is, the "cell" has been defined), the hypothesis that the aimpoints are (for example) normally distributed should be checked for each cell. As mentioned previously, the goodness-of-fit test that can be used is the Chi-square test. That is, the null hypothesis that the random variable aimpoint (x,y) has a normal distribution can be tested. This is done by computing the test statistic "X-sq", which is the sum over the intervals of the squared differences between actual and expected interval frequencies divided by expected interval frequency. These "intervals" are defined here in units of fractions of the standard deviation (sigma). The expected frequency for each interval is calculated as the theoretical percentage of that interval from a standard normal table times the total number of data points for the cell in question. (For example, suppose we are concerned with the interval from the mean to the mean plus one-half sigma and we have one hundred data points; then, the expected number of samples lying in this interval would be .1915 times 100, or 19.15 points.) This X-sq is then compared to the tabulated critical value of "Chi-square" (for a given significance level and with degrees of freedom one less than the number of intervals); and, if X-sq is less than Chi-sq, we cannot reject the normality hypothesis.

As a rule of thumb (see Reference 2), the sample size in each interval should equal at least five in order for the Chi-square test to be valid. This restriction has the effect of limiting the cells for which normality can be checked and limiting the number of intervals into which the given cell can be divided if it is checked. A feasible rule is to use a minimum of the following four intervals: (1) the interval between the mean and the mean plus one-half sigma; (2) the interval between the mean and the mean minus one-half sigma; (3) the interval greater than the mean plus one-half sigma; and (4) the interval less than the mean minus one-half sigma. When worked out for a test of normality, this requires five samples in each of the two inner intervals and eight in each of the two outer ones, or a total of twenty-six samples for the cell. When the number of samples in a cell allows, additional pairs of intervals (one on either side of the mean and each of width one-half sigma) can be considered in the test for that cell.

The overall technique relative to aimpoint distributions consists of performing the following steps in an iterative fashion: determining initial significant variables using a statistical package; establishing the consistency and reasonableness of trends in order to refine the list of truly meaningful variables; and, checking the data for each cell (combination of variables) for normality. For example, for a field test with limited data the statistical package might indicate that altitude and aspect are significant relative to the mean of x, while altitude and target status are significant relative to the mean of y. This would imply cells defined by three variables (altitude, aspect, and target status) and there might not be enough data to support these variables. Possibly all five of the distribution-defining parameters are a slightly less strong function of the same two variables, (for example, altitude and sun status), yet normality for many of the resultant cells is rejected. Consequently, one must "start-over" by investigating, for instance, the combination of data over some altitudes, aspects, target status, or whatever in

order to reach normality (since large data samples tend to exhibit more normal behavior than small ones). Frequently, plots of the defining variables as a function of significant variables can be used as aids to visualize trends and otherwise gain insight into the underlying phenomena.

After the accomplishment of the above steps, the data should be grouped into the defining cells and the five distribution-defining parameters calculated for each cell. A possible rule is that in the absence of overwhelming evidence to the contrary, such calculated parameters would be used for any cell with say ten or greater data points. For cells with fewer than ten samples, however, a data void (or "hole") would be deemed to occur. The five distribution-defining parameters for such cells would have to be obtained from other sources than just the particular data for that cell.

A valid approach for determining an appropriate set of distribution-defining parameters for cells with data voids is multiple regression analysis (see Reference 3). This regression analysis can be performed with the aid of a statistical package. The independent variables chosen for regression should be the same variables that defined the cells (that is, the "most significant" variables) and powers and cross products thereof. The "most predictive" independent variables are determined by choosing a significance level that is sufficiently small to exclude those variables explaining little to none of the variance in the data. This resulting set of "most predictive" variables can then be used to make up the model for each distribution-defining parameter as a function of the cell-defining variables. The model, in turn, can be used to compute the distribution-defining parameters for those cells with fewer than (for example) ten samples.

The above regression analysis approach should be done for each different target type (and sensor, of course) when there is enough data for that particular target. In many cases, however, the paucity of data might not allow for a sufficiently predictive model to be developed in that fashion. In such cases, a model can be constructed that uses the data for all similar targets (that is, whose signatures result in near same sensor performance), and includes target type as an additional independent variable. This will be, to a large extent, an iterative procedure with the model improving at the completion of each iteration. A comparison between the model prediction and the actual data should then be made, at least, for the target(s) with the most data. This comparison should be made to gain insight as to how accurately the model predicts the test results. The model prediction can then be calculated using a weighting determined by the sample sizes in each cell as well as an unweighted prediction. This is done because the model will tend to be driven by the data in the more populous cells; and, as a consequence, the unweighted predictions will not compare very favorably to the actual data for cells with sparse data. This will tend to lead one to the conclusion that the model is not as good as it actually is.

When the development of the model has proceeded to a point where it is deemed sufficient to predict the performance of the system in question, a matrix for each target of the five distribution-defining parameters for each cell can be generated using the model. These values can then be used for those cells that have too few test samples; and, the values as calculated from the actual test data can be used for the cells with sufficient samples.

EXAMPLE

To illustrate the techniques mentioned above, an example problem was developed. First, it was assumed that a seeker had aimpoint tendencies that were functions of various test parameters. Next, a model was developed to randomly generate aimpoints from the assumed distributions. Finally, an analysis of these data was conducted as if none of the underlying tendencies were known.

A seeker was assumed to have the aimpoint distribution characteristics summarized below in Table 1.

Table 1. Sample Aimpoint Distribution

Condition	Mean (x,y)	Sigma x	Sigma y
Target Moving	(5,2)	2	5
Target Idling, High Sun	(0,2)	3	3
Target Idling, Low Sun	(8,3)	4	1
Target Cold	(0,0)	5	5

Additionally, it was assumed that the altitude of the seeker above the target did not influence the mean but did influence the sigmas (standard deviations). At low altitudes, the standard deviations were assumed to be one-half of the above values. At high altitudes, the standard deviations were assumed to be 50 percent larger than above. Finally, it was assumed that additional data were collected on other parameters such as the aspect angle relative to the front of the target, and the target background. The aimpoint generation model randomly generated aimpoints with all of the above characteristics.

Exercising the model for 1000 replications generated the same results as if a seeker having these capabilities were flight tested and 1000 aimpoints collected. The resulting distribution is shown in the scatter plot of Figure 1.

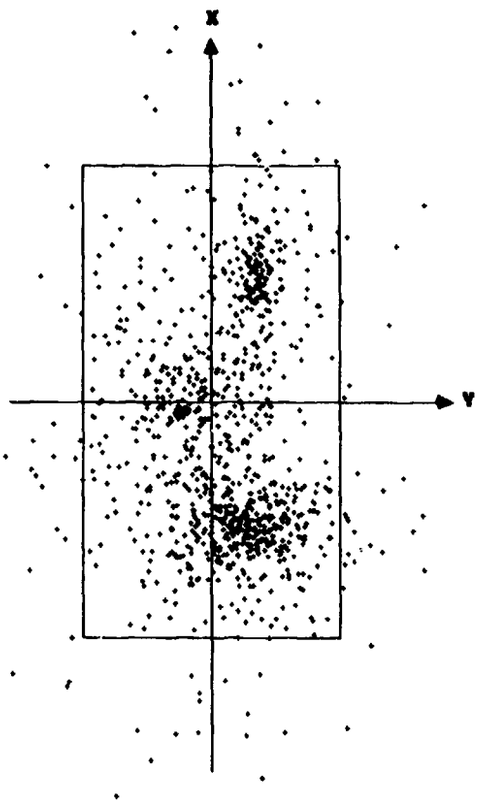

Figure 1. Scatter Plot

A stepwise multiple regression with independent variables of target status, sun status, target aspect, target background, and seeker altitude, was conducted for each of five dependent variables. The first two dependent variables were the x and y aimpoints. The second two dependent variables were the squares of the x and y aimpoints and the final dependent variable was the product of the x and y aimpoints. On the first pair, the analysis indicates whether any of the independent variables influences the means. On the second pair, the analysis indicates whether any of the independent variables influence the standard deviations, and the final analysis indicates whether the correlation between the x and y aimpoint is influenced by any of the independent variables. Since we are using a normal distribution as an example, these five quantities (two means, two standard deviations, and a correlation coefficient) totally define the aimpoint distribution, and will (as mentioned above) be referred to as the five "distribution-defining" parameters.

The results of the regression analysis are shown in Table 2. The F-value is the ratio of the "within-parameter" variance to the total parameter variance. This value, when referred to an F-table with the appropriate degrees of freedom, is indicative of the probability that a given parameter is not significant. It is this probability that is shown in Table 2. To minimize unnecessary calculations, as suggested above, only variables significant above the 95 percent level (i.e., PR>F values less than 0.05) will be selected for the regression analysis.

Table 2. Probability of Parameter Insignificance (PR>F)

Parameter	Mean x	Mean y	Sigma x	Sigma y	Corr Coeff
Tgt Status	.0	.0001	.0001	.0001	.0001
Sun Status	.0001	.0001	.0001	.1599	.0011
Aspect	.7296	.5741	.0681	.2244	.3918
Location	.2333	.7970	.4467	.4433	.1005
Altitude	.9262	.9072	.000	.0001	.9351

The table indicates that two parameters (target status and sun status) were significant in terms of explaining variations in both the x and y mean aimpoint. For the standard deviation about the x aimpoint, three factors (target status, sun status and altitude) were significant while for the y aimpoint, two factors (target status and altitude) were significant. For the correlation between the x and y coordinates of the aimpoint, the analysis of variance indicated that both target status and sun status were significant. Thus, the analysis shows that the distributions of aimpoints to be functions of three parameters: target status, sun status, and altitude.

For situations where the test parameters are discrete variables, such as the case outlined above in the example problem, predictions for the means are simply the cell averages. Table 3 summarizes the predictions (PRED) of the distribution-defining parameters as functions of the appropriate significant variables. Also shown for comparison purposes are the "true" values (ACT for actual) of the distribution parameters. As can be seen the significant variables (i.e., target status, sun status and altitude) were detected and the cell averages are in fairly close agreement with true values.

It should be noted that in situations where the test parameters are continuous variables, (for example, if altitude had been expressed in feet above the target instead of "high", "medium", and "low") a regression technique can be used to predict the values of the distribution-defining parameters. Continuous variable regression techniques are also useful for predicting the cell value in situations where data are lacking.

The hypotheses being tested are that the distributions of the aimpoints about the respective means are normal. To test these, frequency distributions for the distances from the mean of all aimpoints in the x and y directions for each cell are computed. Fourteen data bins are created in both the x and y directions, seven on each side of the mean. Each bin is one-half sigma in width. A count is then made of the number of data points falling within each bin. The difference between the number of data points within each bin and the expected number that should be in each bin, if the data were normally distributed, is then computed. The ratio of the square of these differences to the expected number of points within the cell (X-Sq) used is then summed and compared to a Chi-square distribution with the appropriate degrees of freedom. Should this sum exceed the critical value of the Chi-square distribution (Chi-Sq), the hypothesis would then be rejected. Table 4 gives the comparisons between measured and true distributions for the x direction in the situation where the target is moving, sun status is low and the altitude is low. Table 5 gives the same for the y direction. In neither instance was the null hypothesis rejected. Similar analyses were conducted for the other 17 cells and in no case was the null hypothesis rejected.

We see that for the above example, the methodology suggested herein was able to successfully determine the significant variables, demonstrate normality, and predict the distribution-defining variables such that data voids could be filled as necessary.

Table 3. Predicted and Actual Distribution-Defining Variables

Tgt	Sun		x-Aimpoint Mean		x-Aimpoint Sigma		y-Aimpoint Mean		y-Aimpoint Sigma		x-y Corr Coeff	
Stat	Stat	Alt	Pred	Act	Pred	Act	Pred	Act	Pred	Act	Pred	Act
MOVE	LOW	Low	-5.0	-5	1.58	1	1.76	2	2.7	2.5	0.09	0
MOVE	LOW	Med	-5.0	-5	2.15	2	1.76	2	5.61	5	0.03	0
MOVE	LOW	Hi	-5.0	-5	2.95	3	1.76	2	8.21	7.5	0.02	0
MOVE	HI	Low	-5.1	-5	0.13	1	2.59	2	1.92	2.5	-----	0
MOVE	HI	Med	-5.1	-5	2.8	2	2.59	2	5.28	5	-0.12	0
MOVE	HI	Hi	-5.1	-5	2.55	3	2.59	2	7.99	7.5	-0.09	0
IDLE	LOW	Low	0.4	0	1.5	1.5	-2.06	-2	1.69	1.5	-0.82	0
IDLE	LOW	Med	0.4	0	3.01	3	-2.06	-2	2.36	3	-0.29	0
IDLE	LOW	Hi	0.4	0	4.44	4.5	-2.06	-2	3.53	4.5	-0.13	0
IDLE	HI	Low	7.8	8	2.74	2	2.88	3	----	1.5	----	0
IDLE	HI	Med	7.8	8	4.24	4	2.88	3	1.24	3	-0.02	0
IDLE	HI	Hi	7.8	8	6.65	6	2.88	3	2.9	4.5	0	0
COLD	LOW	Low	-0.4	0	2.6	2.5	0.49	0	2.4	2.5	-0.28	0
COLD	LOW	Med	-0.4	0	4.5	5	0.49	0	5.01	5	-0.08	0
COLD	LOW	Hi	-0.4	0	7.84	7.5	0.49	0	6.88	7.5	-0.03	0
COLD	HI	Low	-0.1	0	2.31	2.5	-1.14	0	2.17	2.5	0.29	0
COLD	HI	Med	-0.1	0	5.1	5	-1.14	0	4.9	5	0.06	0
COLD	HI	Hi	-0.1	0	6.82	7.5	-1.14	0	6.8	7.5	0.03	0

Tgt = Target
Stat = Status
Alt = Altitude
Pred = Predicted
Act = Actual
Corr = Correlation
Coeff = Coefficient
---- = Indeterminate

Table 4. Marginal Normality Analysis, x-Direction

Bin (Std Deviations)	Actual Number	Expected Number	X-Sq
Less than -3	0		
-3.0 to -2.5	0	4.6	.03
-2.5 to -2.0	1		
-2.0 to -1.5	4		
-1.5 to -1.0	7	6.4	.06
-1.0 to -0.5	14	10.5	1.17
-0.5 to 0	11	13.4	.43
0 to 0.5	10	13.4	.86
0.5 to 1.0	13	10.5	.59
1.0 to 1.5	6	6.4	.03
1.5 to 2.0	1		
2.0 to 2.5	2		
2.5 to 3.0	1	4.6	.43
More than 3.0	0		
TOTAL	70	TOTAL	= 3.60

Critical Chi-Sq = 9.24

Therefore, Cannot Reject H_o, Normality

Table 5. Marginal Normality Analysis, y-Direction

Bin (Std Deviations)	Actual Number	Expected Number	X-Sq
Less than -3	0		
-3.0 to -2.5	0	4.6	.56
-2.5 to -2.0	2		
-2.0 to -1.5	1		
-1.5 to -1.0	9	6.4	1.06
-1.0 to -0.5	12	10.5	.21
-0.5 to 0	9	13.4	1.45
0 to 0.5	14	13.4	.03
0.5 to 1.0	13	10.5	.60
1.0 to 1.5	6	6.4	.03
1.5 to 2.0	2		
2.0 to 2.5	1		
2.5 to 3.0	1	4.6	.08
More than 0	0		
TOTAL	70	TOTAL	= 4.02

Critical Chi-Sq = 9.24

Therefore, Cannot Reject H_o, Normality

REFERENCES

1. James T. McClave and Frank H. Dietrich, II, Statistics, Third Edition, San Francisco, California, U.S.A., Dellen Publishing Company and London, U.K., Collier Macmillan Publishers, 1985, p. 669 ff.

2. Ibid., p. 555.

3. Ibid., pp. 637-665.

REPORT DOCUMENTATION PAGE

1. Recipient's Reference	2. Originator's Reference	3. Further Reference	4. Security Classification of Document
	AGARD-CP-435	92-835-0486-0	UNCLASSIFIED

5. Originator Advisory Group for Aerospace Research and Development
North Atlantic Treaty Organization
7 rue Ancelle, 92200 Neuilly sur Seine, France

6. Title GUIDANCE AND CONTROL OF PRECISION GUIDED WEAPONS

7. Presented at the Guidance and Control Panel 46th Symposium held in Geilo, Norway from 3 to 6 May 1988.

8. Author(s)/Editor(s)	9. Date
Various	November 1988
10. Author's/Editor's Address	**11. Pages**
Various	80

12. Distribution Statement This document is distributed in accordance with AGARD policies and regulations, which are outlined on the Outside Back Covers of all AGARD publications.

13. Keywords/Descriptors

Acquisition and guidance sensors
Algorithms
Software
Millimetre-wave sensors
Precision guided munitions

14. Abstract

This volume contains six unclassified papers out of the 25 presented at the Guidance and Control Symposium, held in Geilo, Norway from 3 to 6 May 1988. The remainder of the papers (except papers Nos 11 and 26, not available at time of printing) are included in the classified supplement CP-435(S).

The papers were presented under the following headings: Operational requirements and considerations; Guidance sensors and components; Guidance and control techniques and signal processing; Effectiveness and system evaluation; Systems demonstration.

AGARD Conference Proceedings No.435 Advisory Group for Aerospace Research and Development, NATO GUIDANCE AND CONTROL OF PRECISION GUIDED WEAPONS Published November 1988 80 pages This volume contains six unclassified papers out of the 25 presented at the Guidance and Control Symposium, held in Geilo, Norway from 3 to 6 May 1988. The remainder of the papers (except papers Nos 11 and 26, not available at time of printing) are included in the classified supplement CP-435(S). The papers were presented under the following headings: P.T.O.	AGARD-CP-435 Acquisition and guidance sensors Algorithms Software Millimetre-wave sensors Precision guided munitions	AGARD Conference Proceedings No.435 Advisory Group for Aerospace Research and Development, NATO GUIDANCE AND CONTROL OF PRECISION GUIDED WEAPONS Published November 1988 80 pages This volume contains six unclassified papers out of the 25 presented at the Guidance and Control Symposium, held in Geilo, Norway from 3 to 6 May 1988. The remainder of the papers (except papers Nos 11 and 26, not available at time of printing) are included in the classified supplement CP-435(S). The papers were presented under the following headings: P.T.O.	AGARD-CP-435 Acquisition and guidance sensors Algorithms Software Millimetre-wave sensors Precision guided munitions
AGARD Conference Proceedings No.435 Advisory Group for Aerospace Research and Development, NATO GUIDANCE AND CONTROL OF PRECISION GUIDED WEAPONS Published November 1988 80 pages This volume contains six unclassified papers out of the 25 presented at the Guidance and Control Symposium, held in Geilo, Norway from 3 to 6 May 1988. The remainder of the papers (except papers Nos 11 and 26, not available at time of printing) are included in the classified supplement CP-435(S). The papers were presented under the following headings: P.T.O.	AGARD-CP-435 Acquisition and guidance sensors Algorithms Software Millimetre-wave sensors Precision guided munitions	AGARD Conference Proceedings No.435 Advisory Group for Aerospace Research and Development, NATO GUIDANCE AND CONTROL OF PRECISION GUIDED WEAPONS Published November 1988 80 pages This volume contains six unclassified papers out of the 25 presented at the Guidance and Control Symposium, held in Geilo, Norway from 3 to 6 May 1988. The remainder of the papers (except papers Nos 11 and 26, not available at time of printing) are included in the classified supplement CP-435(S). The papers were presented under the following headings: P.T.O.	AGARD-CP-435 Acquisition and guidance sensors Algorithms Software Millimetre-wave sensors Precision guided munitions

Operational requirements and considerations; Guidance sensors and components; Guidance and control techniques and signal processing; Effectiveness and system evaluation; Systems demonstration. ISBN 92-835-0486-0	*Operational requirements and considerations;* **Guidance sensors and components;** Guidance and control techniques and signal processing; Effectiveness and system evaluation; Systems demonstration. ISBN 92-835-0486-0
Operational requirements and considerations; Guidance sensors and components; Guidance and control techniques and signal processing; Effectiveness and system evaluation; Systems demonstration. ISBN 92-835-0486-0	Operational requirements and considerations; Guidance sensors and components; Guidance and control techniques and signal processing; Effectiveness and system evaluation; Systems demonstration. ISBN 92-835-0486-0